A Synthetic Biology Approach to Bacteria Mediated Tumor Targeting

by

Bahram Zargar

A thesis
presented to the University of Waterloo
in fulfillment of the
thesis requirement for the degree of
Doctor of Philosophy
in
Chemical Engineering

Waterloo, Ontario, Canada, 2014

AUTHOR'S DECLARATION

I hereby declare that I am the sole author of this thesis. This is a true copy of the thesis, including any required final revisions, as accepted by my examiners.

I understand that my thesis may be made electronically available to the public.

Abstract

Development of a drug delivery agent that selectively targets and destroys tumor cells with minimal toxicity to normal tissues is a major challenge in cancer therapy. It has been known for more than 60 years that anaerobic bacteria such as Clostridium can selectively colonize inside the necrotic core of solid tumors. Inoculation of a tumor by wild type Clostridium results in colonization of the necrotic core and consequently significant tumor destruction. This treatment strategy is hampered by the fact that the outer rim of the tumor is typically viable, and so does not present an anaerobic environment. As a result, colonization by Clostridium is unlikely to lead to complete tumor regression, since tumor regrowth occurs from the remaining outer viable rim, as evidenced by clinical trials. This project aims to address the problem of regrowth by developing a novel selectively aerotolerant strain of Clostridium that cannot colonize inside healthy tissue, but that could grow in the viable rim of an infected tumor. We have engineered a gene coding for an aerotolerance enzyme into Clostridium sporogenes. To couple the selective expression of this gene to tumor colonization, it can be placed under the control of a promoter activated by a synthetic quorum sensing circuit. This document describes the foundational work that will allow this system to be implemented. A suitable strain of *C. sporogenes* was selected, and a cloning technique (via conjugation with E. coli) was implemented. Expression of the aerotolerance enzyme and a synthetic quorum sensing circuit were verified in engineered colonies, and appropriate function was confirmed in both cases. Additionally, a model-based design exercise was carried out in order to better understand the system behavior and to identify key parameters for controlling the bacterial population. This analysis was based on mathematical models of the quorum-sensing circuit and of bacterial growth in the tumor environment. Sensitivity analysis reveals the design parameters that have the most significant impact on the extent and specificity of colonization of the viable rim, and thus provides insights into efficient design of the synthetic mechanism.

Acknowledgements

I would like to express my sincere appreciation and thanks to my advisors Dr. Brian Ingalls and Dr. Pu Chen, for giving me the opportunity to work on this interesting project. Your advice on both research as well as on my career have been priceless. I would also like to thank my committee members, Dr. Perry Chou, Dr. Ali Elkamel, and Dr. Trevor Charles for serving as my committee members and helping me throughout this project. I also want to thank Dr. Neil Forbes for accepting to be the external examiner of my thesis despite of his tight schedule. I would especially like to thank Dr. Perry Chou and Dr. Syed Ali Sattar who generously supported me in using their facilities and lab to fulfill this project. Thanks to all my colleagues and the staff at the chemical engineering department of University of Waterloo and at BMI department of University of Ottawa.

A special thanks to my family. Words cannot express how grateful I am to my mother and father, for all of the sacrifices that you have made. I would also like to thank all of my friends who supported me throughout my study, and encouraged me towards my goal.

Table of Contents

List of Figures

List of Tables

Chapter 1

Introduction

1.1 Motivation

Bacteria-mediated cancer therapy has a long history. Almost two centuries ago it was observed that bacterial infections could cause tumor regression. In the 1860's bacteria were used actively in cancer therapy and research on this area started in the mid 1930's. Anaerobic bacteria can colonize inside the necrotic core of a solid tumor, which is oxygen free and rich in nutrition. Most of the research in this area has been focused on *Salmonella* and *Clostridium*, which have been identified as excellent choices for cancer therapy: *Salmonella* because it allows easy genetic manipulation, and *Clostridium* because it colonizes in large numbers in tumors [1,2,3].

Among the strains that have been investigated, *Clostridium sporogenes* seems to be one of the best in tumor targeting and colonization. This strain is motile, non-pathogenic, spore-forming, and colonizes selectively in tumors in large numbers. Colonization of wild-type *C. sporogenes* in the necrotic core of the tumor leads to significant tumor oncolysis, but regrowth occurs from the viable outer rim of the tumor, which is oxygenated[2]. The use of *C. sporogenes* for cancer therapy entered clinical trial in 1967 [2] but was discontinued because of the regrowth problem. Since then, a number of alternative approaches, such as delivery of prodrug-converting enzymes, combined bacteria-radio therapy, and combined bacteria-chemo therapy have been explored in attempt to arrive at a successful therapy [1]. In 2006, the first successful gene transformation protocol for *C. sporogenes* opened a new window in bacteria mediated cancer therapy [4].

On the other hand, new techniques in synthetic biology help us to spatially and temporally control gene expression inside specific environments. The tumor regrowth problem can be solved using recombinant *C. sporogenes* and new techniques in synthetic biology, which allow for specific functions (e.g. aerotolerance, drug release) to be triggered selectively in the tumor environment.

1.2 Objective, Hypothesis and Methodology

This project aims to address the problem of regrowth of tumor tissue after bacteriolytic treatment. Our goal is to develop a novel selectively aerotolerant strain of *Clostridium* that cannot colonize inside healthy tissue, but that could grow in the viable rim of an infected tumor. We hypothesize that aerotolerance is conferred by expression of an aerotolerance enzyme by an engineered strain of *Clostridium sporogenes*. To couple the selective expression of this gene to tumor colonization, it will be placed under the control of a promoter activated by a synthetic quorum sensing circuit.

A synthetic biology approach is used in this project. The quorum sensing mechanism in gram positive and gram negative bacteria are modeled in details to understand the system behavior. System analysis on these models helps us understand the contribution of all components on system behavior. Additionally, modeling of colony growth in tumors and sensitivity analysis of this model reveals the design parameters that have the most significant impact on the extent and specificity of colonization within the viable rim, and thus provides insights into the design of the synthetic mechanism.

We used conjugation to transfer genes into *C. sporogenes*. The *lux* promoter from *Vibrio fischeri* and the *P2* and *P3* promoters from *Staphylococcus aureus* were chosen as candidates to produce density dependent gene expression in *C. sporogenes*. In order to study the behavior of these promoters in *C. sporogenes,* they were cloned upstream of an anaerobic gene reporter with all associated quorum sensing elements. As a positive control, we assayed expression from the thiolase promoter (*thl*) from *C. acetobutylicum*. The three genetic circuits were transformed into *C. sporogenes* and their behavior was compared with the positive control and the native bacteria. The *lux* promoter showed no activity in *C. sporogenes,* but the *P2* and *P3* promoters were active. However, the *P2* promoter showed behavior very similar to the constitutive expression. Expression from *P3* was low at low cell concentrations and increased dramatically as the cell density crossed a threshold, demonstrating a switch-like behavior. Thus the *P3* promoter seems to be a good candidate for cell density expression of an aerotolerance enzyme.

The potential for aerotolerance of *C. Sporogenes* was addressed by measuring the effect of constitutive expression of the *noxA* gene from *C. Aminovalericum,* which express a water-forming NADPH oxidase. The *noxA* gene was cloned upstream of the *thl* promoter, and the resulting plasmid was transformed into *C. sporogenes*. The behavior of the engineered *C. sporogenes* strain was

compared with the native strain in the presence of oxygen. The engineered strain retained its growth while the native strain did not, suggesting that expression of *noxA* can make *C. sporogenes* aerotolerant.

The planned final construct, an engineered *C. sporogenes*, expressing aerotolerance enzyme under the control of the quorum-sensing *P3* promoter, may be capable of destroying the oxygenated part of a tumour, and thus providing a successful therapy. Moreover, this strain can be used as a safe vehicle to deliver therapeutic agents (gene, drugs, prodrugs) into the proliferating and non-proliferating part of the tumor. Because the expression of a single aerotolerance enzyme is not enough to significantly scavenge oxygen in fully oxygenated healthy tissue, there is minimal concern for the engineered colony to grow beyond the rim of the tumor. Moreover, any bacterial cells that escape the tumor environment will have to face the immune system (which is compromised in the tumor itself).

To the best of our knowledge this is the first time that an attempt has been made to express of noxA in C. sporogenes, and the first time that a synthetic quorum sensing has been engineered in C. sporogenes.

Chapter 2
Literature Review

2.1 Introduction

Almost 150 years ago bacterial infections was used actively for the first time to cure cancer patients [2,3]. Since that time, a range of bacterial strains, including E.coli, *Bifidobacteria*, *Salmonela*, and *Clostridia*, have been tested for tumor therapy. This chapter begins with a description of the tumor microenvironment in section 2.2, which will be followed by a review of research on clostridia-mediated and salmonella-mediated bacterial tumor therapy in sections 2.3.

The therapeutic design proposed in this manuscript involves engineering a strain of *Clostridium* so that it will gain aerotolance when germinating to high density in solid tumors. A literature review of oxygen metabolism in *Clostridium* is reported in section 2.4. Section 2.5 describes the quorum sensing mechanism in gram positive and gram negative bacteria, which provides a means to implement density-dependent behavior. Mathematical modelling of quorum sensing mechanism is reviewed in Section 2.6. Finally a brief overview of synthetic biology is presented in Section 2.7.

2.2 Tumor Microenvironment

Every cell in the human body follows a highly regulated cell cycle. If a single cell loses its control over cell cycle, it could proliferate quickly and produce a vast population of cells, resulting in formation of a tumor. As the tumor grows the surrounding blood vessels become inadequate to supply nutrients for the abnormal cells. This triggers the secretion of tumor angiogenic factors (TAFs). TAFs stimulate differentiation, division and migration of endothelial cells of the blood vessels to the tumor site. The imbalance between different TAFs typically causes abnormality in the blood vessels of the tumor. As the tumor grows the distance between microvessels and some tumor cells increases. As a consequence, the oxygen level of the inner part of the tumor is reduced. The low level of oxygen in the inner part of the tumor makes this part highly hypoxic. Some parts of the inner tumor become oxygen-free; cells in these areas undergo necrosis ([1,2]) .

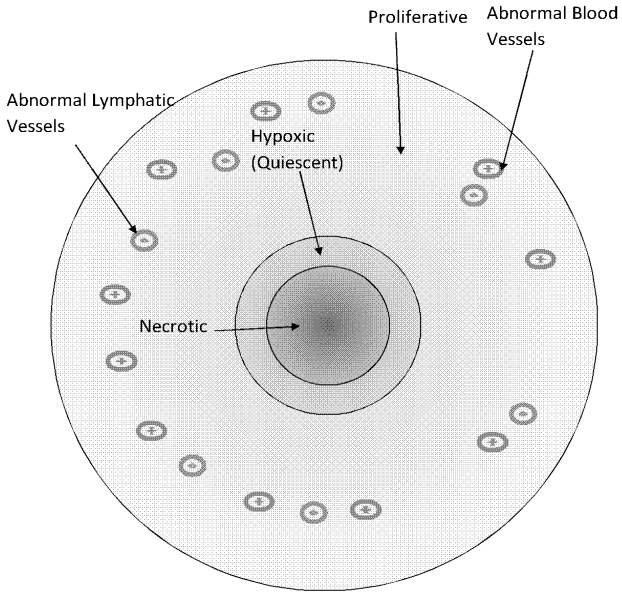

Figure 1: Structure of solid tumors

Figure 1 shows the structure of an idealized solid tumor. In the proliferative part, the abnormal cells are close to blood vessels and receive sufficient nutrition and oxygen. In the quiescent or hypoxic part, the concentration of oxygen is less than 0.33% (2.5 mmHg). (By comparison, the oxygen concentration in normal tissue ranges from 3.1-8.7% (24-66 mmHg) [7,8].) The abnormal cells in this part of the tumor stop proliferating. The necrotic core of the tumor is composed of dead cells. The oxygen level in the necrotic core is almost zero.

The lymphatic vessels in both the hypoxic and necrotic parts of the tumor are abnormal and cannot discharge waste water from inside the tumor. Therefore the interstitial pressure increases in these parts. The high interstitial pressure and low oxygen concentration make hypoxia a barrier against some traditional cancer therapy methods such as chemotherapy and radiotherapy [9].

2.3 Bacteria Mediated Cancer Therapy

Even though hypoxia is a serious barrier against chemotherapy and radiotherapy, it can be used as a marker to distinguish solid tumors from normal tissues. Since the necrotic part of a tumor is oxygen-free and rich in nutrients from dead cells, it is an ideal environment for anaerobic and facultative anaerobic bacteria to germinate. Anaerobic bacteria species such as *Salmonella*, *Bifidobacteria* and *Clostridia* have been used for tumor treatment. Most research on this area is focused on *Salmonella* and *Clostridium*, as reviewed below.

2.3.1 *Salmonella* Mediated Cancer Therapy

Salmonella is a gram negative facultative anaerobic bacterium that causes intestine infection. The early studies on *Salmonella* were focused on reducing its pathogenicity (septic shock). In 1952, Graham and Coleman showed that *Salmonella montevideo* colonizes inside carcinoma tumors [10]. In order to use *Salmonella* as an anti-tumor agent, it must be made non-pathogen or, at least, its potential for harm must be attenuated.

Early works on *Salmonella* were focused on making vaccines; as a side benefit, these works were also helpful for providing a bacterial strain that can be used as an anti-cancer agent. In 1951, Bacon et al. showed that *Salmonella* can be attenuated by auxotrophic mutations, such as those mutations that affect the biosynthesis of purines [11]. In 1981, Hoiseth and Stocker attenuated *Salmonella typhlimurium* by mutations that affect the biosynthesis of aromatic amino acids [12]. They also showed that the attenuated *Salmonella* can be used as a live vaccine.

In 1997 researchers reported that attenuation increases the colonizing capability of *Salmonella typhlimurium* in tumors and that these attenuated strains can be used as gene delivery vectors. To explain the improved colonization, Pawelek et al. hypothesized that the necrotic part of tumors provides essential nutrients for auxotrophs [13]. They conducted their studies in animal models: melanoma-bearing mice and mice implanted with human tumors such as human lung carcinoma A549, human colon carcinoma HCT 116, human breast carcinoma BT20, human renal carcinoma CRL 1611, and human hepatoma HTB 52. They showed that attenuated *Salmonella* strains germinate in tumors 250- to 9000-fold higher than normal tissue, such as liver. They also engineered *Salmonella* to express genes, such as thymidine kinase from herpes simplex virus. Tumor growth regression was observed when the engineered *Salmonella typhlimurium* was injected into the tumor- bearing mice.

In 1999, Low et al. showed *Salmonella* retains its tumor-suppression properties when two genes from its chromosome are deleted. The deletion of the *msbB* gene reduces induction of TNFα (Tumor necrosis factor α), which in turn reduces the risk of septic shock. The deletion of the *purI* gene makes the bacteria dependent on an external source of adenine [14].

In 2005, Ming Zhao et al. reported development of a genetically modified strain of *S. typhlimurium.* This strain, which is also known as *S. typhlimurium A1*, selectively grows in prostate tumors implanted in mice and causes tumor regression [15]. Normal tissue was cleared from *S. typhlimurium A1* bacteria even in immuno-deficient mice. No side effects of the treatment were observed. *S. typhlimurium A1* is auxotrophic (leucine-arginine dependent) and apparently receives sufficient nutritional support only from tumor tissue. When the bacteria were injected intravenously, they germinated inside PC-3 prostate tumors and caused tumor regression.

In 2006, the same group reported on a further modification of *S. typhlimurium A1*, designed to increase its tumor targeting ability [16]. The strain was re-isolated after infection of a human colon tumor growing in mice. They injected the modified strain into the breast tumors in mice models. This strain is known as *S. typhlimurium A1-R* and increases tumor targeting *in vivo* as well as *in vitro* compared to *S. typhlimurium A1*.

Current research on *Salmonella* has focused on delivery and expression of therapeutic agents such as cytokines, prodrug-converting enzymes, and agents toxic to tumors.

Even though attenuated *Salmonella* shows good tumor colonization and regression in animal models, the clinical results on human have been disappointing. Colonization of *Salmonella* in human patients is generally insufficient. Moreover the colonization of attenuated *Salmonella* in normal tissue, even transiently, causes side effects and reduces the specificity of this treatment as a gene transfer system [17].

2.3.2 Clostridium Mediated Cancer Therapy

Clostridia are motile gram positive obligate anaerobic bacteria. Although some strains of *Clostridia*, such as *C. botulinum* or *C. tetani*, are well known as pathogens, most *Clostridia* strains are non-pathogenic.

In 1935 Connell used *C. histolyticum* to treat advanced cancers [18]. He concluded that the production of proteolytic enzymes in *C. histolyticum* causes tumor regression. In 1947, Parker et al. infected tumor-bearing mice by *C. histolyticum* to study tumor regression [19]. (This was the first study of tumor regression by bacteria). They observed considerable regression in a sarcoma tumor, indicating that *Clostridium* spores are good candidates to be used as anti-tumor agents.

In 1955, Malmgren and Flanigan intravenously administered *C. tetani* spores into tumor-bearing and normal mice [20]. All tumor-bearing mice died within 48 hours because of the production of tetanus toxin in the tumor, but the non tumor-bearing mice survived without any tetanus symptoms. The microscopic examination of the tumor and normal tissue sections indicated that the spores germinated exclusively within the tumor and released tetanus toxins, demonstrating specificity of colonization.

In 1964, Möse and Möse intravenously injected *C. butyricum* M55 (later named *C. oncolyticum*, and now classified as *C. sporogenes* ATCC 13732) into mice with solid Ehrlich carcinomas [21]. The bacteria colonized the tumor; the necrotic part of the tumor was discharged as brownish liquid. In the few mice that survived this deadly stage, tumor regrowth was observed from the remaining outer rim. These results were confirmed by other studies with other nonpathogenic spores of *Clostridium* and with different types of tumor models [22, 23]. (In 1967, Möse and Möse also showed that *C. sporogenes* is nonpathogenic by injecting this strain into themselves!)

In 1967, Corey et al. reported on the treatment of five patients with neoplastic diseases by injection of 10^{10} spores of *C. sporogenes*. The patients developed only a mild fever during treatment [24]. However, to prevent patient mortality, surgery was required before completion of oncolysis: because of tumor regrowth from the viable outer rim, the clinical trial discontinued. These studies show that *C. sporogenes* can be safely used as a tumor-targeting agent.

Combined treatments were explored in an attempt to destroy the tumor's outer rim. For example, *Clostridium* administration was accompanied by chemotherapeutic agents such as 5-Fluorodeoxyuridine and cyclophosphamide [23, 25]. Other combined treatments, such as *Clostridium* spores and local irradiation and high frequency hyperthermia showed significant results in mice-bearing melanomas [26]. In 1979, Möse administrated *Clostridium* spores to tumor-bearing rats while the oxygen level in the respiratory air of the animals was decreased to 11-12% [27]. These attempts were unable to resolve the issue of growth from the viable outer rim.

All these studies show that wild type *Clostridium* could colonize well inside the necrotic core of a tumor and destroy a significant portion of the tumor, but regrowth invariably occurs from the remaining outer rim.

Over the last decade, a number of studies have addressed *Clostridium* based therapeutic approaches. Dang et al. screened anaerobic bacterial species such as *bifidobacteria, lactobacilli* and pathogenic *clostridia* for their tumor targeting capability. They reported that *C. novyi* had the best colonizing behaviour [28]. They removed a lethal toxin expressed by this strain and produced a non-toxic strain named *C. novyi-NT*. Intravenous administration of these bacteria into mice bearing Ehrlich ascites tumors resulted in tumor colonization and extensive oncolysis. They also showed that *C. novyi-NT* can efficiently infiltrate and extensively spread throughout the necrotic tumor regions. Similar to *C. butyricum M55*, germination of the spores led to enlargement of the necrotic regions and subsequent delays in tumor growth. The observations were tumor-type dependent; some colonization led to severe toxicity as a consequence of so-called 'tumor lysis' syndrome.

The authors of [29] used a *Clostridium* host as a tumor-specific gene delivery system. Because the required gene delivery systems were only applicable for saccharolytic strains, the initial experiments were undertaken with *C. acetobutylicum* and *C. beijerinckii*. Unfortunately, these strains have been shown to exhibit suboptimal tumor colonization properties. Indeed, upon systemic administration of spores, colonization levels of the saccharolytic *C. acetobutylicum* and *C. beijerinckii* are 1000-fold lower compared to proteolytic *C. sporogenes* strains [30]. Despite their weak tumor colonization properties, the use of saccharolytic strains (as opposed to a proteolytic host) may be beneficial when the introduction of the desired therapeutic gene is required. The use of a proteolytic host may cause increased degradation of extracellular therapeutic protein [31].

There have been efforts on genetic manipulation of strains with good colonization properties, such as *C. sporogenes*. In 2002, Liu et al. described an electroporation protocol for transformation of *C. sporogenes* [32]. They injected engineered *C. sporogenes* accompanied by 5-fluorocytosine (5-FC) prodrug administration into tumor bearing mice. The *C. sporogenes* strain was genetically engineered to express *E. coli* cytosine deaminase, which converts prodrug 5-FC to fluorouracil, an anticancer drug (Figure 2). Unfortunately, their experiments were not repeatable. In 2006, Theys et al. developed a conjugation-based gene transfer protocol that allows the construction of recombinant *C. sporogenes* strains [4]. They genetically engineered *C. sporogenes* to produce Nitrogen reductase (NTR), which converts prodrug CB1954 (5-aziridinyl-2, 4-dinitrobenzamide) to its 10000-fold more toxic 4-

hydroxylamine (4HX) derivative, which can act as an apoptosis agent (Figure 2). As a result of these efforts, it is now possible to design gene therapies using the strain with the highest tumor colonization (i.e. *C. sporogenes*). Not surprisingly, preclinical experiments with recombinant *C. sporogenes* have shown increased anti-tumor efficacy in comparison with *C. acetobutylicum* or *C. beijerinckii* [33].

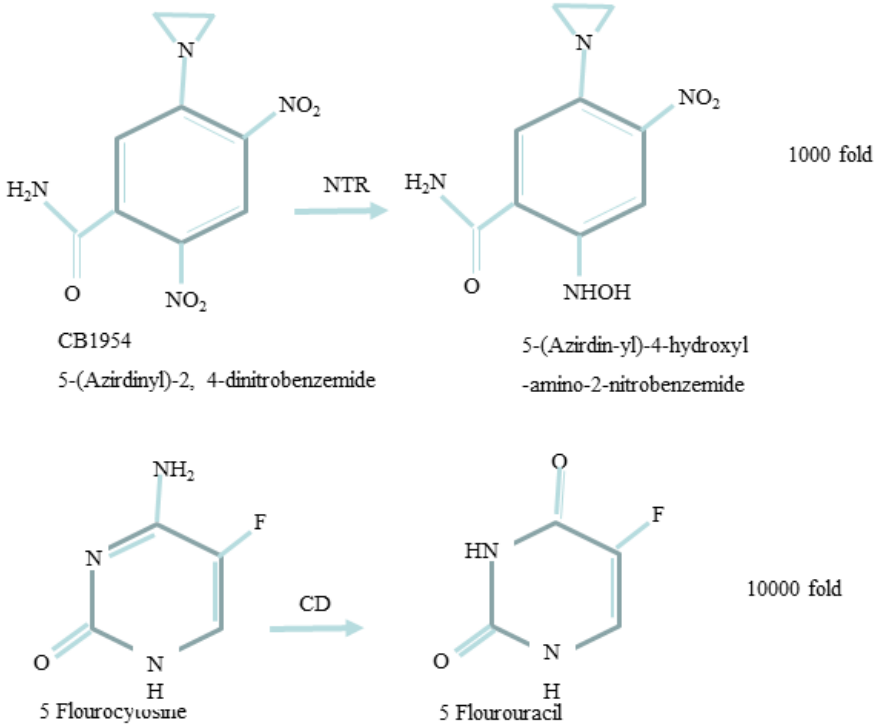

Figure 2: CD and NTR convert prodrug to drugs which are highly toxic [33]

Besides Clostridium, other anaerobic bacteria species such as *Bifidobacterium* can be used to deliver genes to tumors [34]. However, the rather low colonization efficiency and the tendency to clump, rather than distribute within necrotic areas, appeared to make *Bifidobacteria* inferior to the optimal strain of *Clostridia*. However *Bifidobacteria* exhibit inefficient colonization of tumors, in comparison with *Clostidia*. Moreover, *Bifidobacteria* colonies forms clumps, preventing fast and even distribution in tumors.

2.4 The Effect of Oxygen on the Growth of *Clostridium*

This section describes the reasons for growth inhibition of *Clostridium* in the oxygenated parts of a tumor. The study of oxygen metabolism in anaerobic bacteria suggests ways in which these bacteria

may be made oxygen-tolerant, which could allow them to colonize to the outer rim of a tumor, leading to complete oncolysis.

2.4.1 Facultative and obligate anaerobic Clostridia species

Clostridia, *Sporolactobacillus* and *Amphibacillus* are all spore forming gram positive bacteria. They all lack Krebs cycle enzymes and the enzyme catalase, which catalyzes the degradation of hydrogen peroxide. Sporolactobacillus and Amphibacillus are facultative anaeorobes; they can grow well in the presence of oxygen. In contrast, *Clostridia* are known obligate anaerobes; they cannot grow in the presence of oxygen. A number of reasons for this growth inhibition have been proposed. One of the major hypotheses is that *Clostridium* does not have a mechanism to eliminate oxygen derivatives, such as hydrogen peroxide (H_2O_2), superoxide and hydroxyl radicals [35]. Strong evidence for this hypothesis is that almost all *Clostridium* species lack catalase, which catalyzes the degradation of hydrogen peroxide [36]. An alternative hypothesis relates to the reduction in energy production when anaerobic bacteria are exposed to oxygen [37], as follows. Normally, NAD(P)H oxidases are fully engaged in the energy production system of anaerobic bacteria. When these cells are exposed to oxygen, NAD(P)H oxidases are used to eliminate oxygen. Therefore, energy production in the cell is reduced. The reason that the growth rate of *Amphibacillus* is unaffected by presence of oxygen is related to their ability to eliminate oxygen derivatives by NADH oxidase [38], [39]. For example, in *Amphibacillus xylanus*, NADH oxydase can act as a peroxidase, with the final product of oxidation being water [40-42].

Research on the effect of oxygen on *Clostridium butyricum* has revealed that this strain is able to consume oxygen. *C. butyricum* stops growing in the presence of O_2, but when the oxygen has been consumed it grows normally [35]. This finding shows that oxygen does not damage the enzymes involved in the bacteria's metabolism. It can be concluded that suspension of growth is a means of survival for this *Clostridia* species. The conclusion is that the production of water-forming NADH oxidase can make an anaerobic bacteria aerotolerant, with the degree of aerotolerancy dependent on the abundance of the NADH oxidase.

2.4.2 Oxygen Metabolism in Anaerobes

In 2005, Kawazaki et al. hypothesized that *Clostridia* have a metabolic pathway to eliminate oxygen radicals. In *Clostridium aminovalericum* a NADH oxidase gene is characterized named *noxA*. The final

product of this oxidase is H_2O. When the bacteria are exposed to oxygen, the expression of the *noxA* gene strongly increases, indicating that this gene is involved in oxygen metabolism [43].

To identify the genes responsible for eliminating oxygen radicals in *C. acetobutylicum*, Kawazaki et al. searched the genome of *C. acetobutylicum* for genes homologous to *noxA*. The identified genes are listed in Table 1.

The *nror* gene expresses a protein homologue to an NADPH oxidase [44]. NROR does not function as an NADH oxidase. Western blot analysis showed that the *nror*, *fprA2* and *dsr* genes were transcribed by a single promoter and expressed a protein homologue to flavoproteins, which are involved in removal of oxygen radicals. These genes were upregulated after 10 minutes of exposure to 5% O_2. The gene *dsr* is also expressed by a separate promoter, which was upregulated after 30 minutes of oxygen exposure[43].

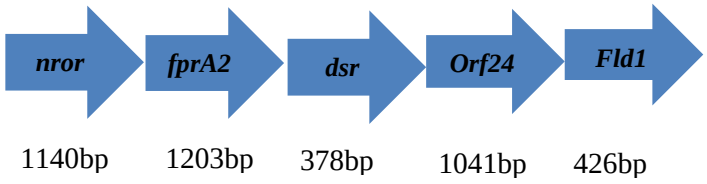

Figure 3: Gene cluster downstream of *nror* gene [43]

Table 1: Genes involved in oxygen metabolism of C. acetobutylicum[43]

Gene identification	**Gene name**	**Primer sequence (5'–3')**
CAC2448	*nror*	F,AGATGATTTATATGAAAAGCAC R,AATGTATTTATCTTCTTGTGCAC2449
CAC2449	fprA2	F, AGTTCTAAATCCTAGTCTCC R, CTCAGATGGAACAAATAAAC
CAC2450,	*dsr*	F, ATGAATAACGATTTATCAATTTAC R, TTATATATCTGCTTTCCATAGG
CAC2451,	*orf2451*	F, GAGCTTAATATAATAGTTCC R, ACATTTATTTAATAGCAGCC
CAC2452,	*fld1*	F, GTCGAGGAGGAATTATTATG R, TCTTCCTTACTAGGTGCCTC

The gene *fprA2* expresses a protein homologue to an oxygen-induced flavoprotein that was already identified by Kawasaki et al [45]. *C. acetobutylicum's* Dsr protein functions as a superoxide reductase (SOR) and produces H_2O as final product. Kawazaki et al. concluded that the proteins encoded by the *nror* operon may form an enzyme complex (Nror-FprA2-Dsr) that functions as a radical oxygen species (ROS) scavenger in oxygen metabolism of *C. acetobutylicum*.

Two other genes located downstream of *dsr* are orf2451 and *fld1* (Figure 3). The gene *fld1* codes for a flavodoxin homologue; orf2451 codes for a methyltransferase-similar protein that is involved in stress response to heavy metals, drugs and oxygen. The expression of these two genes is also highly upregulated 10 minutes after exposure to 5% oxygen.

Kawazaki et al. also found genes transcribing rubrerytherins (ruby, rub), which are O_2 induced proteins. These genes are upregulated when the bacteria are exposed to low levels of oxygen. These proteins function as superoxide dismutases. The authors identified many genes in *C. acetobutylicum* that are upregulated after aeration and that encode peroxidase like proteins. They also showed that the activity of NAD(P)H-dependent (hydrogen) peroxide reductase increases after exposing *C. acetobutylicum* to 5% oxygen [43].

These results verify the existence of oxygen metabolism and show the importance of active oxygen and lipid peroxide scavenging enzymes for the growth of *C. acetobutylicum* in the presence of oxygen.

In 2006, Kawazaki et al. investigated the effects of oxygen levels on the growth of *Bifidobacterium,* which is a gram positive anaerobic bacterium. Oxygen sensitive *Bifidobacterium* accumulates hydrogen peroxide (H_2O_2) in the presence of O_2, inhibiting growth. In the presence of oxygen, the O_2 sensitive *Bifidobacterium* cells recovered their growth rate when the experimenters added catalase to the medium; no accumulation of peroxide was observed in species that tolerate oxygen up to 20%. No significant changes in fermentation were observed, showing that oxygen did not damage the metabolism of the bacteria [46].

The existence of oxygen metabolism in anaerobes strengthened our hypothesis that *Clostridium* can be made aerotolerant by the introduction of a synthetic oxygen metabolism pathway. This synthetic metabolism should be able to scavenge radical oxygen species and produce water as the final product.

2.4.3 *noxA* Gene from *C. aminovalericum* is a Good Candidate to be Engineered in *Clostridium*

In [47] a range of oxidase and related enzymatic activities were observed in *Clostridium* strains. NADH/NADPH oxidase, NADH/NADPH peroxide and super oxide dismutase (SOD) activities were observed in the cytoplasmic fraction of nine strains of *Clostridia* (Table 2). No catalase, fatty acid peroxidase, cytochrome peroxidase, idide peroxidase, ascorbate peroxidase, glutathione peroxides or chloroperoxidase activities were detected in *Clostridium* strains [42]. The production of NADH oxidase in *C. sporogenes*, which is the most anaerobic strain, is much lower than that of *C. aminuvalericum,* which is the most aerotolerant species. (*Clostridium aminovalericum* can grow in low levels of oxygen ($3\%O_2/97\%N_2$).

Table 2: Oxidase and active oxygen-scavenging enzyme activities [47]

	Oxidase activities(O2 nmol/min/mg protein)					*Enzyme activity mU/mg protein*		
	NADH Oxidase		***NADPH oxidase***	***Pyrovate Oxidase***	***Glucose Oxidase***	***NADH Peroxidase***	***NADPH peoxidase***	***SOD (U/mg)***
	H_2O producer	*H_2O_2 Producer*						
C. butyricum	43.4	123	6.0	0	0	5.0	5.8	1.37
C. scatologenes	24.0	40.0	44.6	0	0	35.3	71.1	1.75
C. sporogenes	7.8	16.6	3.5	0	0	11.8	10.2	0.75
C. oceanicurn	40.0	61.4	10.9	0	0	10.0	4.3	0.61
C. ***bifermentans***	7.8	28.0	1.1	5.1	0	6.1	2.5	1.26
C. ***mangenotii***	15.0	106.6	2.7	15.3	0	12.0	8.6	2.60
C. ***barkeri***	40.0	71.0	123.0	0	0	40.0	36.3	0.69
C. innocuum	17.1	252.7	1.1	0	0	27.7	7.8	1.05
C. ***aminovalericum***	78.0	82.9	12.8	0	0	27.0	17.7	ND

Because *C. sporogenes* does not have a system to scavenge hydrogen peroxide, the engineered NADH oxydase should be a water forming type. The production of hydrogen peroxide as the final

product may inhibit the bacteria growth, therefore *noxA* gene from *C. aminovalericum* seems to be the best candidate.

2.5 Quorum Sensing Mechanisms in Bacteria

Constitutive expression of *noxA* gene could make *C. sporogenes* sufficiently aerotolerant that it would lose its tumor-targeting property and colonize healthy oxygenated tissue. Therefore the production of *noxA* gene in a therapeutic strain should be tightly controlled. We propose control by a genetic circuit. The genetic circuit should not express *noxA* before the complete colonization of *C. sporogenes* in the necrotic core of the tumor. When the bacterial concentration in the tumor becomes large enough, the genetic circuit will trigger the expression of the *noxA* gene, thus making the *C. sporogenes* cells aerotolerant. These aerotolerant cells can then invade the outer rim of the tumor. To ensure that the aerotolerant phenotype is exhibited only in the tumor, the genetic circuit should generate a strict switch-like (on/off) behavior. Bacterial quorum sensing mechanisms are good candidates for this design. Quorum sensing involves control of gene expression by local cell population density, as we review next.

Just as the cells of higher organism communicate with one another using hormones, bacteria communicate using small hormone-like molecules called autoinducers. This communication allows bacteria to sense their local population density. Bacteria can respond to their population concentration and synchronize their activities by controlling gene expression when a ‘quorum’ has been reached.

Quorum sensing mechanisms play important roles in a range of bacterial functions. For example, some bacteria, such as *Pseudomonas aeruginosa,* use this mechanism to produce biofilm [48], some, such as *Serrati liquefaciens* [49] and *Erwinia chrysanthemi* [50], use quorum sensing to regulate virulence factors and some, such as *vibrio harveyi* and *vibrio fischeri,* use it to control the production of luminescence [51]. Almost all bacteria use quorum sensing mechanisms to regulate gene expression [52]. There are some similarities and differences between the quorum sensing mechanisms evolved in different bacteria. All quorum sensing mechanisms are based on a positive feedback which results in a switch-like behavior. The cell density in all bacteria is measured by an autoinducer whose concentration represents the cell population. The autoinducer fires a cascade of events that results in gene expression.

This circuit switches on when the autoinducer concentration reaches a threshold. In gram negative bacteria, the autoinducer freely diffuses through the cell membrane, while in gram positive bacteria, a receptor actively exports autoinducer to the extracellular space. In gram positive bacteria, the autoinducer fires the genetic circuit by auto-phosphorylation of a histidine kinase membrane binding receptor. But in gram negative bacteria the complex of autoinducer with a cytoplasmic receptor activates gene transcription.

2.5.1 Quorum Sensing Mechanism in Gram Negative Bacteria

Quorum sensing was first observed in *Vibrio fischeri*, which is a gram negative rod-shaped marine bacteria [53]. It can be found in seawater at a concentration of 10 cells per ml. *Vibrio fischeri* can also grow symbiotically in specialized light organs of the Hawaiian squid *Euprymna scolopes* at a concentration around 10^{10} cells per ml. When the population of bacteria reaches this threshold, a genetic circuit is fired inside the bacteria that results in the production of bioluminescence. The squid uses this light to mask its shadow and hide from its predators, and the bacteria use the squid as a source of nutrition [51].

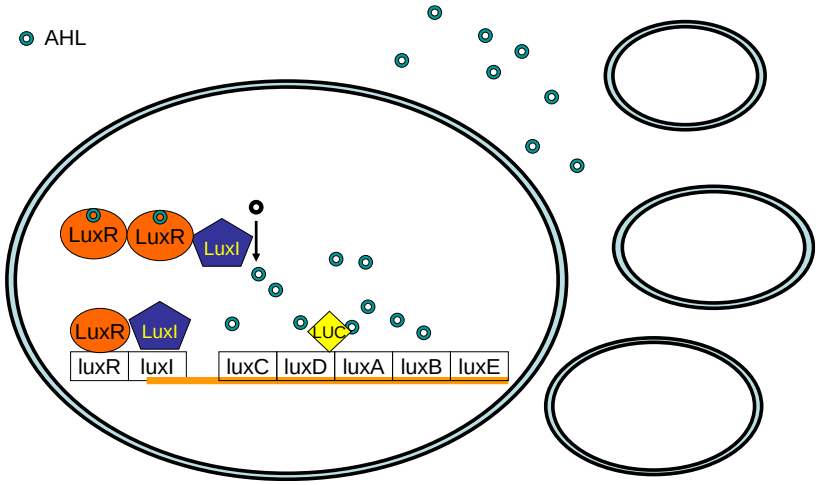

Figure 4: Lux Quorum sensing mechanism in *Vibrio fischeri*

Figure 4 shows the lux quorum sensing circuit of *Vibrio fischeri*. Proteins LuxR and LuxI control production of the luciferase genes (*luxICDABE*) that produce light. LuxI is an autoinducer synthase that

catalyzes the production of acyl-homoseine lactone (AHL), 3OC6-homoserine lactone, from S-adenosylmethionine (SAM) and acyl-acyl carrier protein (acyl-ACP) , which are generated via fatty acid biosynthesis pathways [54]. AHL converts SAM and Acyl-ACP into three components: 3OC6-homoserine lactone, 5′-methylthioadenosine and apo-ACP [55]. Figure 5 shows schematically the synthesis of AHL by LuxI.

:

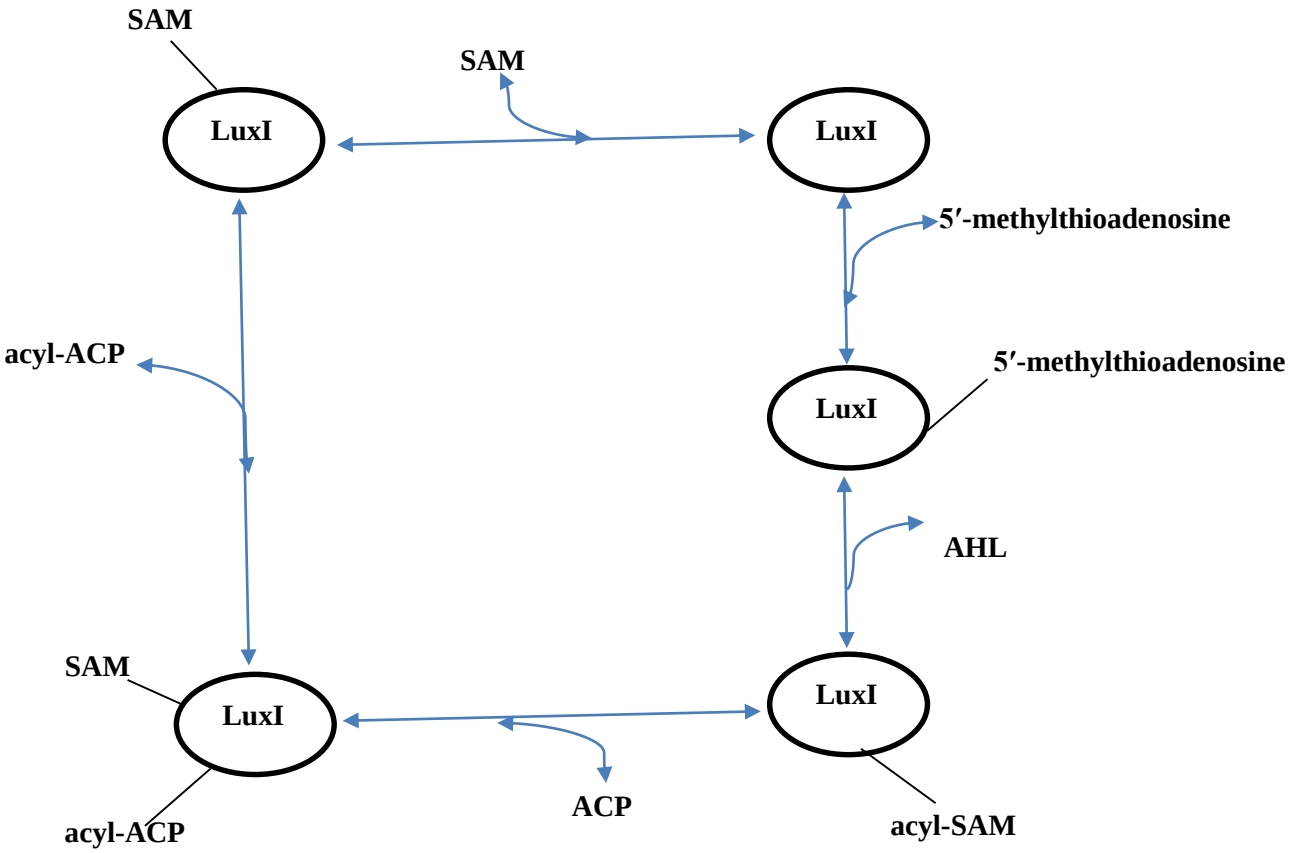

Figure 5: synthesis of Acyl-HSL by LuxI

AHL can diffuse freely across the cell membrane. Therefore the extracellular concentration of AHL increases as the local population increases. When the AHL concentration reaches a threshold, LuxR binds to AHL and the LuxR-AHL dimer acts as a transcriptional activator for the *lux* promoter. The *lux* promoter (*plux*) expresses the luciferase genes (*luxICDABE*) along with *luxR* and *luxI*. The expression of the *luxI* gene by plux results in a positive feedback. This positive feedback is the core of the quorum

sensing mechanism. Since the AHL concentration is a representative of the cell population, the bacteria can sense its population and adjust gene expression accordingly. All gram negative bacteria have similar quorum sensing mechanism elements analogous to LuxI , LuxR and AHL. The AHLs differ in among the gram negative bacteria, with varying acyl chain length.

2.5.2 Quorum Sensing Mechanism in Gram Positive Bacteria

Gram positive bacteria use oligopeptides of 10 to 20 amino acids as autoinducer signals to communicate with each other. Receptor proteins activate transcriptional activators by phosphorylation (and thus play a role analogous to LuxI and LuxR in *V. fischeri*). The transport of autoinducer across the cell membrane is an active process [56] (which is a key difference with the gram-negative mechanism).

An example of quorum sensing in gram positive bacteria is provided by *Staphylococcus aureus*. *S. aureus* infections are benign at low cell density, but become a deadly at high density. At low density the bacteria expresses proteins that enhance its attachment to the human body. At high density it represses this circuit and start expression of toxins and protease. Figure 6 shows the quorum sensing mechanism of *Staphylococcus aureus*.

Protein AgrD produces a peptide autoinducer (AIP). AgrB is a receptor that exports AIP to the extracellular space and adds a thiolactone ring to it. The modified AIP binds to another receptor called AgrC. AIP mediates the auto-phosphorylation of AgrC. Active AgrC mediates the phosphorylation of ArgA. Phospho-ArgA acts as a transcriptional activator for agrB, agrD, agrC, AgrA and RNAIII genes by activating expression from the *P2* and *P3* promoters. RNAIII represses the expression of adhesion factors and induces the expression of toxins and secreted factors. The activation of the *agr* promoter by phospho-ArgA results in a positive feedback which switches on the gene expression when the cell population reaches a threshold [57]. Recently the crystal structure of AgrA has been shown to have a binding site for small molecules that inhibit AgrA from binding to DNA [58]

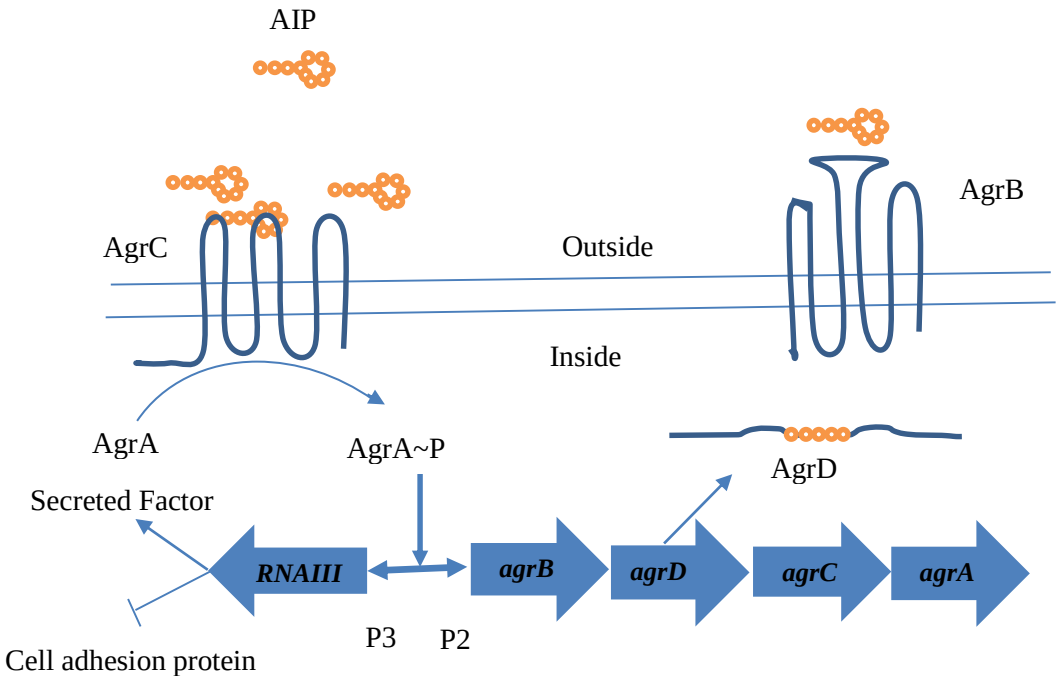

Figure 6: Quorum sensing in *Staphylococcus aureus* [53]

2.6 Mathematical Modeling of Quorum Sensing mechanisms in gram negative and gram positive bacteria

Quorum sensing systems involve networks of components interacting through a range of feedback connections. Consequently, mathematical models may be called for to interpret their behaviour. A complete model analysis will be presented in chapter 3. Here, we review the relevant system analysis in the literature.

Goryachev and Lee [59] performed a computational system analysis on the quorum sensing mechanism of *Vibrio fischeri*, based on a differential equations model. They considered three different layouts for analysis: a minimal QS network, a basal QS network and a basal QS network with dimerization. In the minimal QS network they ignored the auto regulation of the LuxR protein by assuming constitutive expression of the *luxR* gene. In the basal QS system they considered both the *luxR* and *luxI* positive feedback loops but ignored dimerization of the LuxR protein. In the third model they considered the effect of dimerization on the system behaviour. The standard chemical kinetic

approach was used to model the biochemical interactions. Their analysis of these three system reveals that dimerization is important; it improves the stability of the off state and reduces the noise. They concluded that both the luxR positive feedback loop and the dimerization are important for the switch-like behaviour of the system.

Williams et al. [60] used a combination of experiments and modeling to validate the existence of LuxR autoregulation and highlight the effect of this positive feedback loop on the switch-like behaviour of the *V. fischeri* quorum sensing mechanism. They replaced the *lux* genes downstream of the *lux* promoter (i.e. *luxIABCD*) with a green fluorescent gene (*gfp*) and constructed a circuit termed *lux01*. This Lux01 circuit was cloned into *E. coli*. They measured the *gfp* intensity in different autoinducer concentrations and drew null clines. Measurements of the *gfp* signal under dilutions of autoinducer revealed that the system exhibits hysteresis. They also measured the LuxR concentration while varying the autoinducer concentration and showed that at a threshold concentration of autoinducer, the LuxR abundance increases rapidly. This confirms the switch-like response of LuxR, due to the positive feedback in the autoregulatory loop. They developed a mathematical model to further investigate this feedback loop. Their model shows bistability if and only if they include LuxR autoregulation.

Kutter and Hence [61] considered a more comprehensive model of the *V. fischeri* quorum sensing system, which includes the interplay of the *lux* and *ain* systems, a second quorum sensing mechanism involving in bioluminescent regulation in *V. fischeri*. The *ain* system is regulated by an autoinducer known as C8HSL and a transcription activator called LitR, They assumed that LitR is the only transcription activator of the *luxR* gene. They ignored the LuxR auto regulation. They showed that their model validates the experimental results of mutants of two different *Vibrio fischeri* strains (ES114 and MJ1). They also showed that their model exhibits bistability.

Some system analysis of quorum sensing mechanisms of gram positive has also been carried out. Gustafsson et al. [62] developed a mathematical model for the quorum sensing system in *Staphylococcos aureus*, as shown in figure 6 in Section 2.5.2. Mass action principals and fundamental kinetic principals were used to model the interaction between AIP and AgrC, the phosphorylation of AgrA, and expression of the *agrA*, *agrC* and RNAIII genes. By plotting the RNAIII concentration against the AIP concentration, they showed that the system exhibits switch-like behaviour and hysteresis. The protein SarA is known to increase the basal expression of AgrA. The experimental results show that SarA mutants have the same final level of RNAIII, but are induced at a higher concentration of AIP, meaning that decreasing the basal level of AgrA should increase the threshold

concentration but have no effect on the final concentration of RNAIII. Simulation of the mathematical model validate this experimental observation. Gustafsson et al. also studied the effect of inhibitory AIP (from other strains), which decreases the threshold concentration. They concluded that a slight increase in the affinity of AgrC for AIP will reduce considerably the threshold inhibitor concentration required to turn the system off [62].

Karlsson et al. [63] studied the quorum sensing system that regulates competence in *Staphylococcos pneumonia*. Experimental results show that competence is down-regulated a short time after induction. They hypothesised that the down-regulation of competence is due to expression of an inhibitor of the quorum sensing promoter. To study their hypothesis, they developed a mathematical model for the competence quorum sensing system. They plotted the steady state concentration of the transcriptional activator as a function of extracellular concentration of competence stimulation peptide. Their plot shows hysteresis and verifies that the system exhibits bistability. They conducted a sensitivity analysis to identify which parameters are significant in the competence shut down response. This analysis showed that the synthesis of all genes products are important, confirming that a repressor is down regulating all genes at the transcriptional level [63].

Jabbari et al. [64] developed a more comprehensive model for the *Staphylococcos aureus* quorum sensing mechanism. They included the dynamics of AIP production and simulated the whole quorum sensing genetic circuit, including the intra- and extracellular production of AIP and proteins. They developed a dimensionless mathematical model using the initial concentration of a range of proteins and mRNAs. Simulation of their model shows hysteresis and bistability. They used the dimensionless model to explain how the switch-like response in virulence production occurs.

2.7 Synthetic Biology

In this project, a synthetic biology approach is proposed for engineering a quorum sensing system into *Clostridia*. Here, we briefly review some of the relevant literature on synthetic biology.

The term "synthetic biology" was used by Barbara Hobom in 1980 to explain recombinant DNA for engineered bacteria . It was used again in 2000 by Eric Kool to describe the synthesis of unnatural molecules in living systems [66]. During the last decade, researchers have used the term "synthetic biology" to describe the application of an engineering approach into biology, with the goal of designing and constructing new or modified living system with new functions.

Through Synthetic Biology, engineers are treating biology as the physics and chemistry of a new century. They are drawing analogies between proteins and genes and transistors, diodes and resistors. These elements are assembled together to produce genetic or protein devices, similar to logic gates and switches in digital computers. Furthermore these biological gates and switches are connected in such a way to manipulate the genetic and metabolic pathways that are the integrated circuits of biological systems. Finally using these pathways, biological systems can be redesigned to produce new synthetic organisms with novel functions that do not exist in nature [66].

In the engineering approach, an engineer follows standard steps: designing, modeling, implementing, testing and validating to construct a novel system, using tools such as a standardized library, computer aided design (CAD), computer aided engineering (CAE) and computer aided manufacture (CAM) software. The designer may go back and forth between different steps to optimize the design. To apply this approach to biology, researchers in synthetic biology are developing standardized libraries such as BioBrick and BglBrick [67],[68], CAD and CAE software such as Clottho Framework and Eugene language [69][70] and ultimately DNA synthesis machines which plays the role of CAM software and CNC in synthetic biology [71][72]. Although following the route of mature engineering disciplines seems promising, the complexity of biological systems and the context-based behavior of biological parts may makes the route longer than for other engineering fields.

2.7.1 Implications of Quorum sensing in synthetic biology

The elements of bacterial quorum sensing mechanisms have been used widely in synthetic biology. Weiss and Knight [73] used the *Vibrio fischeri* quorum sensing mechanism to develop controlled sender and receiver populations in *E. Coli*. You et al. [74] developed a programed population control circuit by putting a killer gene under the control of the *lux* promoter. They developed a biological feedback circuit to control a cell population. Basu et al. [75] produced a pulse generator using receiver and sender devices by putting the *luxI* gene under the control of the tetracycline promoter (*ptetR*) in their sender device and, in the receiver device, GFP and CI repressor gene of lambda phage under the control of *lux* promoter. They spatially controlled the production of GFP: the receiver bacteria near and far from the sender bacteria did not produce GFP, while the intermediate range cells did. This was the first step toward bacteria pattern formation. Basu et al. [76] reported programmed pattern formation using

the same sender device and similar genetic circuit. They constructed a low-detect plasmid and three high-detect plasmids harboring three different *luxR* genes with three different sensitivity to AHL concentration. They developed their band detector device by combining the low detect plasmid with each of the high detect plasmids. Putting sender strains in different parts of a petri dish, they formed a variety of patterns such as an elipse, a heart and a clover.

The elements of quorum sensing mechanisms were used to develop synthetic inter- and intra-species ecosystems. Ballagade et al. [77] developed a synthetic predator-prey *E.coli* ecosystem using elements of *Vibrio fischeri* and *Pseudomonas aeruginosa* quorum sensing mechanisms. In their system, a killer gene is expressed by a constitutive promoter in the predator strain, while a density-dependent promoter (*plux*) is incorporated into the prey. An antidote gene is expressed by a *lux* promoter in the predator, which inhibits the expression of killer gene in high density. The killer gene is expressed by a density dependent promoter (*plux*) in the prey, thus killing prey at high density. At low prey density the predator will be killed due to the constitutive expression of killer protein in Predator. Prey will grow until they reach a threshold level of AHL production, thus activating the *lux* promoter in the predator and the prey resulting in production of antidote protein in the predator and killing protein in prey. The production of antidote rescues the predator while the production of killing protein kills the prey. This will result a predator-prey ecosystem.

2.7.2 Application of synthetic biology in bacteria mediated cancer therapy

A number of projects have addressed the engineering of *Salmonella* and *E. coli* to be used as anti-tumor devices. Anderson et al. engineered *E. coli* to express the invasin gene (*inv*) from *Yersinia pseudotuburculosis* to invade cancer cells. They developed cell concentration-dependent, hypoxic and arabinose dependent strains by cloning the *inv* gene downstream of *lux* promoters, hypoxia-responsive *fdhF* promoter and the arabinose-inducible *araBAD* promoter respectively.

Royo et al [79] engineered some elements of the naphthalene degradative pathway, which is regulated by acetyl salicylic acid (ASA), from *Pseudomonas putida* into *Salmonella enterica*. ASA is an anti-inflammatory drug. In this pathway the NahR protein is a transcription factor for the *Psal* promoter which in turn activates expression of XylS2. Both NahR and XylS2 are activated by ASA. The activated XylS2 in turn activates the *Pm* promoter, which expresses the target gene cytosine deaminase. Cytosine deaminse converts prodrug 5-FC to fluorouracil, an anticancer drug

Xiang et al. [80] engineered *E. coli* to express the short hairpin RNA (shRNA) invasin gene (*inv*) and two other genes that are necessary for transforming shRNA into mammalian cells. shRNA cleaves the mRNA of a cancer gene termed *CTNNB1*. In most colon cancers, CTNNB1 is overexpressed or mutated. Oral or intravenous administration of *E. coli* into tumor-bearing mice resulted in *shRNA* production in the tumor, which silenced the *CTNNB1* gene at both the mRNA and translation level.

Prindle et al. [81] translated some synthetic genetic circuits already constructed and tested in *E. coli*, such as fast, robust and tunable genetic oscillator, genetic clocks and toggle switch, into *Salmonella thyphimurium*. All of these devices can be used to regulate the dose and duration of drug production in a tumor.

Chapter 3

Mathematical Modeling and analysis of the Quorum Sensing Mechanism

3.1 Introduction

Mathematical modeling is a powerful tool for exploring the dynamic behaviour of a system. From an engineering perspective, it can also be used to guide the modification of a system to produce desired behaviour. This model-based design approach is common in traditional engineering fields, and is also applicable to engineering of biological systems [65]. The chapter contains an analysis of mathematical models of quorum sensing mechanisms in gram negative and gram positive bacteria. Analysis of these models demonstrates the effect of variation in network modules and parameters on the system behaviour, and so highlights key design parameters for engineering of these systems.

As discussed in chapters 5 and 6, we explored the possibility of using either gram-negative or a gram-positive quorum sensing mechanism for controlling gene expression in *C. Sporogenes.* Although the implementation of a gram negative system into *C. Sporogenes* was not successful (Chapter 6), the analysis of this system may still prove useful in alternative implementations, or in improving our understanding of quorum sensing mechanisms in general.

This project investigates the use of quorum sensing to control the aerotolerance of bacteria that have been targeted to solid tumors. Two key performance measures of such a system are (i) the threshold bacterial concentration at which expression of the aerotolerance enzyme is triggered and (ii) the resulting steady-state enzyme concentration. To achieve optimum regression, these values will need to be adjusted depending on tumor size. Analysis of a mathematical model can reveal which design parameters have the most significant impact on these performance measures, and how these parameters should be chosen to arrive at optimum performance.

From a control engineering perspective, we are developing a feedback control system to regulate the production of aerotolerance enzyme in response to the local density of the bacterial population. In the quorum sensing system, the autoinducer acts as a sensor (sensing the cell population) and sends a signal to the controller, which is the transcription and translation mechanism of the bacteria. Although we are unable to separate this control system into a “plant” and “controller” (as in traditional feedback control

design), we can nevertheless aim to tune the gains of the controller to achieve desired behaviour. The sensitivity analysis presented in this chapter indicates how, in both gram positive and gram negative quorum sensing systems, the behaviour of the controlled system can be tuned by changing the gains of the controller.

3.2.1 Modelling a Gram Negative Quorum Sensing Mechanism

As discussed in Section 2.5.1, the quorum sensing mechanism of *Vibrio fischeri* is a prototype of gram negative quorum sensing systems. As shown in the network in Figure 4, on page 16, in this system, the production of bioluminescence results from the quorum sensing loops, with autoinducer 3-oxo-C6. Engineered instances of this system confirm that the Lux loop is sufficient to generate switch-like quorum-sensing behaviour in non-native bacteria [59].

As reviewed in Section 2.6, a number of kinetic models of quorum sensing mechanisms have appeared in the literature. We focus on the model of Goryachev and Lee [59], which describes the lux quorum-sensing loop in *Vibrio* species.

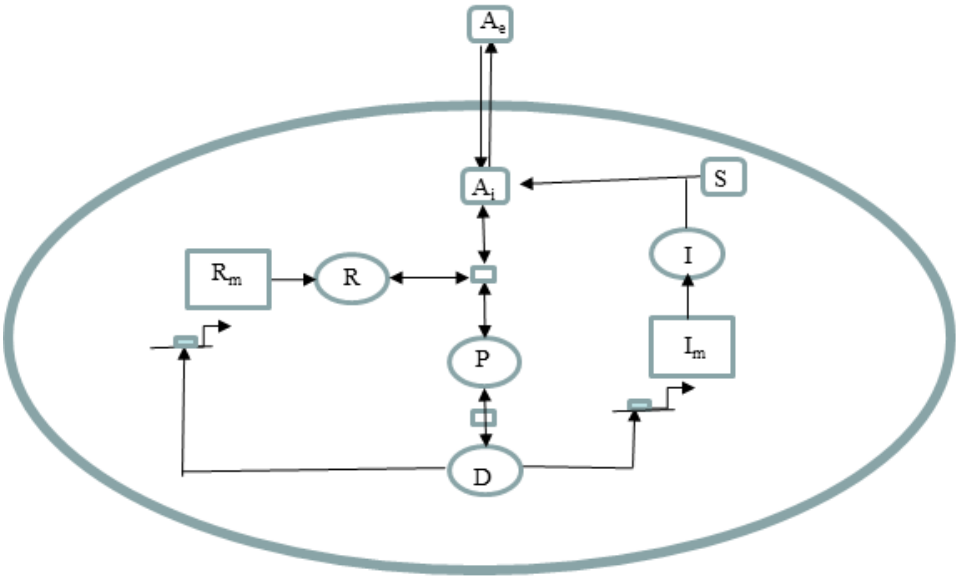

Figure 7: The quorum sensing layout of V. Fischeri used by Goryachev and Lee [59], A_e: extracellular *AHL*, A_e: intercellular *AHL*, *I:LuxI*, *R:LuxI*, *P= LuxR-AHL*, *D:LuxR-AHL* dimer, *S*: **S**-adenosylmethionine (SAM), I_m: LuxI mRNA, R_m: LuxR mRNA

As shown in Figure 7, the authors focused on the two positive feedback loops involving luxI and luxR, while neglecting the effects of the ain and the LuxQ/P loops, as well as the effect of C8 competition with AHL on binding with LuxR protein. Their analysis reveals that the LuxR positive feedback loop and LuxR dimerization are significant contributors to the bistability of the system.

We next review the kinetic formulation of the Goryachev and Lee model [59]. The formation of the LuxR-AHL complex is described by the following reaction

$$A + R \underset{k_{-1}}{\overset{k_1}{\rightleftharpoons}} P \tag{1}$$

where *A,R* and *P* are AHL, LuxR and LuxR-AHL respectively, and k_1 and k_{-1} are the rates of association and dissociation.

Dimerization of the LuxR-AHL complex (*P*) is described as:

$$2P \underset{k_{-2}}{\overset{k_2}{\rightleftharpoons}} D \tag{2}$$

where k_2 is the association rate and k_{-2} is the dissociation rate, and D is the dimer.

These reactions occur quickly on the time-scale of gene expression processes, so we can consider a rapid equilibrium assumption for *P* and *D*. Defining K_1 as the ratio of the association rate k_1 to the dissociation rate k_{-1}, the concentration of *P* is given by:

$$P = \frac{k_1}{k_{-1}} AR = K_1 AR \tag{5}$$

A rapid equilibrium assumption for the formation of *D*, and substituting for *P* from Equation (5) yields:

$$D = \frac{k_2}{k_{-2}} {K_1}^2 A^2 R^2 = K_2 {K_1}^2 A^2 R^2 \tag{6}$$

where K_2 is the ratio of association to the rate of dissociation of the dimer.

The mRNA dynamics for LuxR (R_m) and LuxI (I_m) can be described by:

$$\begin{cases} \frac{dR_m}{dt} = k_5 + \frac{K_3 D}{K_4 + D} - k_6 R_m & (9) \\ \frac{dI_m}{dt} = k_9 + \frac{K_7 D}{K_8 + D} - k_{10} I_m & (10) \end{cases}$$

where k_5 and k_9 are basal transcription rates for R_m and I_m, respectively, K_3 and K_7 are the maximal rates for activated transcription, K_4 and K_8 are dissociation constants for D-promoter binding and k_6 and k_{10} are the corresponding mRNA degradation rates. Considering that mRNA dynamics are much faster than protein dynamics, a quasi-steady-state assumption for the mRNA concentration gives the following equations for R_m an I_m

$$\begin{cases} R_m = \frac{1}{k_6}(k_5 + \frac{K_3 D}{K_4 + D}) & (11) \\ I_m = \frac{1}{k_{10}}(k_9 + \frac{K_7 D}{K_8 + D}) & (12) \end{cases}$$

The concentrations of proteins LuxR (R) and LuxI (I) are described by

$$\begin{cases} \frac{dR}{dt} = k_{11} R_m - k_{12} R & (13) \\ \frac{dI}{dt} = k_{13} I_m - k_{14} I & (14) \end{cases}$$

where k_{12} and k_{14} are the corresponding degradation rates, and k_{11} and k_{13} are per-mRNA translation rates.

Substituting equations (11) and (12) into equations (13) and (14) yields:

$$\frac{dR}{dt} = \frac{k_{11}}{k_6}(k_5 + \frac{K_3 D}{K_4 + D}) - k_{12} R \quad (15)$$

$$\frac{dI}{dt} = \frac{k_{13}}{k_{10}}(k_9 + \frac{K_7 D}{K_8 + D}) - k_{14} I \quad (16)$$

To address the dynamics of AHL (concentration A) , the following assumptions are made: (*i*) the production rate of AHL depends only on the abundance of LuxI (i.e. the substrate concentration is steady), and (*ii*) the rate of diffusion of AHL into the cell is proportional to the difference between the extracellular and intracellular concentrations of AHL. Thus

$$\frac{dA}{dt} = k_{15} I + k_{16}(A_e - A) \quad (17)$$

where k_{15} is the per-LuxI production rate, A_e is the extracellular AHL concentration, and k_{16} is the diffusion rate.

We could now apply equation (6) to write *D* in terms of *A* and *R* to arrive at a model consisting of three differential equations. However, the authors further reduce the description of the dynamics by applying a quasi-steady-state assumption to LuxI ,which is translated from a short *mRNA* compared to *LuxR*. Substituting the quasi steady state for *I* (from Equation (9)) into equation (17) yields:

$$\frac{dA}{dt} = \frac{k_{13}k_{15}}{k_{10}k_{14}}\left(k_9 + \frac{K_7 D}{K_8 + D}\right) + k_{16}(A_e - A) \tag{18}$$

Finally, substituting for *D* from Equation (6) into equations (15) and (18) gives the two-state model:

$$\frac{dR}{dt} = \frac{k_{11}}{k_6}\left(k_5 + \frac{K_3 A^2 R^2}{\frac{K_4}{K_1^{\,2} K_2} + A^2 R^2}\right) - k_{12}R \tag{19}$$

$$\frac{dA}{dt} = \frac{k_{13}k_{15}}{k_{10}k_{14}}\left(k_9 + \frac{K_7 A^2 R^2}{\frac{K_8}{K_1^{\,2} K_2} + A^2 R^2}\right) + k_{16}(A_e - A) \tag{20}$$

The parameter values from [59] are reported in Table 3.

Table 3: Parameters value in the model [59]

Parameters	Value	Parameters	Value
k_1	10^{-4} n$M^{-1}s^{-1}$	k_9	1.5×10^{-4} nMs^{-1}
k_{-1}	$3\times10^{-3}\ s^{-1}$	k_{10}	$6\times10^{-3}\ s^{-1}$
k_2	10^{-5} n$M^{-1}s^{-1}$	k_{11}	$1.28\times10^{-2}\ s^{-1}$
k_{-2}	$10^{-2}\ s^{-1}$	k_{12}	$2\times10^{-4}\ s^{-1}$
K_3	4.8×10^{-3} nMs^{-1}	k_{13}	$1.6\times10^{-2}\ s^{-1}$
K_4	1 nM	k_{14}	$5\times10^{-5}\ s^{-1}$
k_5	3×10^{-4} nMs^{-1}	k_{15}	$0.45\ s^{-1}$
k_6	$6\times10^{-3}\ s^{-1}$	k_{16}	$0.4\ s^{-1}$
K_7	2×10^{-3} nMs^{-1}		
K_8	30 nM		

The authors of [59] explored the behaviour of a range of model variants, with a focus on the switch-like behaviour of the system. Here, we take an alternative approach to model analysis; our focus is on the sensitivity of the system's performance measures to the values of the model parameters. While we do not expect the results of this analysis to be quantitatively accurate, the results will identify the key parameters to be considered in designing our system. To simplify our parametric sensitivity analysis, we lump the model parameters as follows (values in Table 4, below):

$$K_{R1} = \frac{k_{11}k_5}{k_6} \tag{21}$$

$$K_{R3} = \sqrt{\frac{K_4}{{K_1}^2 K_2}} \quad K_{R2} = \frac{K_3 k_{11}}{k_6} \ , \tag{22}$$

$$K_{A1} = \frac{k_{15}k_{13}}{k_{10}k_{14}} k_9, \tag{23}$$

$$K_{A3} = \sqrt{\frac{K_8}{{K_1}^2 K_2}} \quad \text{and} \quad K_{A2} = \frac{k_{15}k_{13}K_7}{k_{10}k_{14}}, \tag{24}$$

This gives a simplified model formulation, from Equations (19) and (20):

$$\frac{dR}{dt} = K_{R1} + \frac{K_{R2}\left(\frac{AR}{K_{R3}}\right)^2}{1+\left(\frac{AR}{K_{R3}}\right)^2} - k_{12}R \tag{25}$$

$$\frac{dA}{dt} = K_{A1} + \frac{K_{A2}\left(\frac{AR}{K_{A3}}\right)^2}{1+\left(\frac{AR}{K_{A3}}\right)^2} + k_{16}(A_e - A) \tag{26}$$

These lumped parameters can be interpreted as follows: expression of LuxR (and consequently, production of AHL) are determined by Hill functions, with Hill coefficient of 2 and Hill constants equal to K_{R3} and K_{A3}, respectively. Parameters K_{R1} and K_{A1} are the basal rates of constitutive expression from the two genes, while K_{R2} and K_{A2} are the maximal rates of activated expression.

In comparing the behaviour of the model to experimental observation, we will most likely be observing the system via a target gene (e.g. *gfp*) that is controlled by the quorum sensing system. The concentration (G) of such a protein can be modeled as:

$$\frac{dG}{dt} = K_{G1} + \frac{K_{G2}\left(\frac{AR}{K_{G3}}\right)^2}{1+\left(\frac{AR}{K_{G3}}\right)^2} - k_{G14}R \quad (27)$$

for appropriate parameters K_{G1}, K_{G2} and K_{G14}. Because this equation has the same form as Equation (25), we will simplify the analysis by assuming that the dynamics of such a target protein product would be identical to the LuxR dynamics.

Table 4: Values of lumped parameters

Parameters	Value	Parameters	Value
K_{R1}	6.4×10^{-4} nMs^{-1}	K_{A2}	24 nMs^{-1}
K_{R2}	0.0102 nMs^{-1}	K_{A3}	519.6152 nM^2
K_{R3}	948.6833 nM^2	K_{12}	2×10^{-4} s^{-1}
K_{A1}	3.6 nMs^{-1}	K_{16}	0.4 s^{-1}

3.2.2 Analysis of the Goryachev and Lee model of gram negative quorum sensing system

The analysis described in this section is novel. The mathematical model in Equations (25) and (26), with parameter values in Table 4, was implemented in Matlab [82]. MATLAB's ode45 function was used to simulate the system of ODE's . The extracellular concentration of AHL (A_e) was taken as an external input, and was considered as representative of the local bacteria population density.

Before performing a sensitivity analysis, we confirm the model's dynamic behaviour. Figure 8 and 9 show phase portraits of the model at two different extracellular concentrations of AHL. As Figure 8 shows, when A_e is equal to 50 *nM*. all trajectories converge to a unique stable state; the system is monostable. In contrast, Figure 9 illustrates that the system exhibits bistability at the lower extracellular AHL concentration of 25 *nM*. These two cases indicate the system's potential behaviours: a bistable switch at lower AHL (lower density), and a monostable system (with the switch 'flipped on') at higher

AHL (higher density). The system also exhibits monostable ('off') behaviour below a threshold AHL level, as shown below.

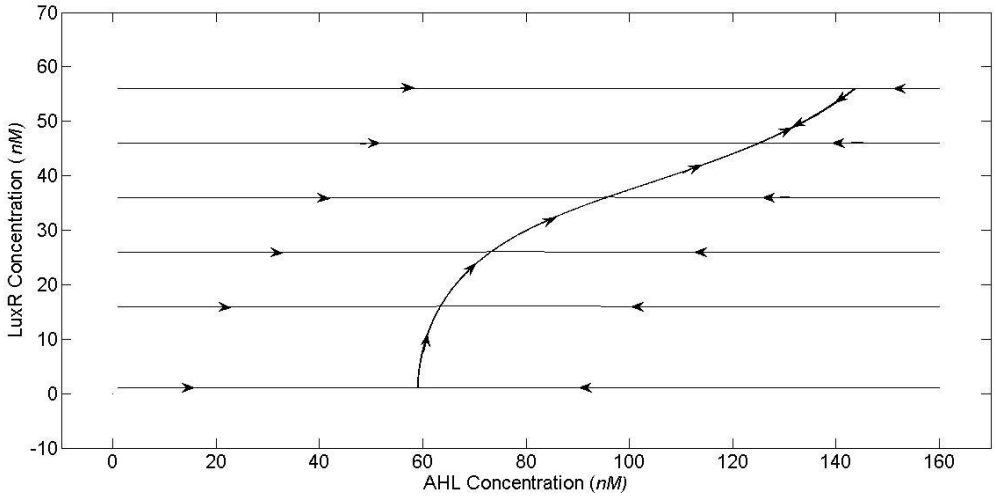

Figure 8: Phase portrait of Goryachev and Lee model at extracellular concentration of AHL equal to 50 *nM*. The system is monostable.

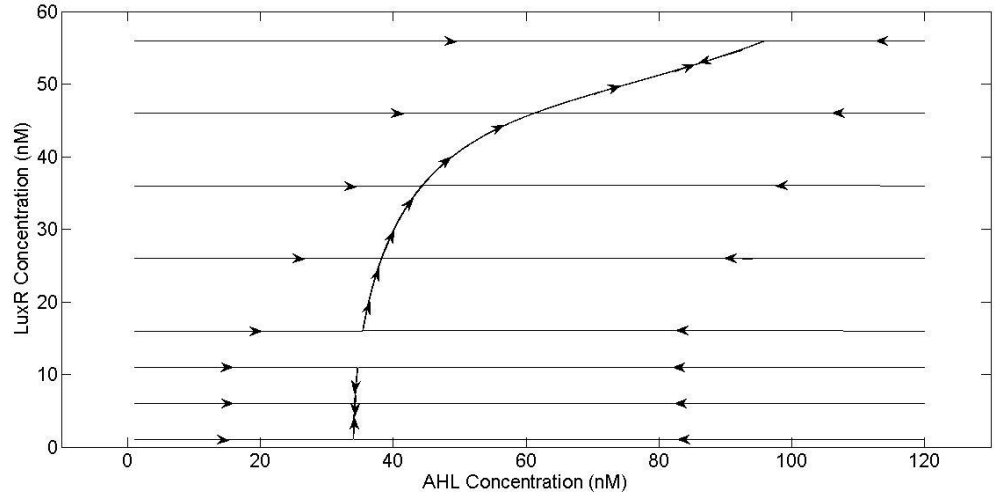

Figure 9: Phase portrait of Goryachev and Lee model at extracellular concentration equal to 25 nM. The system is bistable.

To further explore the change in system behaviour as we ran simulations over a range of AHL (A_e) values. To test for bistability, at each AHL concentration, the model was run to equilibrium from two

initial conditions: one in which intracellular LuxR and AHL levels are low, both equal to 1 *nM* (an 'off' state), and one in which these levels are high, both equal to 10 *nM* (an 'on' state). The steady-state results of these simulations are shown in Figure 10, which is a bifurcation diagram for the model. Similar to Figure 8 above, the system exhibits monostability at low bacteria concentration, when there is insufficient activity to generate a response. As the AHL concentration is increased, the system enters a range of bistablity (for $19<A_e<29\ nM$).

In summary: at low bacteria concentration ($19<A_e$) the genetic circuit is 'off' and for high bacteria concentration ($29<A_e$) system becomes 'on'. As the bacteria grow, A_e increases and when the bacteria concentration reaches a threshold ($A_e=29nM$) the system jumps to the high equilibrium point and the genetic circuit becomes 'on'.

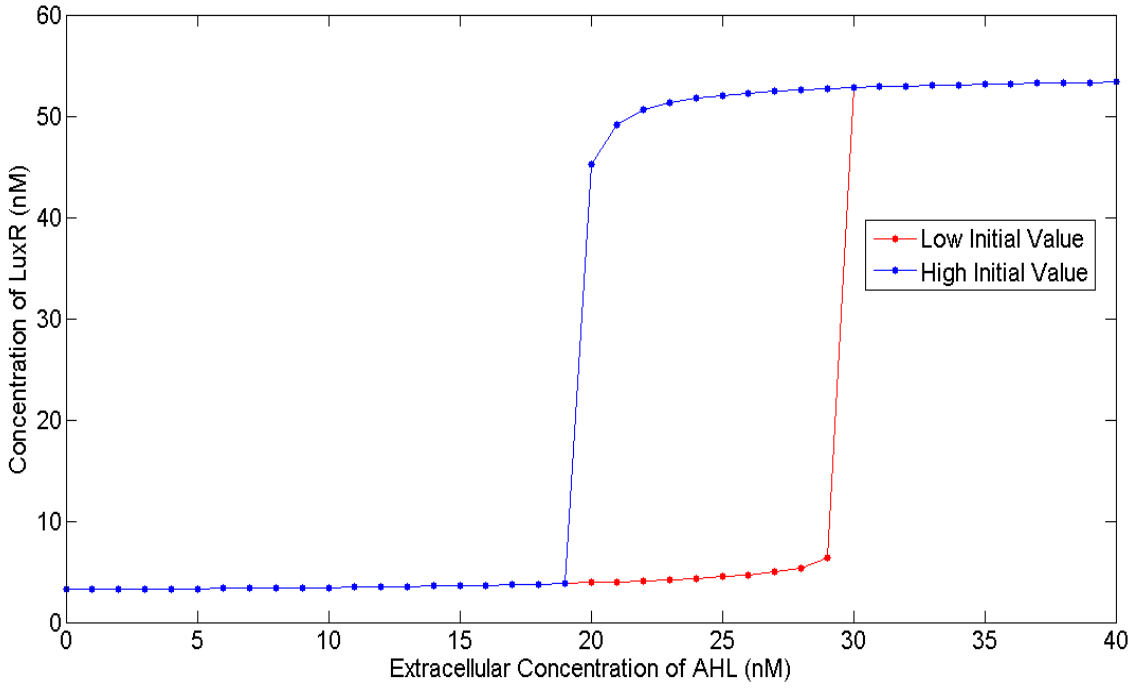

Figure 10: Bifurcation diagram of *V. fischeri* quorum sensing model.

As the figure shows, the system exhibits hysteresis – reducing the AHL level once the system is 'on' will not return the cell to the LuxR-low AHL-low state at the same threshold at which the system jumped to the 'on' state.

The bifurcation structure in Figure 10 is further explored in Figure 11, which is a phase portrait showing nullclines of R and A for various values of A_e. For external AHL concentrations in the range from $19\ nM < A_e < 29\ nM$, the nullclines intersect three times, indicating the existence of three equilibrium points, two stable and one unstable. Parameters that alter the shape of these nullclines can have significant impact on the bifurcation values.

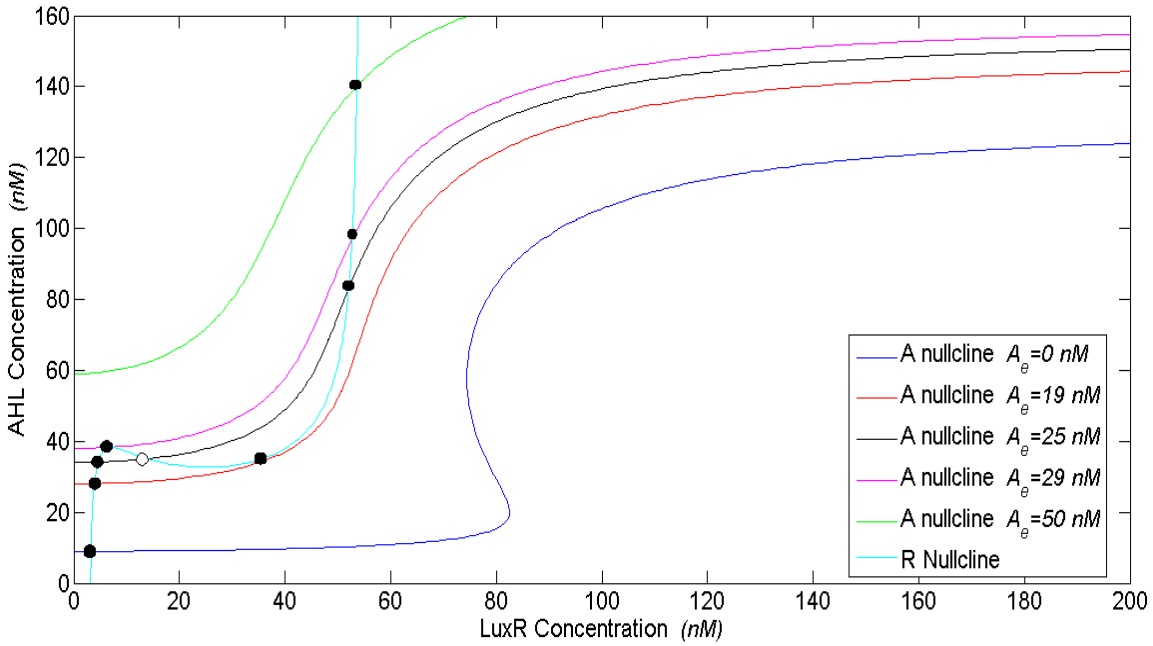

Figure 11: Nullclines of model (25-26) *at* five different external AHL concentrations ($\boldsymbol{A_e}$). The R nullcline is shown in cyan and A nullclines in blue, red, black, magenta and green. Filled and empty circles indicate stable and non-stable equilibrium points, respectively. For $\boldsymbol{A_e}$ between 19 *nM* and 29 *nM*, the system is bistable. Above this interval, only the active (high-***R***, high-***A***) state is present and below this interval only the off state is present.

As mentioned above, in planning to use a quorum sensing system to trigger aerotolerance at the site of solid tumors, we focus on two key performance measures: (i) the threshold concentration of external AHL at which the system switches to the 'on' state, and (ii) the steady-state concentration of the aerotolerance enzyme. We next explore the role of the model parameters, i.e. the design parameters, in tuning system performance.

From a design perspective, natural tuning parameters are the promoter strength and ribosome binding site (RBS) of LuxR and LuxI. These should have a significant impact on system behavior, and can take a range of values corresponding to choice of promoter and RBS. Indeed, as discussed in [83] and [84], changes in the strength of a promoter may alter protein production rate by 1000-fold, while changing the RBS site (and corresponding intergenic region) can have a 100 fold effect.

A preliminary analysis of the role of promoter strength is shown in Figure 12, in which system bifurcation curves are shown for three different values of LuxI and LuxR promoter strength. (To aid in comparing the curves, only the 'turning on' branch of the full bifurcation plot is shown. That is, these equilibria are all reached from the 'off' initial state.)

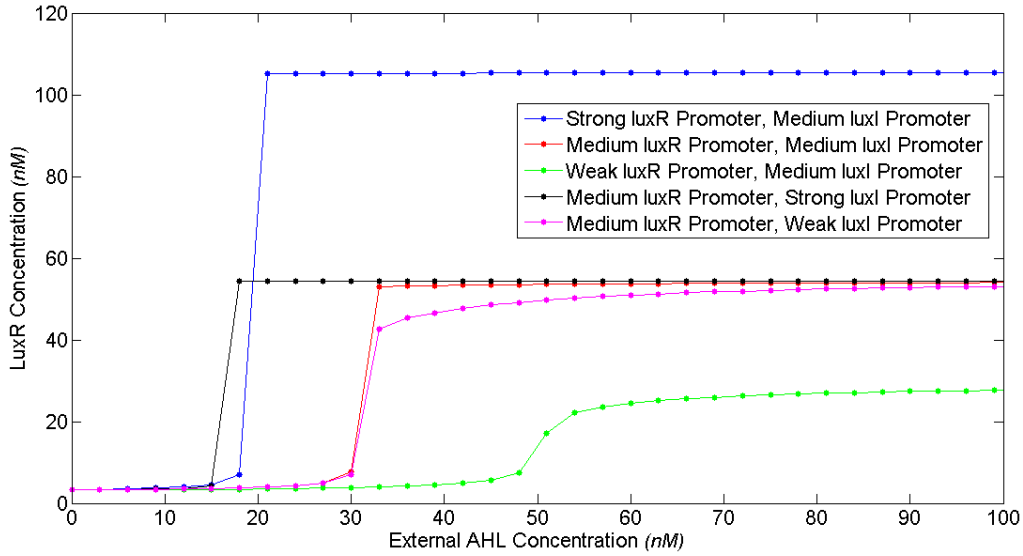

Figure 12: Bifurcation diagrams showing the effects of changes in the promoter strength of the luxR and luxI genes. Strong, medium and weak *luxR* promoters correspond to $\boldsymbol{k_3}$ values of 9.6×10^{-3}, 4.8×10^{-3} 2.4×10^{-3} nMs^{-1}, respectively. Strong, medium and weak *luxI* promoters correspond to $\boldsymbol{k_7}$ values of 9.6×10^{-3}, 4.8×10^{-3} 2.4×10^{-3} nMs^{-1}, respectively. The threshold concentration can be tuned by both promoter strengths. The final concentration of LuxR can be only tuned by strength of *luxR* promoter

The figure shows that the threshold concentration can be tuned by changing the strength of either promoter. In contrast, the final concentration of LuxR can be tuned by the choice of *luxR* promoter, but it is insensitive to the strength of the *luxI* promoter. This insensitivity can be of value in a design strategy, since it allows the concentration threshold to be tuned (via the *luxI* promoter) separately from tuning of the threshold AHL concentration. An analysis of the RBS strength (not shown) reveals a similar effect. This is not surprising, since these parameters play similar roles in describing protein production in the model.

3.2.3 Parametric Sensitivity Analysis

The above analysis sheds some light on the behavior of the system, but addresses the effects of only a few design parameters, and, significantly, may be dependent on the chosen nominal values of the model parameters. Though these nominal values were justified in [59] and [60], they cannot be trusted to be more than estimates of the true representation of the system. To provide more robust design recommendations, a globalized sensitivity analysis was carried out on the system. For each parameter $\boldsymbol{P_i}$, two local sensitivity coefficients are defined

$$S_{ss} = \frac{P_i}{C_{max}} \frac{\partial C_{max}}{\partial P_i} \quad \text{and} \quad S_{thresh} = \frac{P_i}{C_{thres}} \frac{\partial C_{thresh}}{\partial P_i} \tag{28}$$

where S_{ss} and S_{thresh} represent the sensitivity of the steady-state concentration of LuxR and the AHL threshold concentration (off-to-on), respectively. These derivatives are approximated as finite differences, by simulating the effect of a 10 percent change in parameter values as follows:

$$S_{ss} = \frac{P_i}{C_{max}(P_i)} \frac{C_{max}(P_i + 0.1 * P_i) - C_{max}(P_i)}{0.1 * P_i} \quad \text{and} \quad S_{thresh} = \frac{P_i}{C_{thres}(P_i)} \frac{C_{thres}(P_i + 0.1 * P_i) - C_{thres}(P_i)}{0.1 * P_i} \tag{29}$$

In order to carry out globalized analysis, for each parameter presented in Table 3, the bistability range was determined. These ranges are reported in Table 3. Because sampling over a fine mesh in the 8-dimensional parameter spaces would be prohibitively time-consuming, two values were chosen for each parameter: at the ends of the bistability region. Local sensitivity coefficients were calculated at the corresponding 256 (=2^8) points in parameter space. For each parameter, these were then averaged to give a single globalized sensitivity coefficient. These are reported in Table 5.

Table 5: Globalized sensitivity analysis on Gram negative QS mechanism

Parameters	Bistability Range	S_{ss}	S_{thresh}
$\boldsymbol{K_{R1}}$	$(\mathbf{1-4}) \times \mathbf{10^{-4}}$ n$\boldsymbol{Ms^{-1}}$	0.0147	-0.7387
$\boldsymbol{K_{R2}}$	$(\mathbf{1-4}) \times \mathbf{10^{-2}}$ n$\boldsymbol{Ms^{-1}}$	0.9877	-0.5675
$\boldsymbol{K_{R3}}$	$\mathbf{800-1500}$ n$\boldsymbol{M^2}$	-0.0025	1.2096
$\boldsymbol{K_{A1}}$	**0.01-4** n$\boldsymbol{Ms^{-1}}$	0.00001	-0.1749
$\boldsymbol{K_{A2}}$	**10-90** n$\boldsymbol{Ms^{-1}}$	0.0005	-0.1343
$\boldsymbol{K_{A3}}$	**100-900** n$\boldsymbol{M^2}$	0	0
$\boldsymbol{k_{12}}$	$(\mathbf{1-2.3}) \times \mathbf{10^{-4}}$ $\boldsymbol{s^{-1}}$	-0.9028	1.3529
$\boldsymbol{k_{16}}$	$(\mathbf{3-9}) \times \mathbf{10^{-1}}$ $\boldsymbol{s^{-1}}$	-0.0006	0.2061

This globalized sensitivity analysis indicates that (i) the steady-state LuxR concentration is most sensitive to the maximal induced expression rate of LuxR ($\boldsymbol{K_{R2}}$) and the degradation rate of LuxR ($\boldsymbol{k_{12}}$) while (ii) the threshold AHL concentration is most sensitive to the dissociation constant for LuxR activation ($\boldsymbol{K_{R3}}$) and degradation rate of LuxR ($\boldsymbol{k_{12}}$) , and is moderately sensitive to the basal LuxR expression rate ($\boldsymbol{K_{R1}}$). Importantly, consistent with the observation in the preliminary analysis, the analysis reveals that the dissociation constant for LuxR activation ($\boldsymbol{K_{R3}}$) could be used to tune the activation threshold without affecting the steady-state AHL level. While tuning of this parameter value introduces its own design challenges (e.g. by introducing point mutations to the LuxI gene), the independent effect revealed by this analysis could be exploited in the design phase.

The analysis in Table 5 addresses the lumped parameters from the simplified model (25-26). To identify how these effects are related to the kinetic parameters in the original model, we carried out a secondary analysis. To identify the contributions to the sensitivity of RBS strength and promoter strength, another sensitivity analysis was carried out on parameters $\boldsymbol{k_{13}}$, $\boldsymbol{k_{15}}$, $\boldsymbol{k_6}$ and $\boldsymbol{k_{10}}$ which characterize the RBS and promoter strength of the *luxR* and *luxI* genes. For each parameter, three values were chosen: the two endpoints and the midpoint of the bistability region. Local sensitivities were

calculated for each parameter at the corresponding 81 points of parameter space, and again the overall sensitivity of each parameter was calculated by averaging. The results are shown in Table 6.

Table 6: Sensitivity analysis on RBS and promoter strength parameter

Parameters		Range	S_{ss}	S_{thresh}
$\boldsymbol{k_6}$	P_{luxR}	$(\mathbf{2-5})\times\mathbf{10^{-3}}$ $\boldsymbol{s^{-1}}$	1.1627	-0.4935
$\boldsymbol{k_{10}}$	P_{luxI}	$(\mathbf{2.4-9.6})\times\mathbf{10^{-3}}$ $\boldsymbol{s^{-1}}$	0.1590	-0.0494
$\boldsymbol{k_{13}}$	RBS_{luxR}	$(\mathbf{1-2})\times\mathbf{10^{-2}}$ $\boldsymbol{s^{-1}}$	2.3556	-0.7935
$\boldsymbol{k_{15}}$	RBS_{luxI}	$(\mathbf{0.8-2.4})\times\mathbf{10^{-2}}$ $\boldsymbol{s^{-1}}$	0.2168	-0.0672

This analysis confirms the result of Figure 12. The steady-state concentration of LuxR is not sensitive to *luxI* promoter or RBS strength. Moreover, the most significant parameter for the steady-state concentration of LuxR and AHL threshold concentration is the RBS strength of *luxR*. The AHL threshold concentration is sensitive to the RBS and promoter strength of *luxR*. Neither threshold concentration nor final value concentration are sensitive to the parameters of luxI production. Changes in the *luxR* RBS and promoter strength will have opposite effects on the AHL threshold concentration and steady state concentration of *luxR*. Therefore, if we want to increase the threshold concentration, decreasing the *luxR* promoter or RBS strength may increase the threshold concentration but will decrease the final concentration of aerotolerance enzyme. Haseltine and Arnold studied analytically and experimentally the effect of changing *luxR* RBS on the threshold concentration and obtained similar results [85]. These results imply that in the plasmid construction that we have selected, in order to tune the threshold concentration we should carefully consider the choice of *luxR* RBS and promoter strength, which will result in a trade-off effect on the final concentration of the aerotolerance enzyme.

Having discussed quorum sensing in gram-negative organisms, we next turn to a complementary model-based analysis of a gram positive quorum sensing system.

3.3.1 Mathematical Model of Quorum Sensing in Gram Positive Bacteria

As reviewed in Section 2.5.2 the quorum sensing mechanism of *S. aureus* is a canonical example of the gram positive quorum sensing system. There are four different strains of *S. aureus*, each of which

produces a strain-specific autoinducer peptides (AIP). Each AIP activates its own AgrC receptor and inhibits the activity of the receptors in the other strains.

Here we investigate a mathematical model of the quorum sensing mechanism of *S. aureus* introduced in [62].

The model formulation is as follows. Binding of the native (*P*) and any non-native (*X*) autoinducer peptides to the sensor receptor AgrC (*C*) can be described by the following reactions:

$$C + P \underset{k_{c2}}{\overset{k_{c1}}{\rightleftharpoons}} C_p \xrightarrow{d_{cp}} \tag{30}$$

$$C + X \underset{k_{c4}}{\overset{k_{c3}}{\rightleftharpoons}} C_x \xrightarrow{d_{cx}} \tag{31}$$

where C_p and C_x are active and inactive AgrC receptor, respectively, k_{c1} and k_{c3} are association rates, k_{c2} and k_{c4} are dissociation rates and d_{cp} and d_{cx} are degradation rates.

The ODE's governing these reactions are as follows:

$$\frac{dC_p}{dt} = k_{c1}CP - k_{c2}C_p - d_{cp}C_p \tag{32}$$

$$\frac{dC_x}{dt} = k_{c3}CX - k_{c4}C_X - d_{cp}C_X \tag{33}$$

Considering quasi steady state assumption for C_p and C_x we have

$$C_p = \frac{k_{c1}CP}{k_{c2}+d_{cp}} = K_{cp}CP \tag{34}$$

$$C_x = \frac{k_{c3}CX}{k_{c4}+d_{cx}} = K_{cx}CX \tag{35}$$

where $K_{cp} = \frac{k_{c1}}{k_{c2}+d_{cp}}$ and $K_{cx} = \frac{k_{c3}}{k_{c4}+d_{cx}}$

The phosphorylation of *AgrA* (*A*) by *AgrC* (*C*) can be described by the following reactions:

$$\overset{d_A}{\leftarrow} A \underset{k_{dp}}{\overset{k_p}{\rightleftharpoons}} A_p \xrightarrow{d_{Ap}} \qquad C_p \downarrow \tag{36}$$

where A_p is the phosphorylated form of AgrA, k_p and k_{dp} are phosphorylation and dephosphorylation rates of AgrA, d_A and d_{Ap} are degradation of AgrA and phosphorylated AgrA, respectively.

Reaction (36) provide the following description of the phosphorylated form AgrA (A_p):

$$\frac{dA_p}{dt} = k_p C_p A - k_{dp} A_p - d_{Ap} A_p \tag{37}$$

Assuming quasi steady state for A_p gives:

$$A_p = \frac{k_p K_{cp}}{k_{dp}+d_{Ap}} CP \;\Rightarrow\; A_p = K_p CPA \tag{38}$$

where $K_p = \frac{k_p K_{cp}}{k_{dp}+d_{Ap}}$

Since the transcription factor of agr operon is a monomer, we can model the dynamics of AgrA as [62]:

$$\frac{dA}{dt} = k_A \frac{\frac{A_p}{K_{Ap}}}{1+\frac{A_p}{K_{Ap}}} + k_{Aprime} - k_p C_p A + k_{dp} A_p - d_A A \tag{39}$$

where k_{Aprime} is basal transcription rate of expression, k_A is the maximal rate of activated expression, K_{Ap} is the Michaelis constant of activator binding, and d_A is the degradation rate for AgrA.

Substituting A_p and $C_p$from Equation (38) and (34) into equation (39) yields:

$$\frac{dA}{dt} = k_A \frac{\frac{K_p}{K_{Ap}} CPA}{1+\frac{K_p}{K_{Ap}} CPA} + k_{Aprime} - \left(k_p K_{cp} CP - k_{dp} K_p CP + d_A\right) A \tag{40}$$

Because AgrC and AgrA are share a common promoter, the transcription of AgrC follows the same kinetic as AgrA. The dynamics of AgrC (C) can be similarly modeled as follows:

$$\frac{dC}{dt} = k_C \frac{\frac{K_p}{K_{Ap}} CPA}{1+\frac{K_p}{K_{Ap}} CPA} + k_{Cprime} - k_{c1} CP + k_{c2} C_p - k_{c3} CX + k_{c4} C_{cx} - d_c C \tag{41}$$

where k_{Cprime} is basal transcription rate for AgrC (C), k_C is the maximal rate of activated expression and d_C is the degradation rate for AgrC.

Substituting C_p and C_x from equations (34) and (35) into equation (41) yields:

$$\frac{dC}{dt} = k_C \frac{\frac{K_p}{K_{Ap}} CPA}{1+\frac{K_p}{K_{Ap} CP} A} + k_{Cprime} - (k_{c1} P - k_{c2} K_{cp} P + k_{c3} X - k_{c4} K_{cx} X + d_c) C \tag{42}$$

The concentration of AgrD (D) can be described as:

$$\frac{dD}{dt} = k_D \frac{\frac{K_p}{K_{Ap}} CPA}{1+\frac{K_p}{K_{Ap}} CPA} + k_{Dprime} - d_B D \quad (43)$$

where k_{Dprime} is basal transcription rate for AgrD (D), k_D is the maximal rate of activated expression and d_B is the degradation rate for AgrD.

Assuming a linear kinetic for the production of AIP (P) from ArgD we have

$$\frac{dP}{dt} = k_{Dp} D - d_P P \quad (44)$$

here k_{Dp} is the production rate and d_P the degradation rate of AIP (P). Ignoring the dynamics of AHL export by AgrB, we assume that all AIP is rapidly exported to the extracellular space.

Parameter values for the model are given in Table 7.

Table 7: Parameters value in the model [62]

Parameters	Value	Parameter	Value
k_A	$10 s^{-1}$	K_{CP}	$5\times10^{-5} s^{-1}$
k_{Aprime}	$0.1 s^{-1}$	K_{Cx}	$0.45 s^{-1}$
k_C	$10 s^{-1}$	d_A	$2 s^{-1}$
k_{Cprime}	$0.1 s^{-1}$	d_C	$2 s^{-1}$
k_D	$10 s^{-1}$	d_{Ap}	$2 s^{-1}$
k_{Dprime}	$0.1 s^{-1}$	d_{Cp}	$2 s^{-1}$
k_{c1}	$1 nM^{-1} s^{-1}$	d_{Cx}	$2 s^{-1}$
k_{c2}	$0.1 s^{-1}$	K_{AP}	$1 nM$
k_{c3}	$1 nM^{-1}s^{-1}$	K_{Cp}	$0.48 s^{-1}$
k_{c4}	$0.1 s^{-1}$	K_{Cx}	$0.48 s^{-1}$
k_p	$10 nM^{-1}s^{-1}$	K_P	$1.59 s^{-1}$
k_{dp}	$1 s^{-1}$		

3.3.2 Analysis of Quorum Sensing in Gram Positive Bacteria

The analysis described in this section is novel. The mathematical model in Equations (40), (42), (43) and (44), with parameter values in Table 7, derived from [62], was implemented in Matlab [82].

MATLAB's ode45 function was used to simulate the system of ODE's . The AIP concentration (*P*) was taken as an external input, and is considered as representative of the local bacterial population density.

The model behaviour is similar to the bistable behaviour exhibited by the model of gram negative quorum sensing that was presented in section 3.1. Although this model is not 2-dimensional, phase portraits can still be generated by projecting the trajectories onto a 2-dimensional plane showing the AgrA-AgrC dynamics. Figure 13 and 14 show representative phase portraits for the monostable and bistable regions, respectively. In figure 13 the AIP concentration is taken equal to 1.5 nM, which is located in monostable ('on') region. As the figure shows, all trajectories converge toward a single stable point.

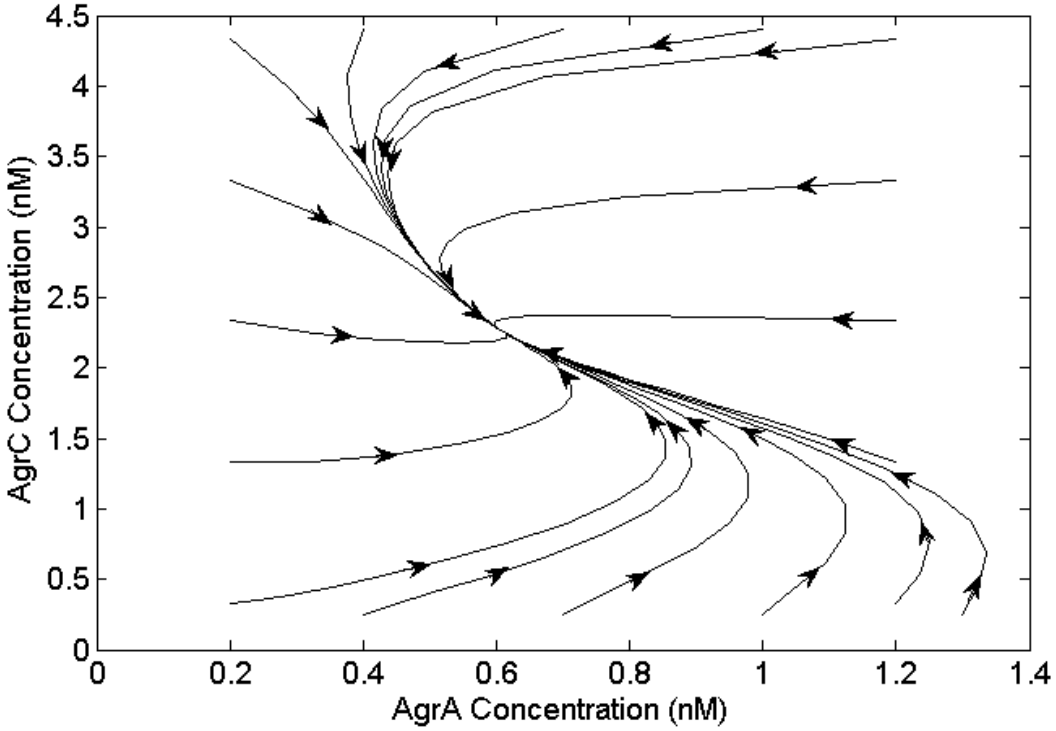

Figure 13: Phase portrait of the system at monostable region, AIP concentration equal to 1.5 *nM*

In Figure 14 the AIP concentration is taken equal to 0.5 nM which is located in the bistable (switching) region. The figure illustrates that the system exhibits bistability: the trajectories of the system converge toward two different stable points depending on the initial condition.

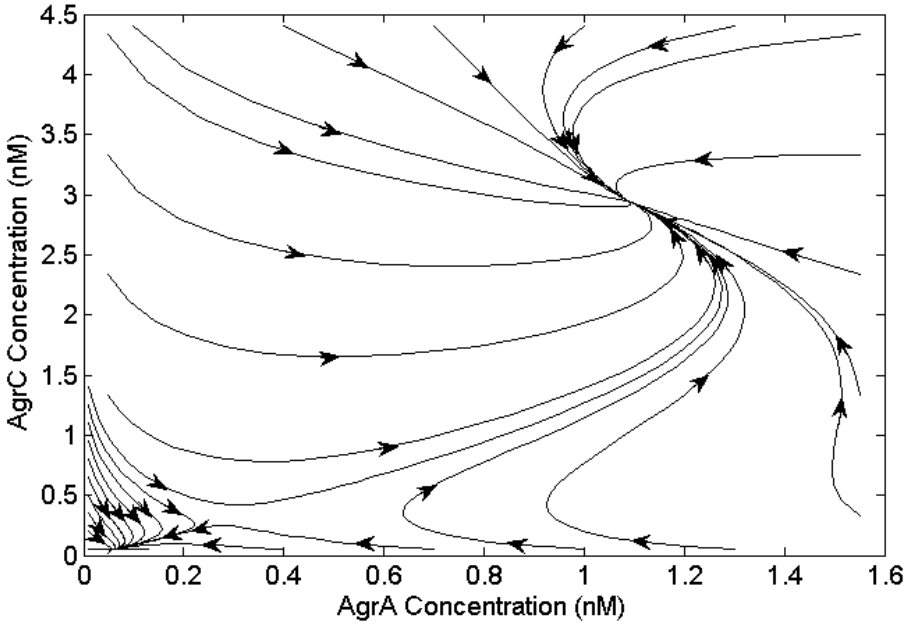

Figure 14: Phase portrait of the system at bistable region
AIP concentration equal to 0.5 *nM*

The bifurcation behaviour of the model is illustrated in Figure 15. To generate this figure, simulations were run for a range of AIP values. In each case, the model was run to equilibrium from two initial conditions: one in which AgrC and AgrA levels are low (an 'off' state, both equal to 0.1 *nM*), and one in which these levels are high (an 'on' state, both equal to 5 *nM*).

As shown in the figure, the system exhibits monostability at low bacterial concentration (*P<0.2 nM*) and at high bacterial concentration (*P>1 nM*). It exhibits bistable behavour for the intermediate range 0.2 nM < *P <1 nM.* At low bacterial concentration the genetic circuit is always 'off'; for high bacteria concentrations it is always 'on'. As a culture grows, the AIP concentration increases; when the bacterial concentration reaches a threshold (*P=0.2 nM*), the system jumps to the high equilibrium point and the genetic circuit becomes 'on'. As the figure shows, the system exhibits hysteresis–it does not return to 'off' state at the same point as it jumps to 'on' state.

Figure 16 shows the nullclines of the model in the absence of AIP. This is representative of the behaviour at low AIP concentration (*P<0.2*): one equilibrium point at the 'off' state.

The system nullclines at AIP concentration equal to 1.5 *nM* (representing high AIP concentration) are shown in Figure 17. Again, the system is monostable: it has one stable equilibrium point at the 'on' state.

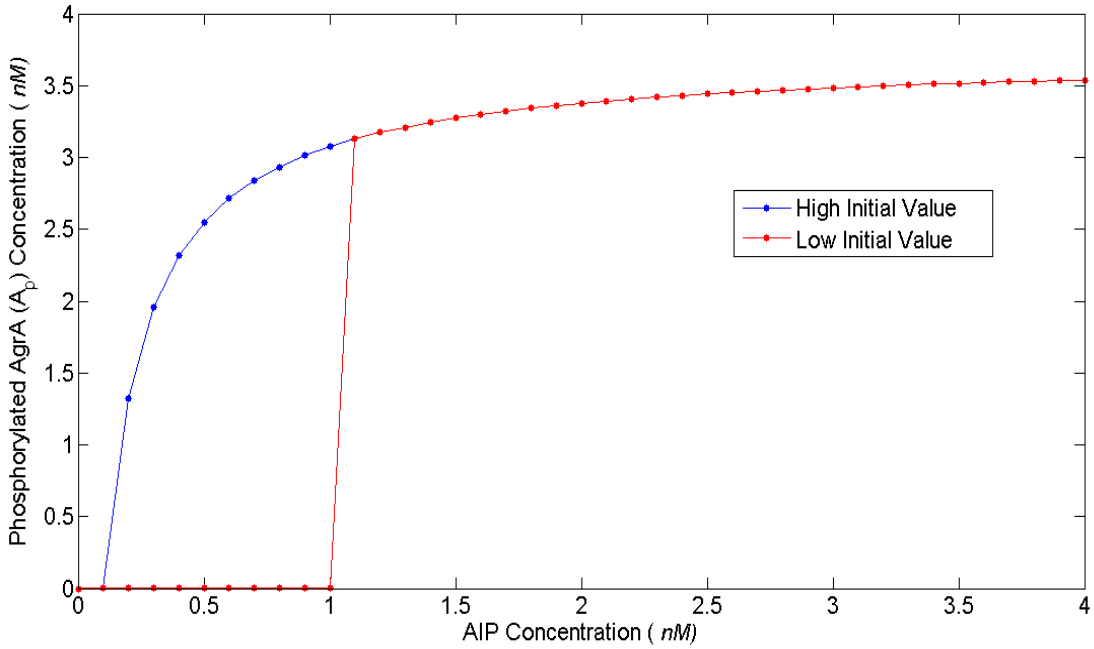

Figure 15: Bifurcation diagram of the *S. aureus* QS mechanism, the initial values of phosphorylated AgrA (*A*) and AgrC(*C*) are equal to 0.1nM for low initial value and 5 nM for high initial value

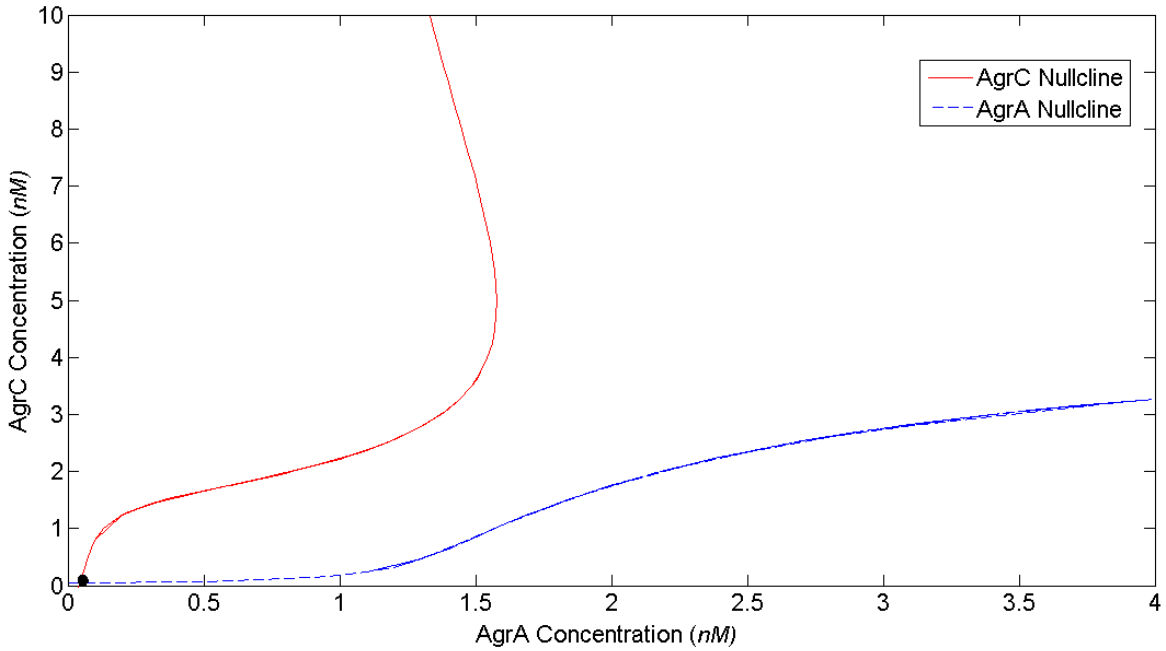

Figure 16: Nullclines of model (40) and (42) in the absence of AIP concentrations (*P*). Filled circle indicate the stable equilibrium point.
For P less than 0.2 *nM* the system is monostable at off state.

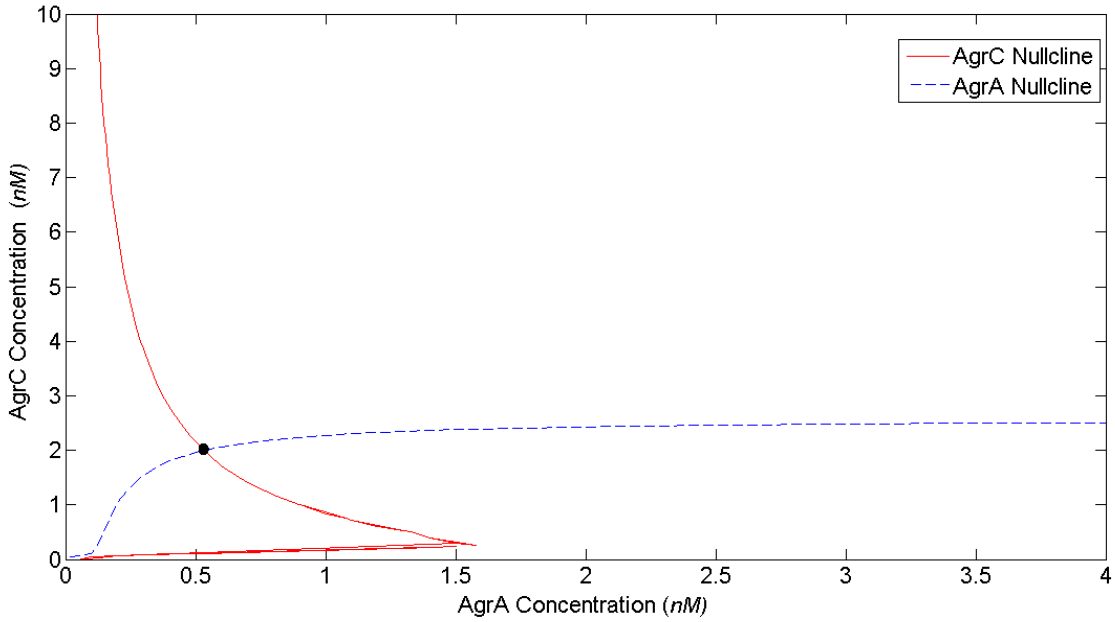

Figure 17: Nullclines of model (40) and (42) at AIP concentrations (*P*) equal to 1.5 *nM*. Filled circle indicate the stable equilibrium point. For *P* higher than 1 *nM* the system is monostable at on state.

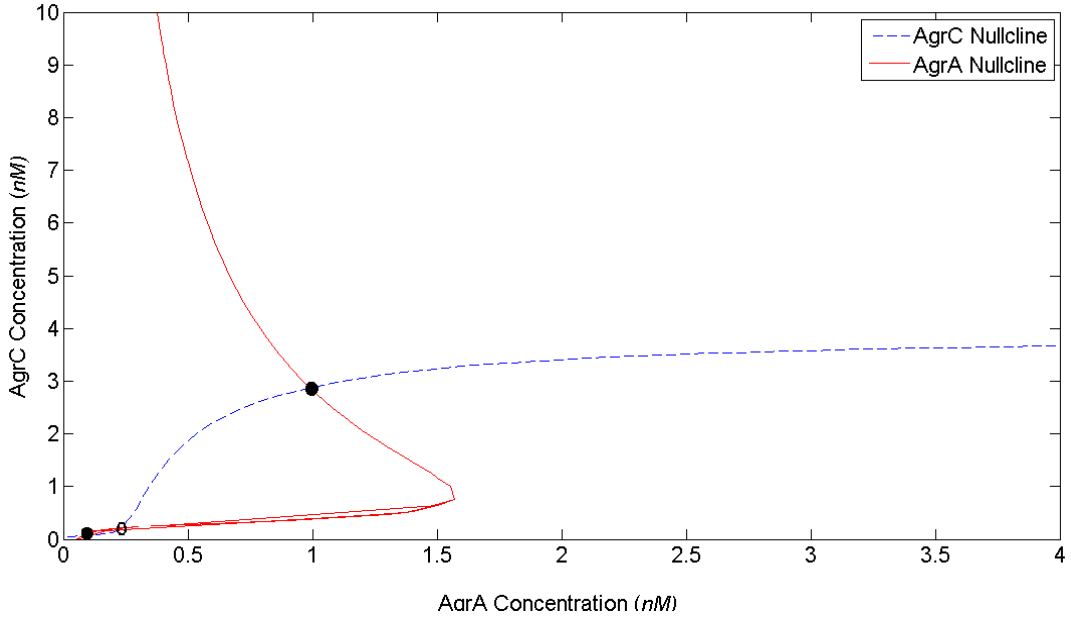

Figure 18 Nullclines of model (40) and (42) at AIP concentrations (P) equal to 0.5 *nM*. Filled and empty circles indicate the stable and non-stable equilibrium points, respectively. The system is bistable at the intermediate concentration of AIP ($0.2<P<1$ *nM*).

At AIP concentration equal to 0.5 *nM*, the system has two stable and one unstable equilibrium points, as illustrated in Figure 18 . The nullclines of the model have similar shape at intermediate concentration of AIP ($0.2<P<1$ *nM*).

We next consider the effect of variation in parameter values on the system behaviour. As in section 3.1, our focus is on two key performance measures: the threshold value of AIP (at which the switch to the 'on' state occurs), and the steady state activity level (the phosphorylated AgrA concentration). Figure 19 shows a preliminary analysis of the role of ribosome binding site (RBS) strength. Variation in the RBS strength of AgrA and AgrC is characterized by changes parameters k_A and k_C respectively. System bifurcation curves are shown over three different values of AgrC and AgrA RBS strengths.

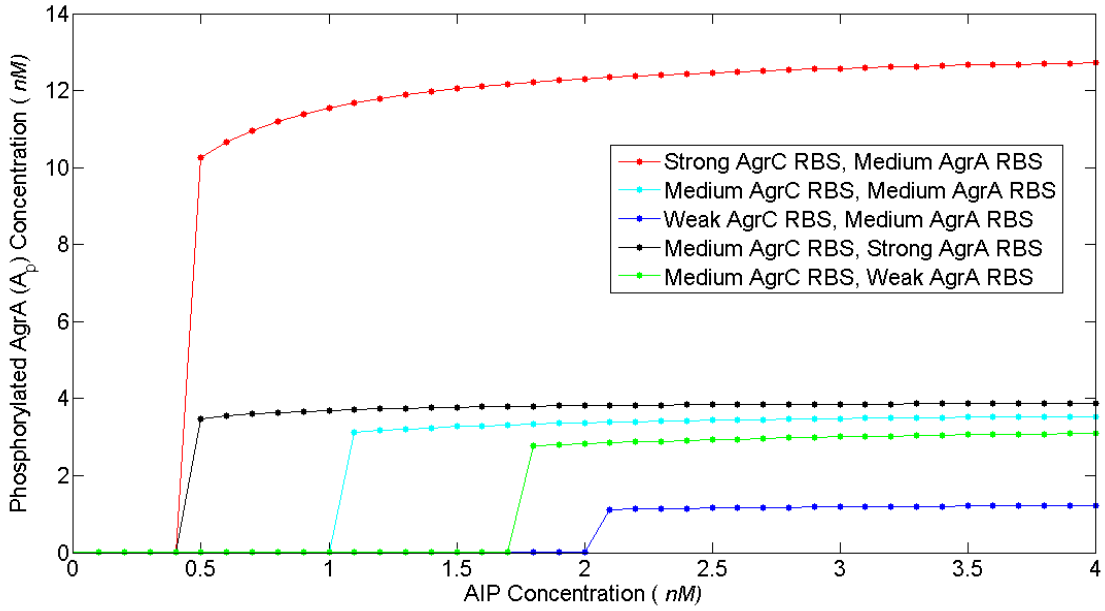

Figure 19 The effects of changes in the ribosome binding strength of AgrA and AgrC. Strong, medium and weak AgrA and AgrC RBS's correspond to $\boldsymbol{k_A}$ **and** $\boldsymbol{k_C}$ equal to **30 , 10** and **5** nMs^{-1} , respectively. The threshold concentration can be tuned by both RBS strength while the final concentration of the transcription factor can be more effectively tuned by strength of AgrC RBS

The figure illustrates that as the strengths of AgrA and AgrC ribosome binding sites increase (increasing k_A, and k_C respectively), the threshold concentration decreases and the final value of transcription factor (A_p) increases. But the effect of RBS strength of AgrC (K_C) on the final concentration is more significant than the effect of RBS strength of AgrC (K_C).

Figure 20 shows the effect of inhibitor autoinducer on the system dynamics. Since our ultimate goal is to engineer quorum sensing mechanism of *S. aureus* into *C. sporogenes*, it is of value to know the effect that inhibitory AIP may have on the engineered system. As shown in the figure, the inhibitor moves the bifurcation points and hysteresis loop to the right, and increases the threshold concentration, but has a minor effect on the final concentration.

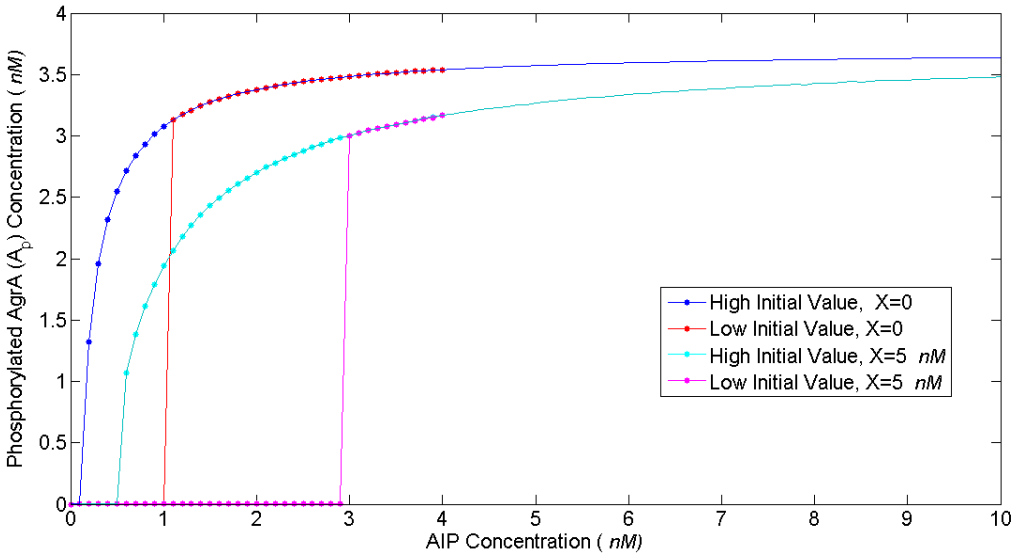

Figure 20: System behavior for different non-native AIP concentration

3.3.3 Parametric Sensitivity Analysis

As in section 3.1, we aim to identify parameters that have significant influence over the system's performance. To obtain robust conclusions, a globalized analysis was carried out over the parameters presented in Table 7. Because sampling over a mesh in the 16-dimensional parameter spaces would be prohibitively expensive, two values were chosen for 7 parameters that we can tune using molecular biology techniques. Each parameter was sampled at the endpoints of the corresponding bistability region, as determined using MATLAB [82]. The other parameters were assigned their nominal values (Table 8). As in Section 3.2.3, Equation (28) was used to define local sensitivity coefficients for each parameter $\boldsymbol{P_i}$ where S_{ss} and S_{thresh} represent the sensitivity of the steady-state concentration of phosphorylated AgrA (A_p) and the AIP (P) threshold concentration, respectively. Equation (29) was used to estimate the derivatives based on 10 percent change in parameter values.

Consequently, the local sensitivity coefficients were calculated at 128 (=2^7) points in the parameter space. For each parameter, these were then averaged to give a single globalized sensitivity coefficient. These are reported in Table 8.

Table 8: Globalized sensitivity analysis of gram negative quorum sensing mechanism

Parameters	Bistability Range	S_{ss}	S_{thresh}
$\boldsymbol{K_p}$	$5-15$	-0.0749	-1.1763
$\boldsymbol{k_c}$	5-15	1.5685	-1.2223
$\boldsymbol{k_A}$	5-15	-0.3368	-0.2313
$\boldsymbol{k_{Aprime}}$	.05-0.15	0.2726	-0.2352
$\boldsymbol{k_{Cprime}}$	.05-0.15	0.2073	-0.9171
$\boldsymbol{d_C}$	1.5-3	0.0902	1.0988
$\boldsymbol{d_A}$	$1.5-3$	-0.7420	1.3924
$\boldsymbol{K_{AP}}$	1	-0.7969	1.8490
$\boldsymbol{k_{c1}}$	1	-0.0186	-0.8906
$\boldsymbol{k_{c2}}$	0.1	-0.0159	0.0208
$\boldsymbol{k_{c3}}$	1	0	0
$\boldsymbol{k_{c4}}$	0.1	0	0
$\boldsymbol{k_{dp}}$	1	0.0158	0.4809
$\boldsymbol{d_{cp}}$	2	0.0724	1.3771
$\boldsymbol{d_{Ap}}$	2	-0.8389	1.2981

The threshold value of AIP is most sensitive to $\boldsymbol{K_{AP}}$, the Michaelis constant for activator binding, and is also highly sensitive to the degradation rates for AgrA and AgrC (in both unphosphorylated and phosphorylated forms, $\boldsymbol{d_C}$, $\boldsymbol{d_C}$, $\boldsymbol{d_{cp}}$, $\boldsymbol{d_{Ap}}$). This threshold is also sensitive to parameter $\boldsymbol{k_c}$, which characterizes the maximal activated expression rate of AgrC. The steady state activity level (i.e. steady state phosphorylated AgrA concentration), is sensitive to the same parameters, with the noteworthy exception of the rate of degradation of AgrC ($\boldsymbol{d_C}$ and $\boldsymbol{d_{Cp}}$).

This analysis presents some design strategies for manipulation of the steady-state activity (e.g. tuning of the degradation rate of AgrA or expression rate of AgrC), and an avenue for separate adjustment of the threshold AIP level (via tuning of the rate of degradation of AgrC).

These results are complementary to our findings in Section 3.3.2. Together, they provide a useful set of strategies for the design of quorum sensing systems as functional switches to trigger desired activity.

Chapter 4
Mathematical Model and Sensitivity Analysis of Aerotolerant Bacteria Growth in Solid Tumors

4.1 Introduction

The results in this chapter were published in [86]. In Section 2.2 the structure of solid tumor was explained. In solid tumors, the proliferation of abnormal cells is much faster than development of vasculature; therefore, the inner part of the tumor becomes avascular. This phenomenon together with the abnormality in lymphatic and blood vessels makes the inner part of the tumor hypoxic [87]. Hypoxia imposes a barrier for conventional cancer therapies such as chemotherapy and radiotherapy. Conversely, it is the mechanism for specificity in a bacteria-mediated therapy, since the hypoxic part of a tumor provides an attractive site of colonization for anaerobic bacteria such as C. sporogenes. Intravenous injection of C. sporogenes into tumor-bearing mice shows that the bacteria can germinate in a tumor up to a density of 2×10^8 C.F.U./g, with resulting oncolysis [88]. Bacterial expression of a therapeutic agent such as nitrogen reductase (NTR) or cytosine deaminase (CD) can further enhance oncolysis.

As was explained in section 2.3, because anaerobic bacteria germinate only in the necrotic part of the tumor, tumor regrowth can occur from the outer viable rim. This problem can be addressed by allowing the bacteria to migrate to less hypoxic parts of the tumor. As discussed in Chapter 2, research on the oxygen metabolism of anaerobic bacteria (such as *Clostridium* and *Bifidobacterium*) has shown that they can germinate in low oxygen environments if they are producing an NADPH oxidase, such as NoxA ([43],[44],[45]). The strain *C. Aminovalericum*, which is able to grow in low oxygen levels, expresses the *noxA* gene at elevated levels under exposure to low oxygen conditions, indicating a role for NoxA in *Clostridium* oxygen metabolism [43]. Other candidate aerotolerance enzymes include *nox-1* and *nox-2* gene from lactic acid bacteria [89], and the *nox* gene from *L. mesendteroides* [90].

The genome of wild-type *C. sporogenes* does not include a *nox* gene. An engineered strain expressing *nox* constitutively would show little specificity in targeting tumors. In order to target colonization, we will place the gene under the control of an inducible promoter that will be active only in the presence of the high-density colony in the necrotic core. Bacterial quorum sensing mechanisms

provide this action: triggering the production of a gene only when the bacterial density surpasses a threshold.

Bacterial quorum sensing was explained in Section 2.5. The two well-characterized quorum sensing mechanism are that of *V. fischeri* and *S. aurous*. While the former is known as the typical quorum sensing mechanism for gram negative bacteria, the latter is used as a typical one for gram positive bacteria. The *Vibrio fischeri* quorum sensing mechanism engineered in *E. Coli* has already been used to increase cell density in selective invasion of mammalian cells [78]. This mechanism can be introduced into *C. Sporogenes* by cloning the *luxI* and *luxR* genes under the control of the *pLux* promoter [51]. Figure 21 shows the proposed genetic circuit using the *V. fischeri* qourum sensing mechanism.

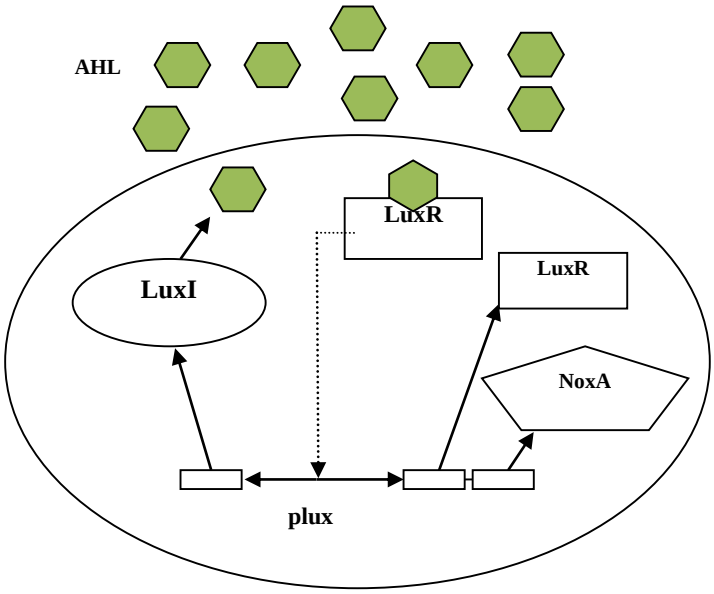

`Figure 21: Proposed aerotolerant genetic circuit using *V. Fischeri* quorum sensing

The *S. aurous* quorum sensing mechanism can be introduced into *C. sporogenes* by cloning *agrA*, *agrB*, a*grC*, *agrD* genes down stream of the *P2* promoter. The aerotolerance enzyme gene can be cloned either downstream of *P2* or *P3* promoter. Figure 22 shows the two proposed layout of the genetic circuit using *S. aureus* quorum sensing.

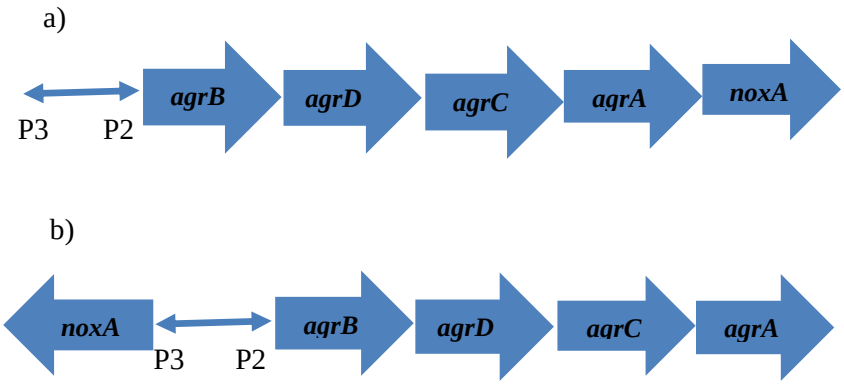

Figure 22: The proposed aerotolerant genetic circuit using *S. aureus* quorum sensing mechanism

The engineered bacteria are expected to germinate in the necrotic part of a solid tumor at a specific concentration (about 10^8 C.F.U./g) [87]. The model-based analysis in Chapter 3 suggests strategies for tuning a quorum sensing mechanism to a threshold by careful design of the synthetic genetic circuit by, for example, modifying the ribosome binding site of the promoter or by the choice of a specific *luxR* gene [76]. As a result, the aerotolerance enzyme will not be expressed in healthy (oxygenated) tissue, but will be produced at the site of a tumor, allowing the local bacteria to migrate to less hypoxic parts of the tumor and hence enhance tumor regression.

To complement our model-based design of the circuit, we next present a mathematical model of tumor colonization by the engineered strain, which will provide insight into design choices that will influence population-level behavior.

4.2 Oxygen profile and tumor structure

Tumor structure was explained in section 2.1. In this section, to simplify the geometric complexity of a tumor, we consider an ideal tumor as a radially symmetric sphere.

Figure 23 shows the oxygen profile and structure of such a tumor as presented in [4]. The radii of the necrotic and hypoxic cores are denoted by R_N and R_H. Oxygen does not diffuse more than 70 µm into the tumor [5]. Considering a tumor with R = 90 µm, we expect to have $R_N = 20\ \mu m$. The hypoxic radius of such a tumor is around $R_H = 36\ \mu m$. The oxygen profile shown in Figure 23 is based on the data in [4] and is used to describe the environment in which a colony forms in the simulation in the

next section. The oxygen level in the necrotic core is almost zero. In the quiescent or hypoxic part, the oxygen concentration is less than 0.33% (2.5 *mmHg*). Table 9 shows the data points extracted from information in [4].

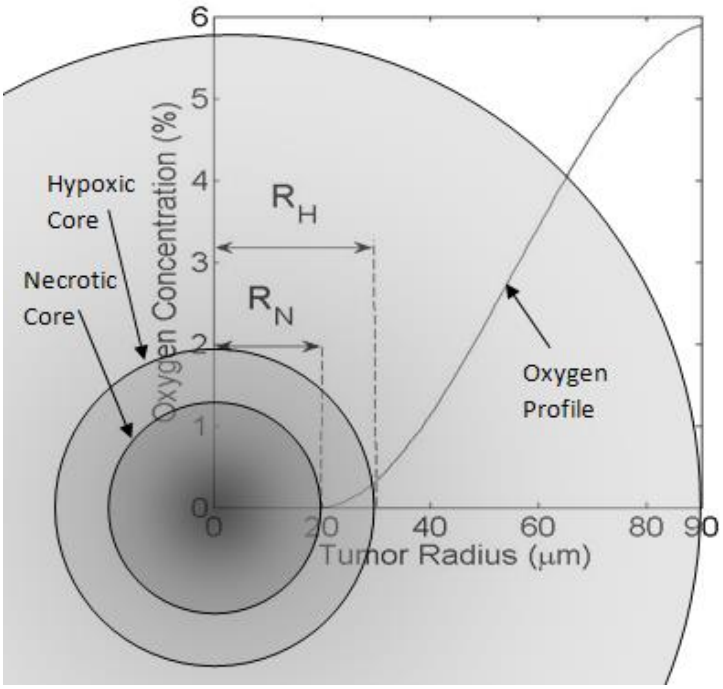

Figure 23: Tumor structure, and oxygen profile based on the data in [4]

Table 9: Data point for fitting Oxygen profile in Tumor based on data in [4]

R(*μm*)	O %	PO_2 (*mmHg*)
0<R<20	0	0
R=20	0	0
R=36	0.33	2.5
R=90	5.9	45
R>90	5.9	45

A cubic curve was fit to the data in Table 9, using the MATLAB curve fitting toolbox [82]. This curve is used in the next section to represent the oxygen profile as a function of radial distance r:

$$O = -3.044 \times 10^{-5} \times r^3 + 5.116 \times 10^{-3} \times r^2 - 0.165 \times r + 1.497 \qquad (45)$$

where r is in μm and oxygen in percent

4.3 Mathematical Model of Bacterial Growth in Solid Tumors

We consider the time-varying growth of the engineered bacterial colony in a radially symmetric spherical tumor.

The degradation, production and diffusion of aerotolerance enzyme (*E*) and autoinducer (*A*) are modeled by reaction-diffusion equations (convective transport is negligible in tumors due to the high intestinal pressure, and so diffusion plays the main role in transport of molecules):

$$\begin{cases} \dfrac{\partial E}{\partial t} = \dfrac{D_E}{r^2}\dfrac{\partial}{\partial r}(r^2 \dfrac{\partial E}{\partial r}) + K_E C_B \dfrac{A}{A+k} - d_E E & (46) \\ \dfrac{\partial A}{\partial t} = \dfrac{D_A}{r^2}\dfrac{\partial}{\partial r}(r^2 \dfrac{\partial A}{\partial r}) + K_A C_B - d_A A & (47) \end{cases}$$

The first terms on the right hand side of the equations describe diffusion. D_A and D_E are the diffusion coefficient of autoinducer and aerotolerance enzyme, respectively. Degradation of autoinducer and aerotolerance enzyme follow a first order kinetic with rate constants d_A and d_E, respectively. The rate of production of autoinducer is proportional to the bacterial concentration C_B, with a rate constant of K_A. The production of the aerotolerance enzyme depends linearly on the bacterial concentration, with rate constant K_E, and hyperbolically on the abundance of autoinducer, with a half-saturation value of *k*. The core of the quorum sensing mechanism, which is the positive feedback loop, is retained in this simplified model. (The model represents the quorum sensing mechanisms of both gram positive and gram negative bacteria. You et al. [74] used a similar simplified description of the quorum sensing mechanism, which lumps production of LuxR (or AgrA), production of LuxR-AHL (or AgrC-AIP) complex, activation of the promoter and expression of target gene.)

The bacterial population dynamics are modeled as

$$\frac{\partial C_B}{\partial t} = \frac{D_B}{r^2}\frac{\partial}{\partial r}(r^2 \frac{\partial C_B}{\partial r}) + K_B C_B (1 - \frac{C_B}{C_M}) - \frac{d_B}{O_{\max} - \dfrac{O}{k_v E + 1}} C_B \qquad (48)$$

Again, the first term describes diffusion, with D_B the diffusion coefficient of the bacteria. In the absence of oxygen and aerotolerance enzyme, the bacteria follow density dependent growth with a maximal rate equal to K_B and a maximal concentration of C_M. A death term, which models the effect of oxygen (O), increases with the oxygen concentration. The aerotolerance enzyme counteracts this effect. The strength of the aerotolerance enzyme is characterized by the parameter k_v. (Since (k_vE+1) is always larger than one, the denominator of the third term (death term) will never become negative.)

To minimize the model parameter set, we non-dimensionalized the mathematical model. Considering A_M and E_M as the maximal concentration of autoinducer and aerotolerance enzyme produced by constitutive promoters, and T_{EM} and T_{AM}, their maximal life time, respectively, we scaled each variable in Equation (46), (47) and (48) by its maximal value to arrive at

$$\frac{R^2}{T_{EM}D_E}\frac{\partial\frac{E}{E_m}}{\partial\frac{t}{T_{EM}}} = \frac{1}{\frac{r^2}{R^2}}\frac{\partial}{\partial\frac{r}{R}}\left(\frac{r}{R^2}^2\frac{\partial\frac{E}{E_m}}{\partial\frac{r}{R}}\right) + \frac{R^2C_MK_E}{D_EE_m}\frac{C_B}{C_M}\frac{\frac{A}{A_M}}{\frac{A}{A_M}+\frac{k}{A_M}} - \frac{R^2d_E}{D_E}\frac{E}{E_m} \tag{49}$$

$$\frac{R^2}{T_{AM}D_A}\frac{\partial\frac{A}{A_m}}{\partial\frac{t}{T_{AM}}} = \frac{1}{\frac{r^2}{R^2}}\frac{\partial}{\partial\frac{r}{R}}\left(\frac{r}{R^2}^2\frac{\partial\frac{A}{A_m}}{\partial\frac{r}{R}}\right) + \frac{R^2C_MK_A}{D_AA_m}\frac{C_B}{C_M} - \frac{R^2d_A}{D_A}\frac{A}{A_m} \tag{50}$$

$$\frac{\boldsymbol{R^2}}{\boldsymbol{T_{BM}D_C}}\frac{\boldsymbol{\partial\frac{C_B}{C_M}}}{\boldsymbol{\partial\frac{t}{T_{AM}}}} = \frac{\mathbf{1}}{\frac{r^2}{R^2}}\frac{\boldsymbol{\partial}}{\boldsymbol{\partial\frac{r}{R}}}\left(\frac{r}{R^2}^2\frac{\boldsymbol{\partial\frac{C_B}{C_M}}}{\boldsymbol{\partial\frac{r}{R}}}\right) + \boldsymbol{K_B}\frac{\boldsymbol{R^2}}{\boldsymbol{D_C}}\frac{\boldsymbol{C_B}}{\boldsymbol{C_M}}\left(\mathbf{1}-\frac{\boldsymbol{C_B}}{\boldsymbol{C_M}}\right) - \frac{\boldsymbol{R^2}}{\boldsymbol{D_C}}\frac{\boldsymbol{d_BC_M}}{\boldsymbol{O_{max}}}\frac{\boldsymbol{\frac{C_B}{C_M}}}{\mathbf{1}-\frac{\boldsymbol{\frac{O}{O_{max}}}}{\boldsymbol{k_{vE_m}\frac{E}{E_m}+1}}} \tag{51}$$

where R is the tumor radius.

We then wrote equations (49), (50) and (51) in nondimensional form as follows:

$$\begin{cases} \frac{1}{\alpha}\frac{\partial \bar{E}}{\partial \bar{t}} = \frac{1}{\bar{r}^2}\frac{\partial}{\partial r}(\bar{r}^2\frac{\partial \bar{E}}{\partial \bar{r}}) + M_E\bar{C}_B\frac{\bar{A}}{\bar{A}+K} - N_E\bar{E} & (52) \\ \frac{1}{\gamma}\frac{\partial \bar{A}}{\partial \bar{t}} = \frac{1}{\bar{r}^2}\frac{\partial}{\partial \bar{r}}(\bar{r}^2\frac{\partial \bar{A}}{\partial \bar{r}}) + M_A\bar{C}_B - N_A\bar{A} & (53) \\ \frac{1}{\beta}\frac{\partial \bar{C}_B}{\partial \bar{t}} = \frac{1}{r^2}\frac{\partial}{\partial r}(r^2\frac{\partial C_B}{\partial r}) + M_B\bar{C}_B(1-\bar{C}_B) - \frac{N_B\bar{C}_B}{1-\frac{\bar{O}}{K_v\bar{E}+1}} & (54) \end{cases}$$

with

$$M_B = \frac{K_B R^2}{D_B},\ N_B = \frac{d_B R^2}{D_B C_M O_{\max}},\ M_A = \frac{K_A R^2 C_M}{A_M D_A},\ K_v = k_v E_M \quad (55)$$

$$N_A = \frac{d_A R^2}{D_A},\ M_E = \frac{K_E R^2 C_M}{E_M D_E},\ N_E = \frac{d_E R^2}{D_E},\ K = \frac{k}{A_M} \quad (56)$$

$$\alpha = \frac{T_{EM} D_E}{R^2}, \gamma = \frac{T_{AM} D_A}{R^2}, \beta = \frac{T_{BM} D_B}{R^2}, \quad (57)$$

The resulting dimensionless parameters are bacterial growth rate (M_B), bacterial death rate (N_B), AHL production rate (M_A), AHL degradation rate (N_A), aerotolerance enzyme production rate (M_E), aerotolerance enzyme degradation rate (N_E), half-saturation constant (K), strength of aerotolerance enzyme (K_v), diffusion coefficient of AHL (α), diffusion coefficient of aerotolance enzyme (β) and diffusion coefficient of bacteria (γ).

The mathematical model in Equations (52) - (57) and Equation (45), with parameter values in Table 10, was implemented in Matlab [82]. MATLAB's PDEPE function was used to solve the system of PDE's (Appendix C). We simulate the situation in which a small number of spores diffuse into the necrotic part of the tumor and germinate, therefore we assume the initial bacterial concentration to be small and the initial autoinducer and aerotolerance enzyme abundance to be zero. Since the boundary of the tumor is well oxygenated, no anaerobic bacteria can grow at the edge of the tumor (and so no autoinducer or aerotolerance enzyme can be produced), therefore the concentration of all species are considered to be zero at the edge of the tumor (r=R). The gradient of all species are assumed to be zero at the center of the tumor; therefore, for each species in the model a symmetric boundary condition is

applied at the center of the tumor ($r = 0$) while a zero boundary condition is applied at the edge of the tumor ($r = R$). In Equation (54), maximum production rate (M_B) and maximum death rate (N_B) are specified by the choice of host bacteria and cannot be altered by genetic circuit. We chose values for those parameters so that for the wild-type (that is, in the absence of the aerotolerance enzyme) colonization is supported only inside the necrotic and hypoxic part of the tumor. The other parameters were estimating from parameters introduced in [74] and [59], using Equations (55)-(57).

Table 10: parameters value in the model

Parameters	Value	Parameters	Value
M_B	20000	N_E	0.1
M_E	50	N_A	0.1
M_A	50	γ	0.01
K_v	23	β	0.0001
K	0.01	α	0.1
N_B	18500		

Figure 22 compares the model predictions of steady-state bacterial populations for wild-type and engineered strains. The engineered circuit confers a marked enhancement of bacterial growth due to the expression of the aerotolerance enzyme.

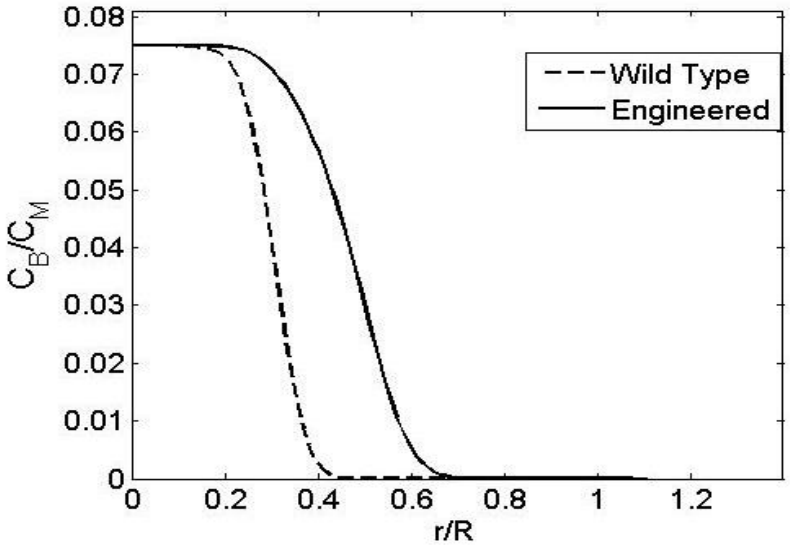

Figure 24: Comparison of steady state bacterial colonization profiles for wild-type and engineered strains.

4.4 Sensitivity Analysis of Aerotolerant Bacterial Growth in Solid Tumors

As in Chapter 3, we carried out a parametric sensitivity analysis of the model to identify which aspects of the mechanism are most significant in determining the targeted growth of the bacteria inside the tumor. While certain aspects of the process, such as diffusion and bacterial growth rate, are likely out of our control, other features present themselves as design parameters. These include the strength of the aerotolerance enzyme, which can be altered by the choice of the specific oxidase, and the production and degradation rates of the aerotolerance enzyme and autoinducer, which can be altered by the choice of promoters, ribosome binding sites, specific *luxR* genes, and degradation tags.

As performance measures of the engineered strain, we considered the overall colony size in steady state, represented by the area under the curve (AUC) in Figure 24, and the degree of specificity (*sp*) of the colony, represented by the width between the points at which the bacteria achieve 10% and 90% of their maximal concentration. An alternative performance measure, not considered here, would be the rate at which the bacteria disperse through the tissue.

Local sensitivity coefficients and their derivatives are defined as Section 3.2.3 using equations (28) and (29). The range of each parameter in which the system performance is sensitive was chosen by first exploring the range over which each individual parameter (with the others fixed at the nominal

values of Table 10, has an impact on system behavior. This procedure lead to upper and lower boundaries for each parameter. Since the parameter values themselves are unknown, a "globalized" analysis was carried out in which the local sensitivity was calculated at $\mathbf{3^5} = 243$ different points in parameter space, chosen by setting each parameter at the two ends of the identified range, and at the midpoint on the log-scale. The sensitivity coefficients for each parameter were then averaged.

Table 11: Globalized parametric sensitivities

Parameters	Range	S_{AUC}	S_{sp}
M_A	70-130	0.1939	0.0428
M_E	70-130	0.5270	0.0404
K	0.01-1	5.6677	0.1977
N_A	0.01-10	-0.0381	-0.0072
N_E	0.01-10	-0.0920	0.0523

The results, shown in Table 11, indicate that for both performance measures the production parameters, M_A, M_E and K, play a more significant role than the degradation rates, N_A and N_E. (From the model structure, the sensitivity to K_v is the same as that to M_E). The behavior is most sensitive to the half-saturation constant K. Consequently, in the design of the synthetic circuit, attention should be directed primarily at the choice of aerotolerance enzyme and at the production of that enzyme and of the autoinducer. These production processes can be controlled through, for instance, selection of promoters and ribosome binding sites, and choice of a form of the *luxR* gene which has a particular affinity for AHL [60].

To conclude, the analysis of the mathematical model of this process indicates that the size and specificity of the destructive colony can be manipulated by careful design of the processes leading to production of quorum-sensing autoinducer and aerotolerance enzyme.

The modelling results in this and the previous chapter will be useful tools to guide design once the synthetic circuit has been finalized an it's behavior has been confirmed. The next chapters describe important first steps in that direction.

Chapter 5
Material and Methods

5.1 Bacteria Strains and Plasmids

Table 12 includes a complete list of palsmids and strains used in this study. *Clostridium sporogenes* ATCC 3584 was bought from American Type Culture Collection (Manassas, VA, USA). *Clostridium sporogenes* NCIMB 10696, *E. coli* S.17, and *E. coli* CA434 were gifts from Dr. Minton (University of Nottingham), Dr. Charles (University of Waterloo) and Dr. Young (Aberystwyth University) respectively.

Two shuttle vectors, pJIR1457 and pMTL825x were used for conjugation. pJIR1457 was a gift from Dr. Rood (Monash University) and pMTL825x from Dr. Minton (University of Nottingham). Standard parts from the biobricks registry were used to construct quorum sensing plasmid: BBA-F1610, I1305 and BBA_F2621 were gifts from iGEM group of the University of Waterloo. Plasmid pGlow-Xn-Pp1-CI was bought from BioCat GmbH (Heidelberg, Germany).

Table 12: List of the plasmids and the method of construction

Strain or Plasmid Vector	**Relevant Characteristics**	**Reference or source**
Bacteria Strains		
E. coli DH5α	*fhuA2 Δ(argF-lacZ)U169 phoA glnV44 Φ80 Δ(lacZ)M15 gyrA96 recA1 relA1 endA1 thi-1 hsdR17*	New England Biolab (NEB)
dam$^-$/dcm$^-$ Competent *E. coli*	*ara-14 leuB6 fhuA31 lacY1 tsx78 glnV44 galK2 galT22 mcrA dcm-6 hisG4 rfbD1 R(zgb210::Tn10)* Tet^S*endA1 rspL136* (Str^R) *dam13::Tn9* (Cam^R) *xylA-5 mtl-1 thi-1 mcrB1 hsdR2*	New England Biolab (NEB)

One Shot® TOP10 Chemically Competent *E. coli*	*F- mcrA (mrr-hsdRMS-mcrBC) 80lacZ M15 lacX74 recA1 ara 139 (ara-leu)7697 galU galK rpsL (StrR) endA1 nupG.*	Invitrogen
E.coli CA434	F- *hsdS2O* (re, me) *recAl3 ara-I4 lacy1 proA2 galK2 rpsL20* (Sm^R) *xyl-5 mtl-1 supE44 (A-)* (HB101 carrying R0702 plasmid) R702 (Tra^+ Mob^+ IncP Km^R Tc^R Sm^R Su^R Hg^R)	[91]
E coli S.17-1	Tp^R Sm^R recA, thi, pro, hsdR-M+RP4: 2-Tc:Mu: Km Tn7 λpir	[92]
C. sporogenes	ATCC 3584	ATCC, Manassas, VA, USA
C. sporogenes	NCIMB 10696	Craibstone Estate, Bucksburn, Aberdeen. UK
Plasmids		
BBa_F2621	BioBrick part, designed by: Barry Canton Group: Antiquity (2004-08-09)	[93]
BBa_C0261	BioBrick part, RBS+*luxI* gene	[94]
BBa_I13504	BioBrick part including E0034, E0040, B0015	[95]
pMTL8225x	Shuttle vector for conjugation transform from *Ecoli* into *Clostridium* Developed by Dr. N. Minton	[96]
pJIR1475	Shuttle vector for conjugation transform from *Ecoli* into *Clostridium*, developed by Dr. J. Roodi	[97]

pGlow-XN-pp1-CI	Containing anaerobic *gfp* (*evoglow*) gene downstream of *thl* promoter	[98]
pGEM®-T Easy	Cloning vector for PCR-generated DNA fragments, Amp^R	New England Biolab (NEB)
CG	C0261 harboring *evoglow* from pGlow-XN-pp1-CI	This study
FCG	F2621 harboring *luxI* and *evolglow* genes from C021 and pGlow-XN-pp1-CI	This study
FG	F2621 harboring *evoglow* gene from pGlow-XN-pp1-CI	This study
TTG	pGEM®-T Easy harboring *evoglow* and *thl* promoter from pGlow-XN-pp1-CI plasmid	This study
PTG	pMTL8225x harboring *thl* and *evoglow* from pGlow-XN-pp1-CI	This study
PAgr	pMTL8225x harboring *agr* operon	This study
PAG2	pMTL8225x harboring *agr* operon and *evoglow* gene downstream of p2 promoter	This study
PAG3	pMTL8225x harboring *agr* operon and *evoglow* gene downstream of p2 promoter	This study
Clonejet_NoxA	Clonejet vector harboring *noxA* gene	This study
PTN	pMTL8225x harboring *thl* promoter and *noxA* gene downstream of *thl* promoter	This study
PAGN2	pMTL8225x harboring *agr* operon, and *evoglow* and *noxA* genes downstream of p2 promoter	This study
PAGN3	pMTL8225x harboring *agr* operon, and *evoglow* and *noxA* genes downstream of p2 promoter	This study
PFCI	pMTL8225x harboring *luxI, luxR, lux pR and lux pL* from lux operon, and *gfp* gene downstream of *lux pR* promoter	This study

PFCG	pMTL8225x harboring *luxI, luxR, lux pR and lux pL* from lux operon, and *evoglow* gene downstream of *lux pR* promoter	This study
PFCGN	pMTL8225x harboring *luxI, luxR, lux pR and lux pL* from *lux* operon, and *evoglow* and *noxA* genes downstream of *lux pR* promoter	This study

5.2 Bacterial growth and storage condition

Clostridium were grown anaerobically in an 830 anaerobic chamber (PLAS Labs). The atmosphere of nitrogen (N2), carbon dioxide (C02), and hydrogen (H2) was maintained at a ratio of 80% (v/v), 10% (v/v), and 10% (v/v) respectively and at a temperature of 37°C. Clostridium were grown in TPYG medium (3% trypticase, 0.5% peptone, 0.1% glucose, 0.5 % yeast extract and 0.1% cysteine-HCL) or in TYG medium (3% trypticase, 2% yeast extract, and 0.1% sodium thioglycollate). Whereas *E. coli* strains were grown in L-broth (1% trypticase, 0.5 % yeast extract and 1 % NaCL) and on L-agar (1.5% agar) at 37°C. For *E. coli* strains, growth culture was supplemented with 500 $\mu g.ml^{-1}$ erythromycin, 50 $\mu g.ml^{-1}$ ampicillin and 100 $\mu g.ml^{-1}$ ampicillin to counter select desired plasmid bearing bacteria. For *Clostridium sporogenes*, antibiotics concentrations were 5 $\mu g.ml^{-1}$ (erythromycin) and 500 $\mu g.ml^{-1}$ (D-cyclocerine).

E. coli and *C. sporogenes* were stored at -80 ^{o}C in glass cryovials containing 15% v/v and 10% v/v glycerol, respectively.

5.3 Molecular Biology Techniques

5.3.1 Plasmid Isolation and Manipulation

Plasmid isolation from *E. coli* and gel extraction were done with miniprep kits and gel extraction kits from QIAGEN (Toronto, ON) or Invitrogen (Burlington, ON) by following the manufacturer's instruction. Plasmid isolation from *C. sporogenes* was done with the standard miniprep with an added lysozyme step. 1 $mg.ml^{-1}$ lysozyme was added to the re-suspended cell pellet, which was then incubated at 37°C for 10 minutes before performing cell lysis and the rest of the procedure.

All restriction enzymes were purchased from New England Biolab (Whitby, ON). For ligation, either Quick ligation kit (NEB, Whitby, ON) or T4 DNA ligase (Invitrogen or NEB) were used. Calf intestine alkaline phosphates were purchased from Invitrogen (Burlington, ON).

5.3.2 PCR

A GS4822 muti block thermo cycler (G-STORM, Somerton. Somerset, UK) was used for PCR. PCR reaction was prepared using Taq DNA polymerase and PCR reagents from New England Biolabs Ltd, (NEB, Whitby, ON) following the manufacturer's protocol for Taq DNA Polymerase with Standard Taq Buffer.

The PCR product was run on a 0.8% agarose gel and the band corresponding to the size of the product were cut and purified using a gel extraction kit from QIAGEN (Toronto, ON) following manufacturer's instruction.

When the PCR product includes the restriction enzyme sites, the purified PCR product was digested with appropriate restriction enzymes and was cloned onto the target vector using T4 DNA ligation kit form NEB (Whitby, ON) . The blunt ended PCR product were cloned into vector pCRII-TOPO TA (Invitrogen, Burlington, ON) using the TOPO TA cloning kit from Invitrogen or into a jet vector using the cloneJET PCR cloning kit (Thermo Scientific). The QuickChange Lightening Multi Site-Directed Mutagenesis Kit from Stratagene (La Jolla, CA) was used for changing the ribosome binding sites.

The primers used in this studied were purchased from Sigma-Aldrich (Oakville, ON) and are listed in Table 13

Table 13: Primers used in PCR

Primer	Tm ^{0}C	USE	Primer sequence
Agr_f_Ecoli	53	Forward primer for amplifying *agr* operon from *C. aminovalericum* genome	GAATTCcAGTTATATTAAAACATGCTAAAAGC
Agr_r_kpnI	56	Reverse primer for amplifying *agr* operon from *C. aminovalericum* genome	GGTACCCCGTTAACTGACTTTATTATCTTAT
pglow_f_xbaI	65	Forward primer to amplify *evoglow* gene from pglow plasmid	GGCATTCTAGAGTAGGATCAAGGAGGTTAGTTAGAATGGG
pglow_r_pstI_spei	72	Reverse primer to amplify *evoglow* gene from pglow plasmid	CTGCAGCGGCCGCTACTAGTCTGGCAAATCATTAAGT GGCGCCTT
thl_f	70	Forward primer to amplify thl promoter from pglow plasmid	GGCATGAATTCGGTTGGAATGGCGTGTGTGTTAGCCA
thl_r	72	Reverse primer to amplify *thl* promoter from pglow plasmid	GGCATTCTAGATCTAACTAACCTCCTTGATCCTA CGGGG
Pglow_f_XhoI	68	Forward primer to amplify *evoglow* gene from pglow plasmid with XhoI restriction site	GGCATGCTAGCGTAGGATCAAGGAGGTTAGTTAGA ATGGG
pglow_r_NehI	71	Forward primer to amplify *evoglow* gene from pglow plasmid with NheI restriction site	GGCATCGATCGCTGGCAAATCATTAAGTGGCGCCTT

To be continued on the next page……..

Table 14: Continued from previous page

Primer	Tm ^{0}C	USE	Primer sequence
NoxA_XhoI	68	Forward primer to amplify *noxa* gene from *C. aminovalericum* genome with XhoI restriction site	GGCATCTCGAGCCGCTTGAGGAGGTCTGTTAATGAAA ATTGTAGTAATT
NoxA_NheI	72	Reverse primer to amplify *noxa* gene from *C. aminovalericum* genome with NheI restriction site	GGCATGCTAGCCTCTCGCCTGTCCCCTCAGTTTATAATC CTTCTTGTTCT AGAACAAGAAGGATTATAAACTGAGGGAGAGGCGAGA GGCTAGCATGCC
GFP_XhoI	66		CGCG CTCGAGATG GGATCCATA AATGCAAAAC
GFP_NheI	65		CGCGGCTAGC TTA ATGTTT TGC TTGTCC TTGT
Mut_F2621_f	61	Forward primer to mutating *luxR* RBS	ATAGGTAATACTAGAGAAAGAGGAGGAATACTAG ATGAAAAACATAAATGC
Mut_F2621_r	61	Reverse primer to mutating *luxR* RBS	GCATTTATGTTTTTCATCTAGTATTCCTCCTCTTTCT CTAGTATTACCTAT
Mut_F1610_f	63	Forward primer to mutating *luxI* RBS	CCGCTTCTAGAGAAAGAGGAGGAATACTAGATGAC TATAATGA
Mut_F1610_r	63	Reverse primer to mutating *luxI* RBS	TCATTATAGTCATCTAGTATTCCTCCTCTTTCTCTA GAAGCGG

5.3.3 DNA Sequencing

All sequencing was done using Applied Biosystems 3130 Genetic Analyzer (Applied Biosystems, Foster City, CA, USA), either at the University of Waterloo sequencing facility, or at Ottawa Hospital Research Institute.

5.4 Gene Transformation Protocols

5.4.1 Conjugation

The protocol used for conjugation is as follows:

The plasmid was transformed into competent *E. coli* CA434 cells by electroporation using a Gene Pulser Xcell Electrooration System (Bio-Rad Laboratories (Canada) Ltd, Mississauga, Ontario). The pre-set bacterial protocol for E.coli was used for a 2mm cuvette.

The procedure for Conjugation was as follows:

Day One:

1. A 5 ml LB broth (with appropriate selection) with the transformed donor E. coli was inoculated . The culture was incubated at 37°C and 225 rpm shaking overnight.

2. 1 ml of an appropriate anaerobic liquid growth medium (e.g. TYG) with the target *C. sporogenes* strain was inoculated and incubated at 37°C under anaerobic conditions overnight.

Day Two:

1. 1 ml of the overnight CA434 donor culture was pelleted by centrifugation at 8000 rpm for 1 minute. The supernatant was discarded and cells were washed by re-suspending in 0.5 ml sterile PBS buffer. The centrifugation step was repeated as before and the supernatant was discarded.

2. The donor E. coli pellet was re-suspended in 200 µl of the overnight *C. sporogenes* culture to produce a conjugation mixture.

3. The entire conjugation mixture was pipetted onto a single non-selective plate containing an appropriate anaerobic growth medium in discrete spots as illustrated in Figure 25.

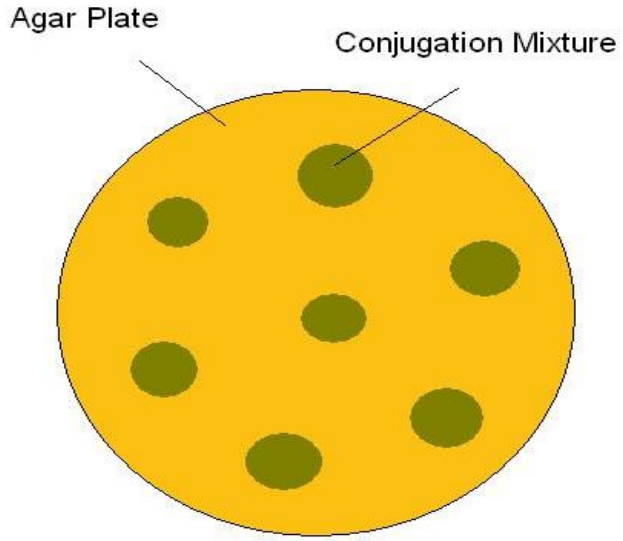

Figure 25: Discrete spots of conjugation mixture on Agar plate

4. The plate was not inverted. The plate was incubated at 37°C for 4-8 hours under anaerobic conditions to allow conjugal transfer of the plasmid from the E. coli donor to the *C. sporogenes* recipient.

5. 1ml of anaerobic sterile PBS was pipetted onto the conjugation plate. Using a sterile spreader, The layer of cells was scraped off the plate and was re-suspended in the PBS.

6. Using a pipette, the cell-PBS slurry was transfered into a fresh microtube as much as possible. 100 µl of the neat and 10-fold diluted slurry were spread onto fresh plates containing an appropriate anaerobic solid growth medium, supplemented with 250 µg/ml cycloserine to select against the E. coli conjugal donor and any other antibiotic to select for the plasmid.

7. After incubation at 37°C for 24-72 hours colonies were large enough to pick.

5.5 GFP Assay

GFP intensity was measured by plate reader or spectrophotometer and spectroflurometer. When using a spectroflurometer and spectrophotometer, first the bacteria were grown to their maximum concentration and then the dilution ratio was determined to avoid saturation of the

spectroflurometer. The bacteria was cultured in a 15 ml tube containing 10 ml of media and with an initial OD around 0.1. At each sampling time, 1 ml of bacteria was stored in a 1.5 ml tube. The OD was read by spectrophotometer. The bacteria were washed twice by PBS and were then diluted in a 1 ml cuvette by the obtained dilution factor. The fluorescent intensity was measured by spectroflurometer.

When the plate reader was used, a 500 µl bacterial culture was centrifuged, and after discarding the supernatant, the pellet was washed with 500 µl PBS twice and was suspended in 500 µl of BPS. Three samples of 150 µl were placed in a black 96 Well plate. A Synergy 2 micro-mode multi-plate reader was used to measure OD600 and the fluorescent intensity of the samples. In order to measure the fluorescent intensity of the bacteria harboring *evoglow* gene, the excitation and emission wavelength were set to 448 µm and 496 µm, respectively. For bacteria harboring *gfp* gene from I1305, the excitation and emission wavelength were 395 µm and 509 µm. The OD was read with absorbtion wavelength of 600 µm.

Chapter 6:

Experimental Results and Discussion

6.1 Introduction

Targeting cancer cells with the minimal side effect on healthy cells and tissue is a major challenge in cancer therapy. By using spore forming strictly anaerobes bacteria such as Clostridium as a drug delivery system, anticancer drugs can be delivered to the necrotic part of a tumor but, the abnormal cells in more oxygenated parts remain unaffected and the tumor will regrow from this viable outer rim. To address this problem, we designed a genetic circuit that controls the production of an aerotolerance enzyme via a quorum sensing promoter. The behavior of the engineered bacteria is the same as the native strain until the population density reaches a threshold. At the threshold density the genetic circuit is activated and the bacteria become aerotolerant.

In order to develop a density dependent aerotolerance strain of *C. sporogenes*, we followed two routes in the experimental side of this project. First we engineered three different quorum sensing promoters into C. sporogenes and secondly we expressed an aerotolerance gene in C. sporogenes and studied the growth of the bacteria in the present of oxygen. The candidate promoters for quorum sensing are: the *lux* promoter from *V. fischeri*, and the *P2* and *P3* promoters from *S. aureus* (ATCC 700699). The behavior of these promoters had not previously been characterized in *C. sporogenes*. In order to quantify the behavior of each promoter, the n*oxA* gene in genetic circuits proposed in Figure 21 and 22 (section 4.1) was replaced by the green fluorescent protein (GPF) gene. As was explained in Section 5.4, three different plasmids were constructed which contain the proposed genetic circuits. The three genetic circuits were cloned on the pMTL822x shuttle vector and were transformed into the *E. coli* donor strain (*E. coli* CA434 from the Younge lab) by electroporation. In order to transform the plasmids into *C. sporogenes*, the CA434 strains harboring the three different shuttle vectors were conjugated with *C. sporogenes*. Conjugated colonies were screened by GFP assay as described in Section 5.5. As the data in the following sections shows, the GFP assay revealed that the *V. fischeri* promoter was not activate in *C. sporogenes*, the *P2* promoter exhibited constitutive activity, and the *P3* promoter was observed to be activate at high concentration of the bacteria and exhibited a switch-like response to

concentration. Therefore the *P3* promoter from *agr* operon of *S. aureus* appears to be the best candidate for implementing synthetic quorum sensing in *C. sporogenes*

In order to demonstrate the effect to which the NoxA protein from *C. aminuvalericum* is able to confer aerotolerance on *C. sporogens*, the *noxA* gene from *C. aminuvalericum* genome (ATCC 13725) was cloned in front of *thl* promoter and the result was cloned into the shuttle vector. The shuttle vector was then transform into *C. sporogenes* by conjugation. The growth of the engineered C. sporogenes in the present of oxygen was compared with native strain. As the data in the following sections shows, the engineered *C. sporogenes* was able to grow in the presence of oxygen while the native strain could not.

6.2 Construction of devices and plasmids

Four different series of plasmids were constructed in this project, a gram negative quorum sensing construct, a gram positive quorum sensing construct, a constitutive construct and an aerotolerance construct. The gram negative quorum sensing construct includes *lux* operon elements of *V. fischeri* such as the *lux* promoter and the *luxR* and *luxI* gene. The gram positive quorum sensing construct includes the *agr* operon and other elements of *S. aureus* such as the *agrA*, *agrB*, *agrC*, *agrD* genes and the *p2* and *p3* promoters. The constitutive construct includes the thiolase promoter (*thl*) which is a strong promoter from *C. acetobotericum*. The aerotolerance construct includes the *noxA* gene from *C. aminovalericum*. Table 13 summarizes the list of the plasmids and the method used to construct both the subcloning and final plasmids.

In order to demonstrate the behaviour of the *V. fischeri* quorum sensing mechanism in *E. coli* and *C. sporogenes*, a sender device that produces AHL and a receiver device that expresses a GFP protein in response to AHL were constructed. The two devices were then combined into a single genetic circuit to construct the final plasmid called "E. coli QS GFP" which contains all required genes and promoters of the *V. fischeri* quorum sensing (*luxR*, *luxI*, *lux pR* and *lux pL*). The behaviour of the combination of sender and receiver devices was compared with that of "E. coli QS GFP" in *E. coli* and show similar behaviour. *E. coli* QS GFP plasmid was chosen to be transformed into *C. sporogenes* to investigate the behaviour of *V. fischeri* quorum sensing in *C. sporogenes*. In order to arrive at a construct that can express the reporter gene in an anaerobic system, the *gfp* genes from I1305 in the constructed plasmids were substituted with the *evoglow* gene from pGlow-XN-pp1-CI to construct pMTL-QS-evoglow.

Two different plasmids were constructed to investigate the behaviour of the *P2* and *P3* promoters (from the *agr* operon of *S. aureus)* in *E. coli* and *C. sporogenes*. These plasmids were called PAG2 and PAG3. The *noxA* gene was cloned downstream of the *thl* promoter to construct plasmid PTN. In order to quantify the production of the aerotolerance protein *noxA*, the *gfp* gene was fused into the *noxA* gene in plasmid PTGN.

6.2.1 Sender and Receiver plasmids, and QS plasmid with reporter gene for *E. coli*

Bacteria carrying the sender plasmid produce AHL; those that carry the receiver plasmid express a reporter gene when exposed to AHL. In order to construct receiver and sender plasmids, two Biobrick standard parts were chosen: BBa_F1610 and BBa_F2621. Figure 26 shows the schematic plot of these two plasmids.

BBa_F1610 contains the *luxI* gene and BBa_F2621 contains the *luxR* gene and the left and right promoters of the lux operon (*lux pR* and *lux pL*). Since we wanted to use these devices in gram positive bacteria, the first step was to change the sequence of the ribosome binding site of the *luxR* and *luxI* genes (AGGAGA) to those of gram positive bacteria (AGGAGG). The RBS's were changed using PCR and QuikChange II Site-Directed Mutagenesis Kit. The primers used for PCR were Mut_F2621_f, Mut_F2621_r, Mut_F1610_f and Mut_F1610_r. The result was validated by sequencing.

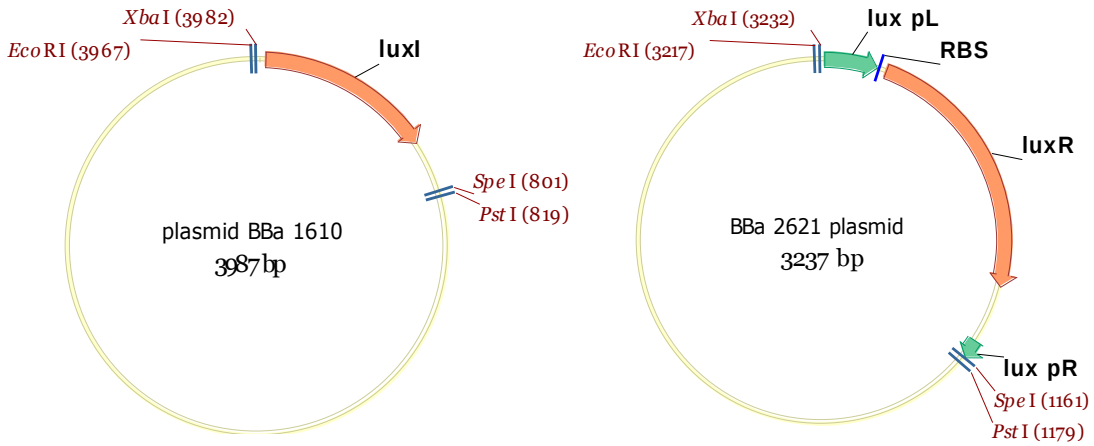

Figure 26: Biobrick parts a) BBa_F1610 and b) BBa_F2621

In order to construct the sender device, the *luxI* gene with gram positive RBS was digested from mutated BBa_F1610 using XbaI and PstI restriction enzymes and was cloned into mutated

BBa_F2621 at the SpeI and PstI site (XbaI and SpeI have compatible ends). Figure 27 shows the schematic map of the sender device

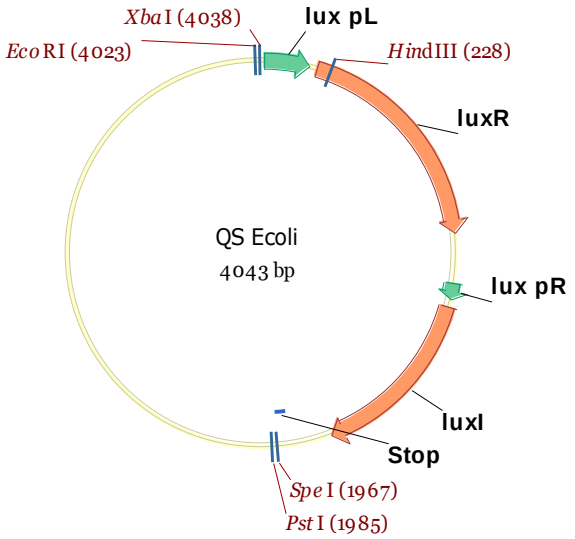

Figure 27: Sender plasmid containing *luxI* and *luxI* genes with gram positive RBS

To construct the receiver plasmid, a reporter gene was cloned downstream of the *lux* promoter. The *gfp* gene from Biobrick part I13504 was digested by XbaI and PstI and the resulting insert was cloned at the SpeI-PstI site of BBa 2621 plasmid. Figure 28 shows the schematic map of I13504 and the receiver plasmid.

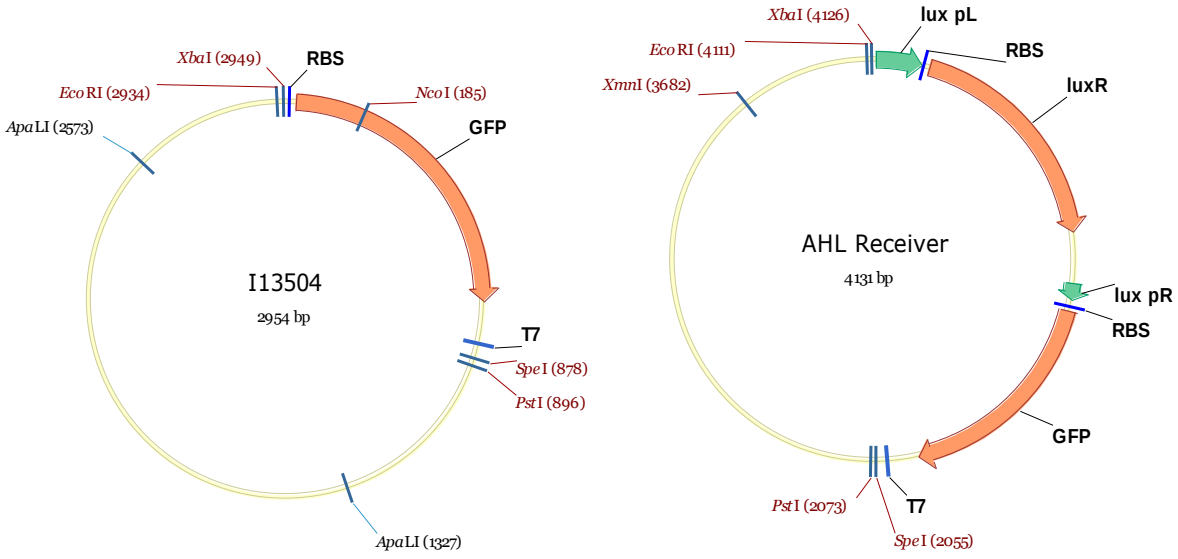

Figure 28: Schematic map of I13504 biobrick part and AHL receiver plasmid

The reporter gene (*gfp*) from I13504 was cloned downstream of the *luxI* gene in the sender plasmid to construct an integrated plasmid. This plasmid includes all the required lux quorum sensing elements and could be used to characterize the behavior of the *Vibrio fischeri* quorum sensing mechanism in *E. coli*. Figure 29 shows the schematic image of QS plasmid with the reporter gene.

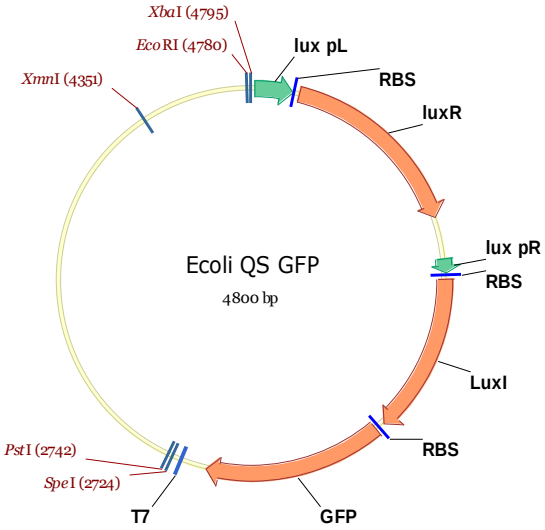

Figure 29: The schematic image of QS plasmids with reporter gene

6.2.2 Sender and receiver plasmids, and QS plasmid with reporter gene for *C. sporogenes*

As a preliminary confirmation, the constructed plasmids were used to demonstrate the behavior of the *V. fischeri* quorum sensing mechanism in *E. coli* (results shown in chapter 6). To demonstrate the behavior of the *V. fischeri* quorum sensing in *C. sporogenes*, the genes and promoters from the plasmids described in Section 6.3.2 were cloned into the Pmtl8225x shuttle vector. Both receiver and sender plasmids were digested was digested by EcoR1 and XbaI , and the 2005 bp and 2700 bp inserts were subcloned into EcoR1-XbaI site of Pmtl8225x. Figure 30 shows the plasmid QS-pmtl and QS-pmtl, with the GFP plasmid, that were used to implement the gram negative bacteria quorum sensing in *Clostridium sporogenes.*

The *QS_Ecoli* plamid was digested by *EcoR1* and XbaI and the 2000 bp insert was subcloned into EcoR1-SpeI site of Pmtl8225x. Figure 30 shows the plasmid QS-pmtl.

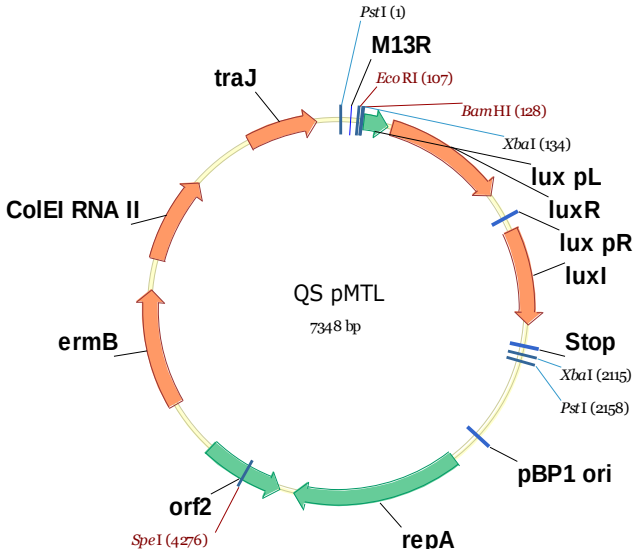

Figure 30: QS-pmtl plasmid for transforming quorum sensing mechanism of gram negative bacteria into gram positive bacteria

In order to construct a receiver plasmid that can be functional in *Clostridium*, the receiver plasmid was digested by EcoR1 and SpeI and the insert was cloned into EcoR1-XbaI of Pmtl8225x.

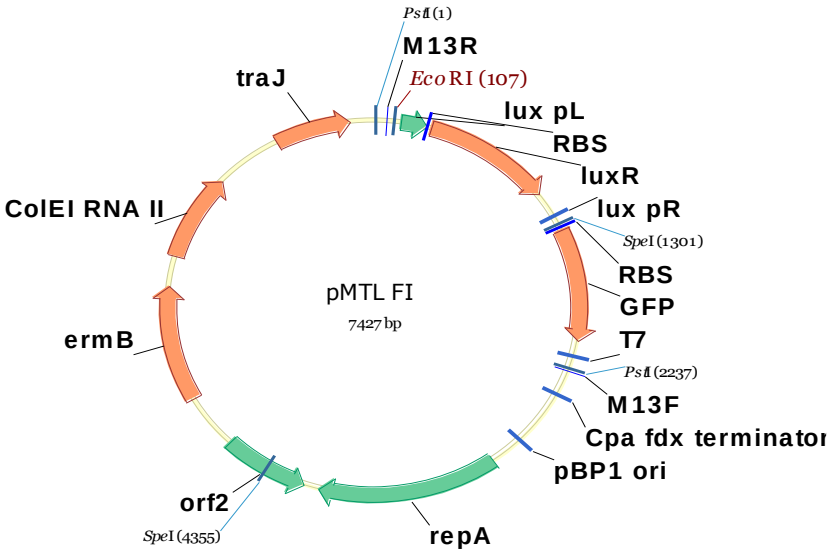

Figure 31: Pmtl-FI, the sender plasmid for Clostridium

Figure 31 shows the schematic image of pmt-FI, which acts as a receiver plasmid in *Clostridium sporogenes*.

In order to implement the quorum sensing mechanism mechanism of *Vibrio fischeri* into *Clostridium sporogenes* using a single plasmid, the E. coli_QS_GFP plasmid was digested by EcoR1 and XbaI and the 2700 bp insert was subcloned into EcoR1-XbaI site of Pmtl8225x. Figure 32 shows the schematic image of pMTL_QS_GFP plasmid.

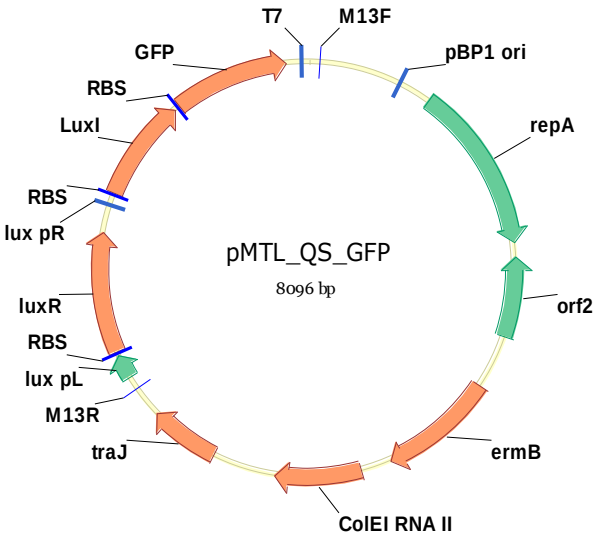

Figure 32: Schematic image of PmtL_QS_GFP

6.2.3 Anaerobic GFP (Flavin Mononucleaotide (FMN)- based fluorescent)

Most of the commercially available *gfp* genes cannot function as reporters in anaerobic systems because oxygen is needed for the synthesis of fluorophores. The flavin mononucleotide (FMN)-based fluorescent proteins (FbFPs) were developed to overcome this problem. The *evoglow* series from BioCat GmbH is a FMN-based fluorescent protein that is functional under both aerobic and anaerobic conditions [98]. Figure 33 shows the map of the pGlow-XN-pp1-CI (pGlow) plasmid, which contains the *evoglow-pp1-CI* (*evoglow*) gene which is expressed by the *thl* promoter. The *thl* promoter is a strong constitutive promoter for *C. acetobutericum* [98]. The *evoglow* gene originated from the Gram-positive

bacterium *Bacillus subtilis*. It was modified using codon usage optimization techniques to be expressed effectively in Clostridium [98].

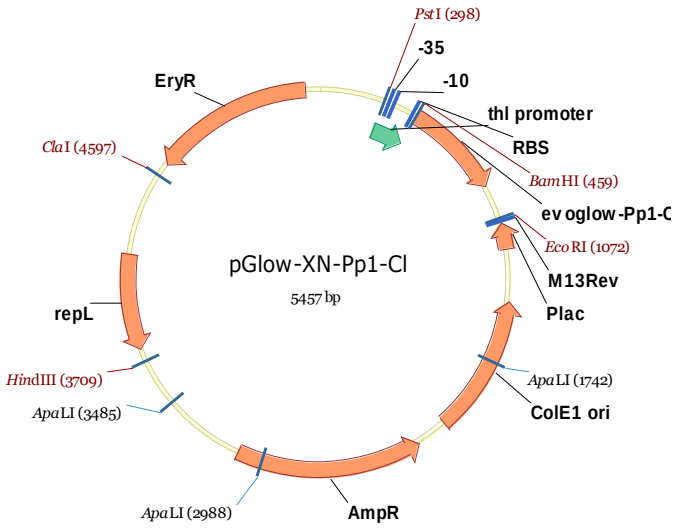

Figure 33: Schematic map of pGlow [98]

The *evoglow* gene was amplified from pGlow plasmid by PCR, using pglow_f_XbaI and pglow_r_pstI_spei primers. The result was inserted into a Teasy plasmid using pGEM®-T Easy Vector Systems from Promega to construct a *Teasy-evoglow* plasmid.

6.2.4 QS plasmid with anaerobic reporter gene

Teasy-evoglow was digested by XbaI and PstI and the resulting insert was cloned into the SpeI-PstI site of F1610 to construct the F1610_evoglow plasmid. This F1610_evoglow plasmid was similarly digested by XbaI and PstI and was cloned into the SpeI-PstI site of F2620 plasmid to construct the Ecoli_QS_pglow plasmid. Finally the Ecoli_QS_pglow was digested by EcoR1 and XbaI and the resulting insert was cloned into the XbaI-EcoR1 site of the pMTL8225x plasmid to construct the pmt_QS-pglow plasmid. Figure 34 shows the schematic image of Ecoli_QS_pglow and pmt_QS-pglow plasmids .

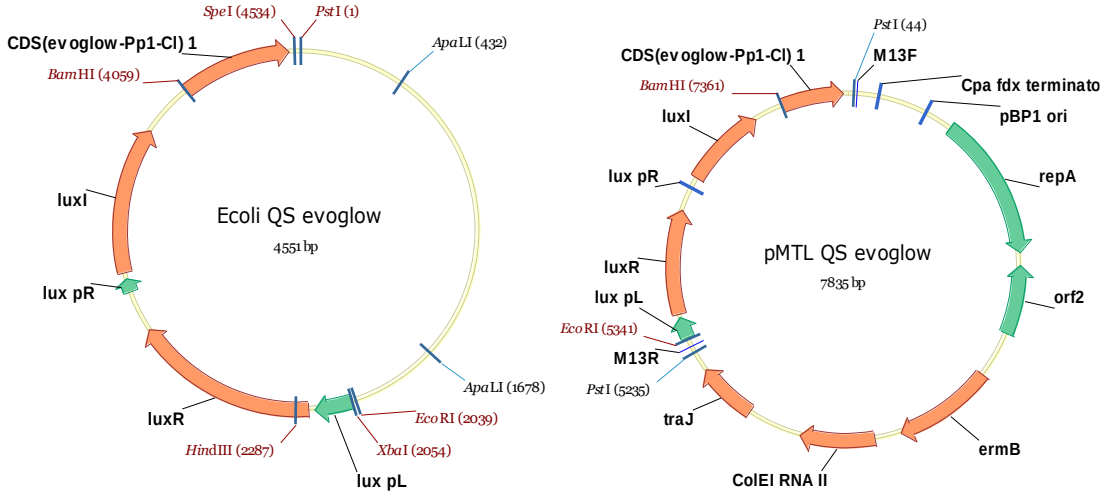

Figure 34: Schematic image of Ecoli_QS_evoglow and pMTL_QS_evoglow

The existence of the insert was verified by sequencing the plasmids

6.2.5 Constitutive GFP Plasmid

To construct a positive control for *Clostridium*, the evoglow gene was cloned downstream of the *thl* promoter on the pMTL8225x shuttle vector. The *thl* promoter and *evoglow* gene were amplified from the pGlow plasmid using PCR with *thl_f* and pGlow_SpeI_PstI primers. The PCR product was cloned into the Teasy plasmid. The Teasy plasmid was digested by EcoR1 and SpeI and the resulting insert was cloned into the EcoR1-XbaI site of the shuttle vector to construct the Pmtl_Thl_glow plasmid.

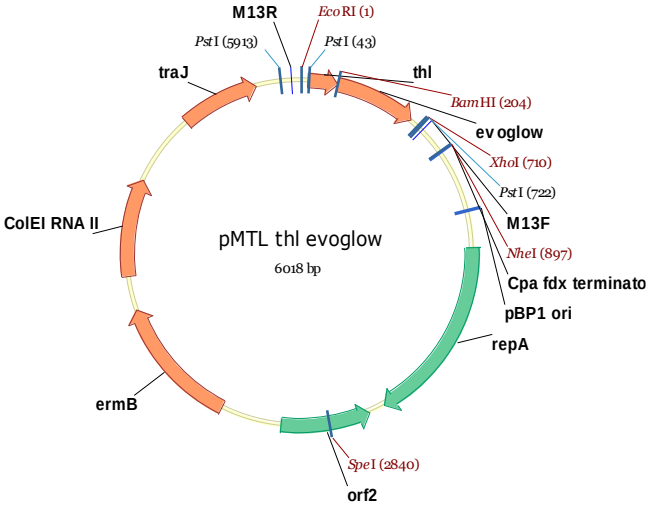

Figure 35: The schematic image of the pMTL_thl_evoglow plasmid

Figure 35 show the schematic image of the Pmtl_Thl_glow plasmid. The existence of the insert was confirmed by sequencing.

6.2.6 Gram Negative quorum sensing mechanism with Anaerobic GFP

To construct the receiver plasmid, the *Evoglow* gene was amplified by PCR from the pGlow-Xn-Pp1-CI plasmid. Two primers, pglow_r and pglow_r, were used for PCR. The PCR product was inserted on pGEM®-T Easy Vector (Promega) to construct the pGEM_evoglow plasmid. The pGEM_evoglow plasmid was digested by XbaI and pstI and the resulting insert was cloned into the SpeI-PstI site of the I13504 plasmid to construct the I13504_evoglow plasmid. The I13504_evoglow plasmid was digested by XbaI and PstI and the resulting insert was cloned into the SpeI-PstI site of the F2621 plasmid to construct the FI_evoglow plasmid. Figure 36 shows schematic images of the FI_evoglow and I13504_evoglow plasmids.

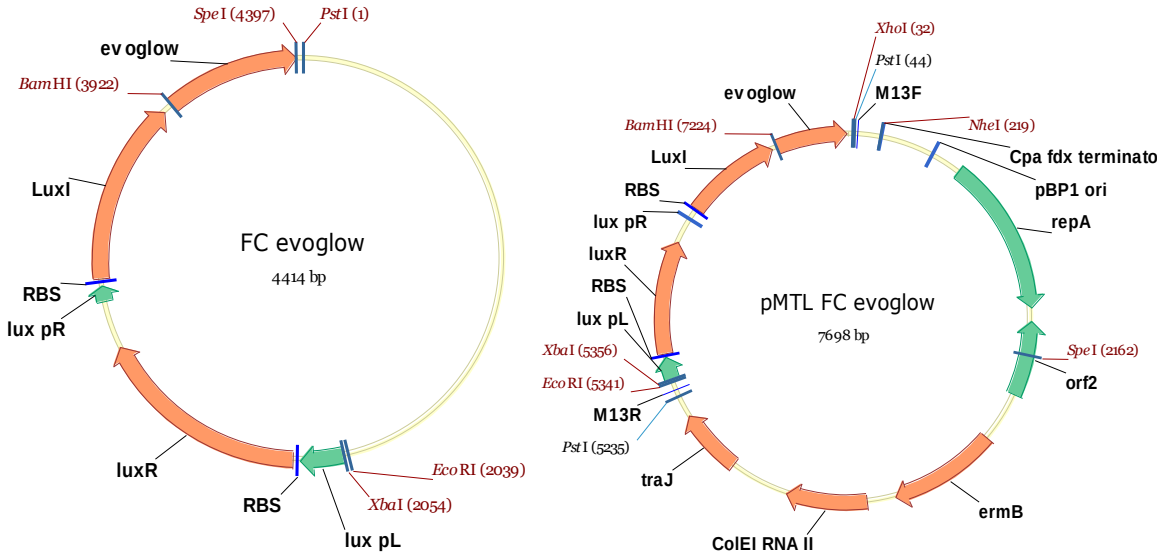

Figure 36: Schematic image of FC_evoglow and pMTL_FC_evoglow

6.2.7 Gram Positive Quorum Sensing Mechanism with Anaerobic GFP using *P2* promoter

To construct a plasmid with gram positive quorum sensing elements, the *agr* operon (~3 kbp) was amplified from the *S. aureus* (ATCC 700699) chromosome using GenBank sequence BA000017.4 by PCR with *agr_r* and *agr_f* primers which had EcoR1 and XbaI site on them respectively.

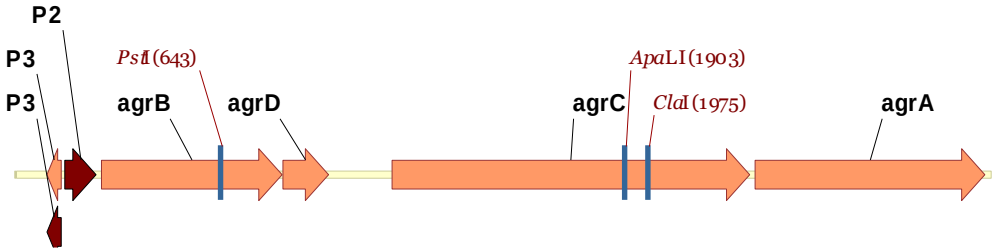

Figure 37: the schematic map of agr operon on the C. acetobutericum

As Figure 37 shows, the *agr* operon consists of three genes (*agrA*, *agrB*, *agrC* and *agrD*) and two promoters (*P2* and *P3*). The PCR product was digested by EcoR1 and XbaI and the resulting segment was cloned into the EcoR1-XbaI site of Pmtl8225x.

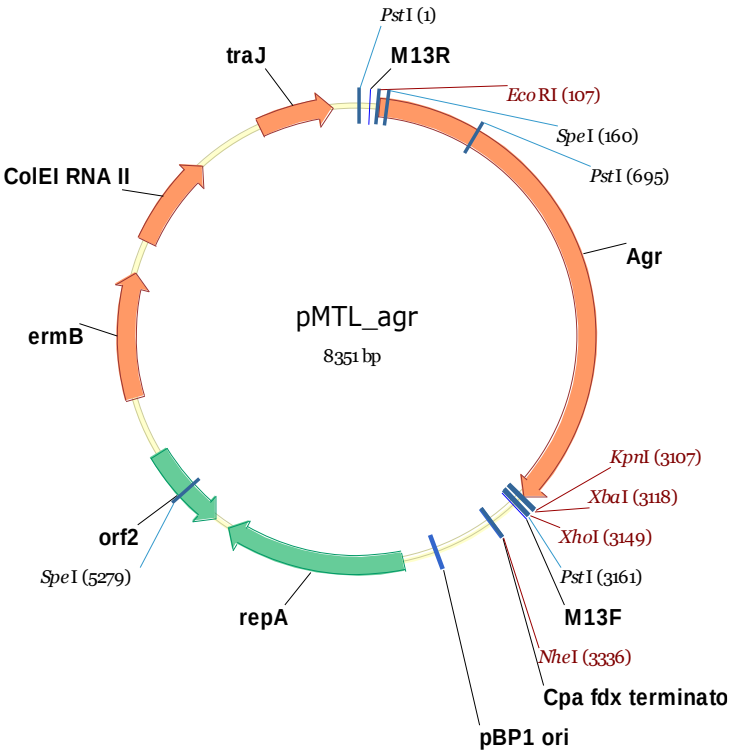

Figure 38: Schematic map of pmtl_Agr plasmid

Figure 38 shows the pmtl_agr plasmid, which has the *agr* operon on the shuttle vector.

In order to quantify the activity of the agr quorum sensing mechanism, the evoglow gene was fused downstream of the agr operon. The evoglow gene was amplified from the pGlow-Xn-Pp1-CI plasmid using the glow_f and glow_r primers (glow_f includes the kpnI restriction site; glow_r contains the XbaI site). The PCR product was digested by KpnI and XbaI and was inserted into the KpnI-XbaI site of Pmtl_agr plasmid. Figure 39 shows the schematic map of the resulting plasmid.

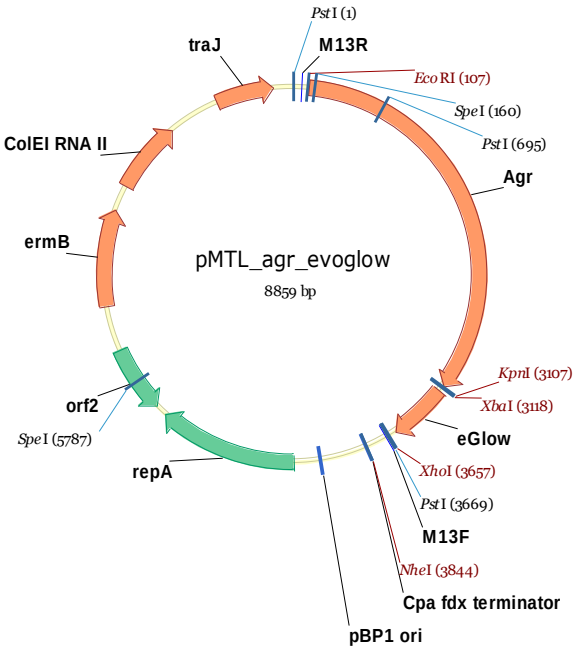

Figure 39: Schematic map of Pmtl_agr_glow plasmid

The existence of *agr* operon and *evoglow* gene was validated by gel electrophoresis and sequencing

6.2.8 Gram Positive QS Mechanism with Anaerobic GFP using *P3* Promoter

The *P2* and *P3* promoters of the *agr* operon of *Staphylococcus aureus* regulate RNAII and RNAIII transcripts, respectively. The expression of evoglow can be controlled either by *P3* promoter or *P2* promoter. To quantitatively measure the activity of the p3 promoter in *Clostridium sporogenes*, the *evoglow* gene was amplified from the pGlow-Xn-Pp1-CI plasmid, using the pglow_f_XbaI and pglow_r_pstI_spei primers. The resulting PCR product was cloned into PGEM_T_Easy plasmid to construct the PGEM-T_evoglow plasmid. Figure 40 shows the schematic image of PGEM-T_evoglow plasmid.

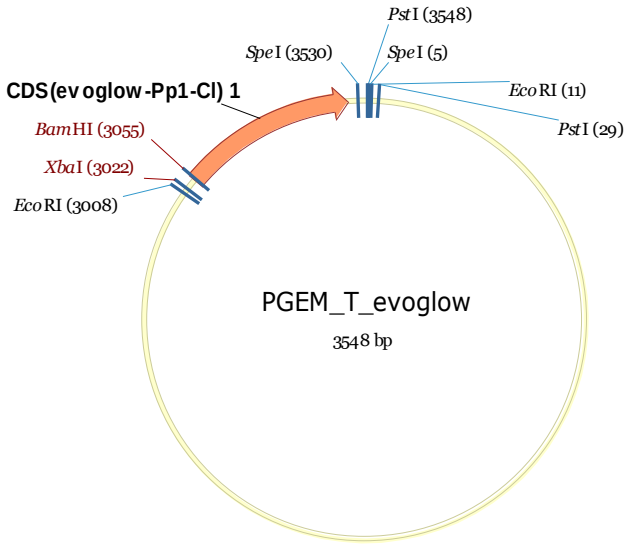

Figure 40: Schematic image of PGEM-T_evoglow

The PGEM-T_evoglow plasmid was digested by EcoR1 and the resulting fragment was cloned in the EcoR1 site of pMTL_agr plasmid to construct pMTL_agr_evoglow_p3 (.PagrG_p3) Gel electrophoresis image was used to pick up the right colonies.

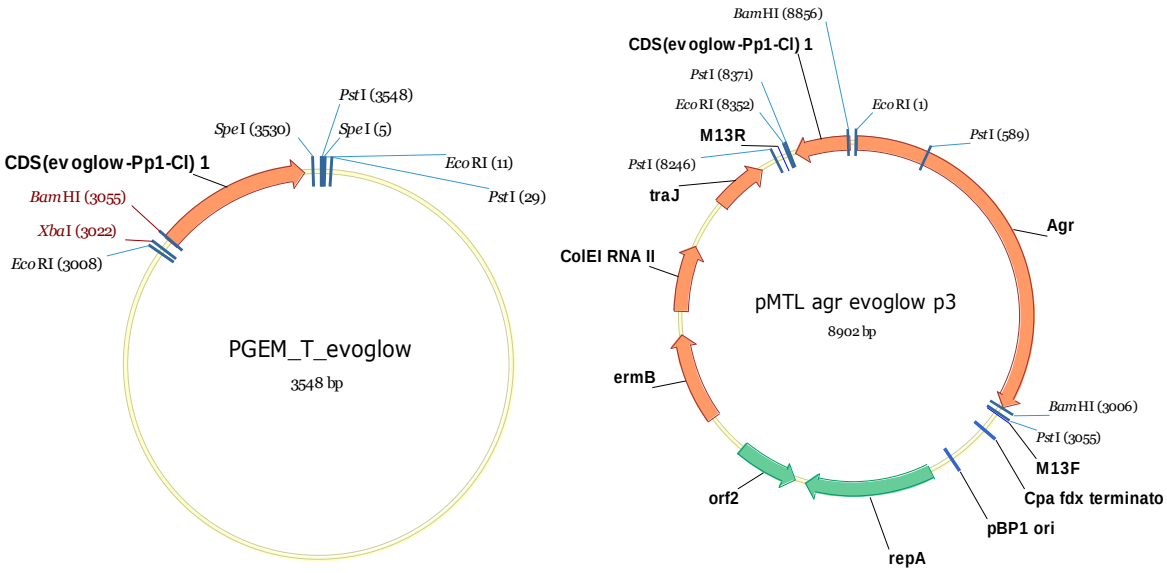

Figure 41: Schematic image of PGEM_T_evoglow and pagrG_p3

Figure 41 shows the schematic image of PagrG_p3. Sequencing and gel electrophoresis was used to pick up the colony with the proper insertion.

6.2.9 Constitutive, gram negative and gram positive aerotolerant plasmid

In order to put the aerotolerance enzyme (NoxA) production under the control of *thl* promoters and quorum sensing promoters of gram negative and gram positive bacteria, the *noxA* gene was amplified from the *C. aminovalericum* (ATCC 13725) chromosome using GenBank sequence AB219226.1 by PCR with primers *noxA_XhoI* and *noxA_NheI*.

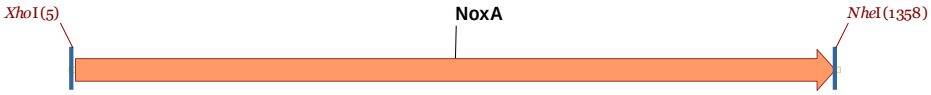

Figure 42: *noxA* gene on the chromosome of *C. aminovalericum*

Figure 42 shows the schematic map of the PCR product. The PCR product was cloned into a clonejet vector as shown in figure 43.

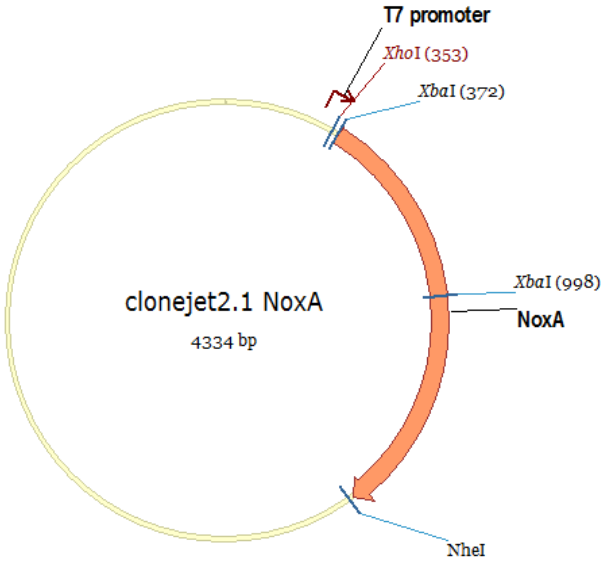

Figure 43: Schematic image of clonejet2.1_noxA plasmid

The *cloneget_noxA* was digested by *NheI* and *XhoI* and the resulting insert was cloned into the *XhoI-NheI* sites of the *pMTL_thl_evoglow*, *pMTL_FC_evoglow*, and *pMTL_agr_evoglow_p2* plasmids.

Figure 44 shows the schematic image of the pMTL_thl_evoglow_noxA, pMTL_FC_evoglow_noxA, and pMTL_agr_evoglow_noxA *P2* plasmids. pMTL_thl_evoglow_noxA provides constitutive

expression of the aerotolerance enzyme NoxA. The *evoglow* reporter gene was used to quantify the level of the aerotolerance enzyme production. pMTL_FC_evoglow_noxA can control the expression of aerotolerance enzyme by quorum sensing mechanism of gram negative bacteria (*V. fischeri*). pMTL_agr_evoglow_noxA P2 can control the expression of aerotolerance enzyme by quorum sensing mechanism of gram positive bacteria (*S. aureus*).

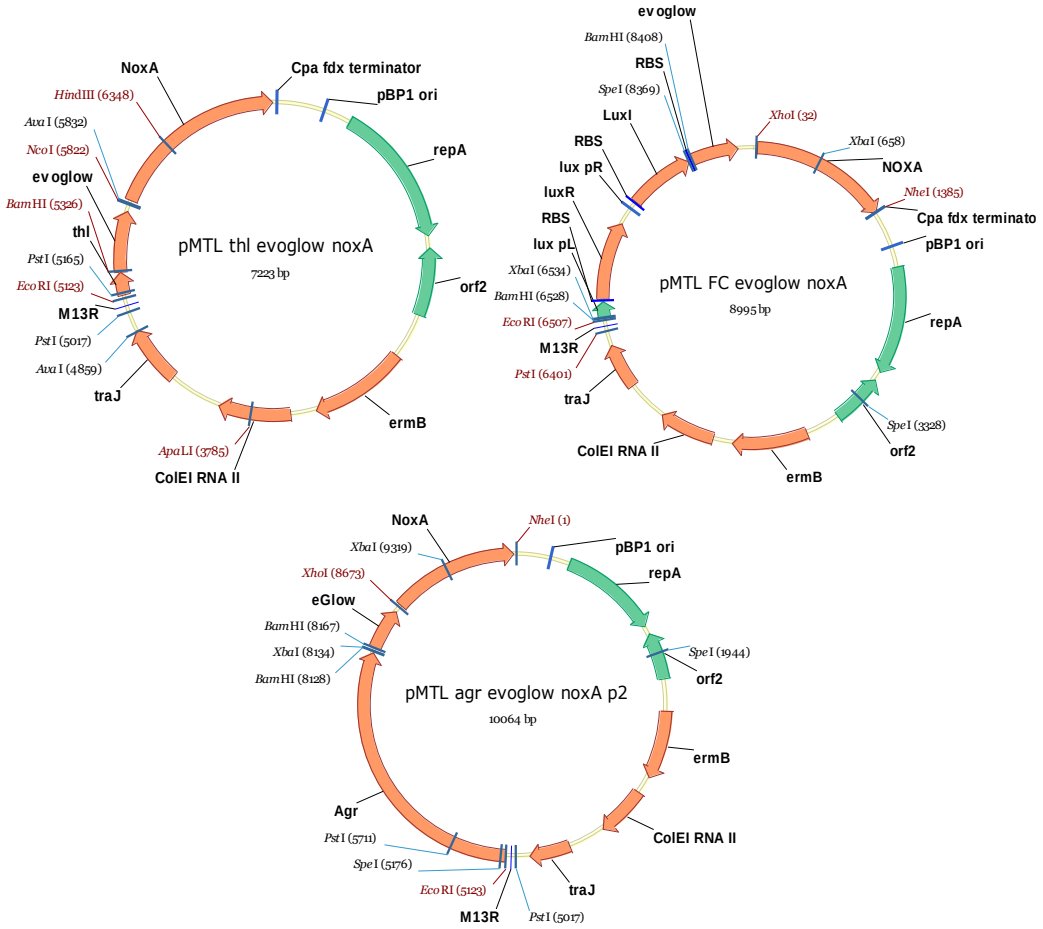

Figure 44: Schematic image of pMTL_thl_evoglow_noxA, pMTL_FC_evoglow_noxA, and pMTL_agr_evoglow_noxA_P2

6.3 Plasmid transformation into *C. sporogenes*

Both electroporation and conjugation were investigated as techniques to transfer genes into *C. sporogenes*. The electroporation attempts were unsuccessful. A protocol was provided by Liu et al which made use of an *E.coli* Pulser with a capacitance of 25 μF [29]. This device was not available,

and so electroporation attempts were made with a Micropulser, which has a capacitance of 10 μF. The reduced capacitance meant that the time constant (product of the resistance and the capacitance) of the original protocol could not be replicated. Initially, the time constant was about 1.5 *ms* (much lower than the constant of 3 *ms* in the protocol). Attempts were made to increase the time constant by increasing the resistance, by using an electroporation buffer with lower concentration of salts, and by using a smaller volume of electroporation buffer. A range of concentrations of $MgCl_2$ and Na phosphate and a range of sample volume were tested, but none could significantly increase the time constant. The highest time constant attained in these investigations was about 2 *ms*, which is much lower than prescribed in the protocol. In the last attempt, a 0.4 cm electroporation cuvette was used which brought the time constant to about 3 *ms*. Ultimately, the electroporation attempts were discontinued because it was determined that conjugation could be used to successfully transform plasmids into *C. sporogenes*.

Initial attempts at conjugation were focused on *C. sporogenes* strain ATCC 3584. *E.coli* strains S.17 and CA434 were used as the donor strains to transfer plasmid pJIR1457 and pMTL8225x into ATCC 3584 (using the protocol outlined in Chapter 5), but the conjugative transfers were not successful. A subsequent round of conjugation attempts were performed with an alternative strain: *C. sporogenes* strain NCIMB 10696. The two shuttle vectors (pMTL8225x and pJIR1457) were successfully transferred into *Clostridium sporogenes* NCIMB 10696 using *E .coli* CA434 as the donor strain. The conjugative transfer of the plasmid was confirmed by plasmid isolation from *C. sporogenes*. The transferred strain was also inoculated aerobically and no bacteria growth was observed, indicating that there was no *E. coli* contamination in transferred culture of *C. sporogenes*.

National Collection of Industrial and Marine Bacteria (NCIMB) claims that *C. sporogenes* ATCC 3584 is the same strain as NCIMB 10696. But these results show that ATCC 3584 is different from NCIMB at least in gene transformation.

6.4 The Behaviour of a Gram Negative Quorum Sensing Mechanism in E.coli

In order to validate the phenotype of the designed genetic circuit, we first transformed it into *E. coli* and studied the reporter gene expression as the cell density varied.

The receiver and sender plasmids (pMTL_FI and pMTL_QS) were transformed separately into *E. coli CA434*. The receiver and sender *E. coli* were cultured together in a tube overnight. Figure 45

compares the fluorescent image of the tube containing mixed receiver and sender *E. coli* with the tube containing only the receiver *E. coli*. The isolated receiver *E. coli* did not produce GFP but the mixed culture shows GFP production at high bacteria concentration (OD600=1).

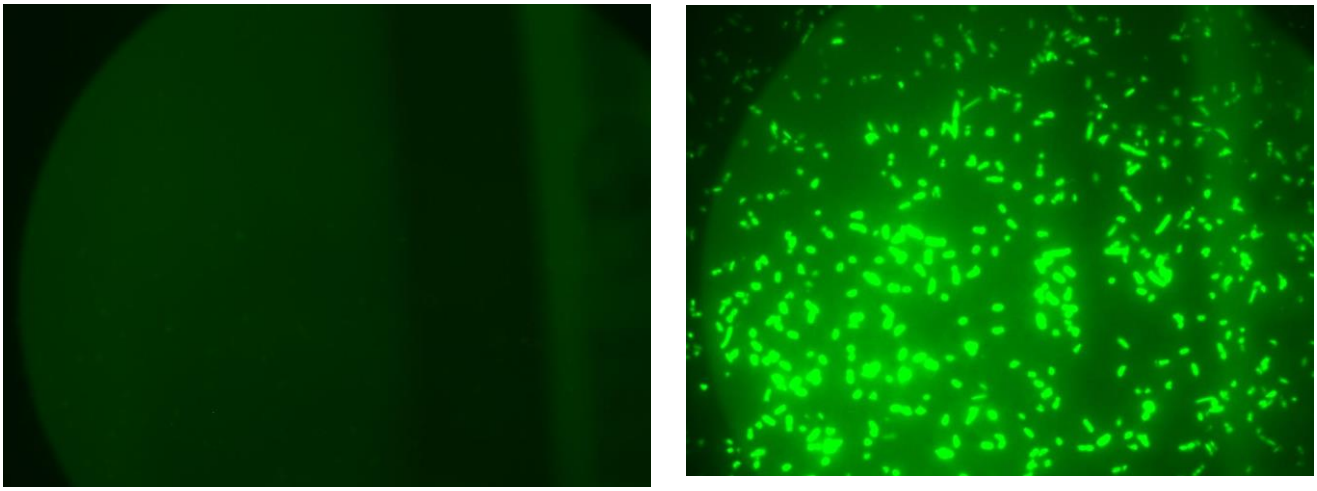

Figure 45: a) Receiver *E. coli* b) Receiver *E. coli* mixed with sender *E. coli*

The quorum-sensing device plasmid Pmtl_QS_GFP was transformed into *E. coli* CA434. The resulting colony showed minimal GFP expression (not visible under microscope) at low concentration, but when OD600 reached 1, the GFP become visible. Figure 46 shows fluorescent production of the *lux* promoter in *E. coli* CA434 harboring Pmtl_QS_GFP plasmid.

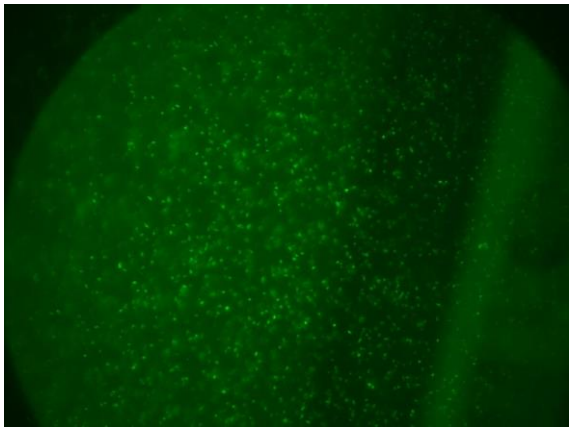

Figure 46: The fluorescent image of the *E. coli*, which harbors

To further validate the switch-like behavior of the quorum-sending mechanism in *E. coli*, fluorescent intensity and cell density were measured in three different strains by spectrofluorometery.

Three tubes of *E. coli* were inoculated. The first tube contained native *E. coli*, two other tubes contained the engineered *E.coli* harboring the QS_GFP plasmid. As a positive control, 1 mg/ml AHL was added to the second tube. The bacterial concentration and the GFP intensity were measured by spectrophotometery and spectrofluorometery (as described in Section 5.). The results are shown in Figure 47.

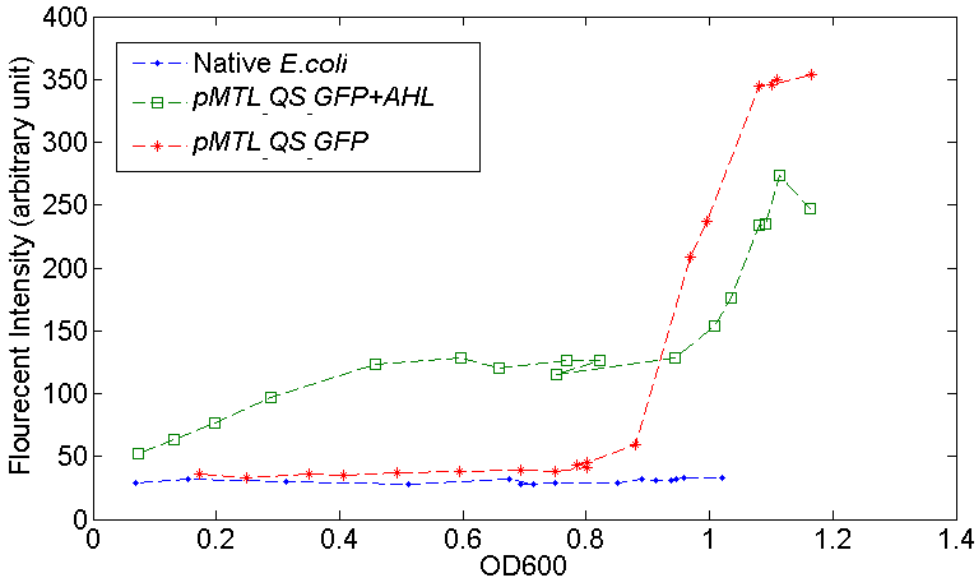

Figure 47: Comparison of GFP expression of native *E. coli* with the engineered *E.coli* harboring pMTL_QS_GFP plasmid with and without AHL in the media

The florescence intensity of the colony without the quorum-sensing plasmid was constant for all cell densities. In contrast, the florescence intensity of the colony harboring the QS plasmid (with reporter gene) was similar to the negative control at low densities (below OD600 of 0.9), but increased dramatically as the colony approached its maximal density. The transition occurred between OD600 0.9 and 1.1, above which the florescence intensity reached a plateau. The positive control colony (engineered *E.coli* with AHL) showed a linear increase in fluorescence until OD600 of 0.45, followed by a plateau until OD600 of 0.9, after which it increased rapidly and reached its maximum at OD600 of 1.1. The linear increase of fluorescence in this positive control tube can be associated with the activation of *lux* promoter by AHL. It is likely that the AHL concentration was enough to activate the *lux* promoter of bacteria up to OD 0.45, and above this population size, there was not enough AHL to activate *lux* promoters across the colony, leading to saturation. At OD600 of 0.9 the lux promoter was activated by the quorum-sensing mechanism, at which point the switch-like behavior was exhibited.

6.5 The Behaviour of Gram Negative QS Mechanism in C. sporogenes

The pMTL_FC_evoglow (PFCG) and pMTL_FC_GFP (PFCI) plasmid were transformed into *E.coli* CA434 by electroporation and then pMTL_FC_evoglow (PFCG) was transformed into *Clostridium sporogenes* by conjugation with *E. coli* CA434. The fluorescence intensity and cell density of *E. coli* harboring pMTL_FC_evoglow (PFCG) and pMTL_FC_GFP (PFCI) plasmid and *C.sporogenes* harboring *pMTL_FC_evoglow (PFCG)* plasmid were measured during colony growth using the method explained in Section 5.4.

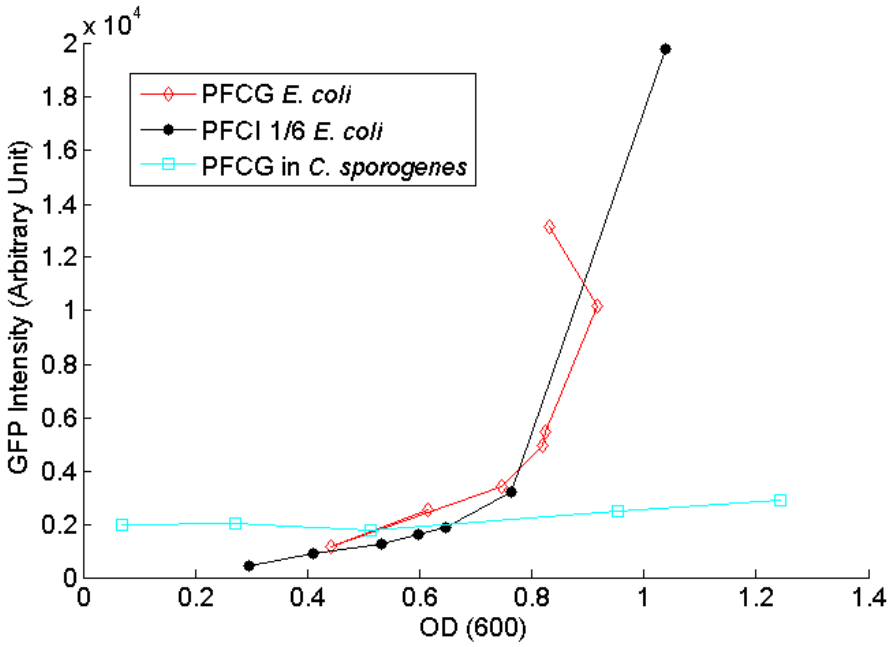

Figure 48: Florescent intensity of *C.sporogenes* and *E. coli* harboring pMTL_FC_evoglow(PFCG) *and* pMTL_QS_GFP (PFCI) plasmids

As Figure 48 shows, the *lux* promoter was not activated in *C. sporogenes*, while it produced the expected switch-like behavior in *E. coli*. The fluorescence intensity of GFP (PFCI) is 6 fold higher than evoglow (PFCG), therefore for comparison of the behavior, the fluorescence intensities of GFP were divided by six. The lack of activation of *lux* promoter in *C. sporogenes* may be associated to the thick cell wall membrane of *C. sporogenes*, which does not allow AHL to freely defuse in and out of the cell. Another possibility is quorum sensing quenching, caused by enzymes that can hydrolyze the lactone bond of AHL [99].

6.6 Behaviour of Gram Positive Quorum Sensing Mechanism in *C. sporogenes*

6.6.1 Behavior of the *P2* promoter in *C. sporogenes*

The pMTL_agr_evoglow_p2 (PAG2-1) and pMTL_thl_evoglow (PTG) plasmids were transformed into *C. sporogenes* by the conjugation method described in Section 5.4.2. The colonies recovered from conjugation were screened by GFP assay and gel electrophoresis of digested plasmid to select the transformed colonies. To investigate the *P2* promoter behavior, one colony of each type of transformed *C. sporogenes* was inoculated into a 15 ml falcon tube with 500 µg/ml D-Cyclocerine and 30 µg/ml of Erthromycin. A colony of *E. coli* CA434 harboring pMTL_agr_evoglow_p2 (PAG2-1) was also inoculated aerobically with 300 µg/ml of Erthromycin and 50 µg/ml of Kanamycin. The fluorescence intensity and cell density were measured using the method described in Section 5.4. Figure 49 shows the fluorescence production of *C. sporogenes* harboring pMTL_agr_evoglow_p2 (PAG2-1), pMTL_thl_evoglow (PTG) with the native *C. sporogenes* and the *E. coli* CA434 harboring pMTL_agr_evoglow_p2(PAG2-1).

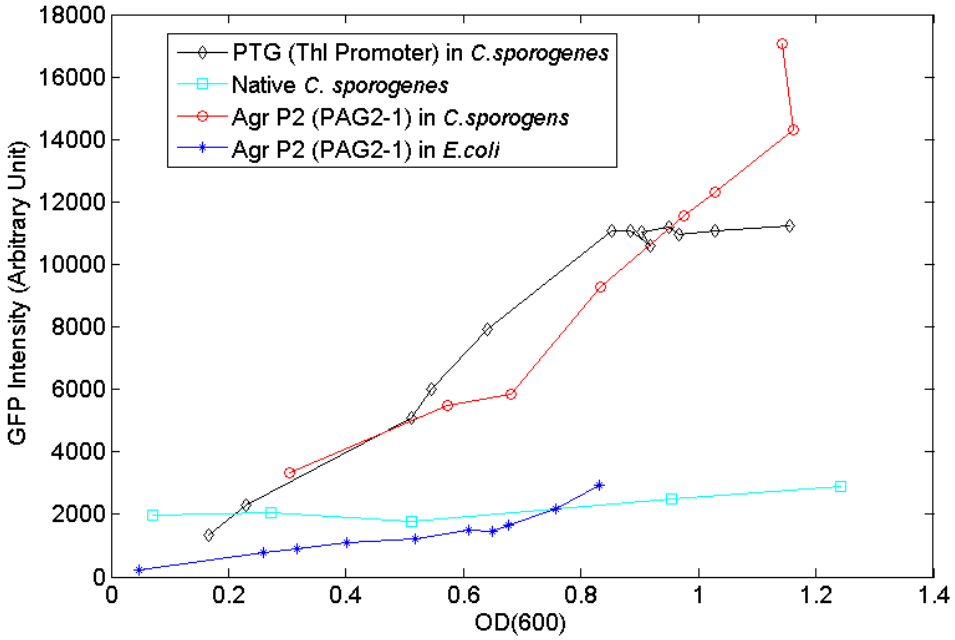

Figure 49: The behavior of the *S.aureus* quorum sensing mechanism with *P2* promoter in *C. sporogenes* and *E.coli* , fluorescence intensity versus cell density

As the figure shows, the *P2* promoter of the gram-positive quorum sensing mechanism (from *S.aureus*) does not show a switch like behavior and behaves more like a constitutive promoter in *Clostridium sporogenes*. This experiment was repeated three times with similar results. One potential reason for this behavior, as was reported by Koeing et.al [100], is that AgrA has a stronger affinity for *P2* promoter in low density than *P3* and a poor affinity in high density. Therefore at low density the low concentration of AgrA may be compensated by its strong affinity, with the result that the promoter shows a behavior similar to constitutive activity. As figure 49 shows, the *P2* promoter did not express GFP in *E. coli*. It has been shown that AIP can be produced by expression of *agrB* and *agrD* in *E. coli* [101], therefore, the lack of activation of *P2* promoter in *E. coli* could be due to the lack of AIP transport from cell wall by AgrB . The constitutive plasmid (PTG) has a linear trend until OD600=1 and then reaches a plateau. The native bacteria shows almost constant fluorescent intensity which is due to the background.

6.6.2 Behavior of the *P3* promoter in *C. sporogenes*

The Pmtl_thl_evoglow plasmid (PTG) and the pMTL_agr_evoglow_p3 plasmid were transformed into *E. coli* CA434 by electroporation to create the donor bacteria for conjugation. Plasmids were transformed into *C. sporogenes* by the conjugation method explained in Section 5.4.2. Transformation of the plasmids was verified by extracting the plasmid from *C. sporogenes* and using gel electrophoresis and sequencing.

To quantify the *P3* promoter behavior, *C. sporogenes* harboring Pmtl_thl_evoglow plasmid (PTG), and pMTL_agr_evoglow_p3 were inoculated into 15 ml falcon tubes with 500 µg/ml D-Cyclocerine and 30 µg/ml of Erthromycin. *E.coli* CA434 harboring pMTL_agr_evoglow_p3(PAG3-3) was inoculated aerobically with 300 µg/ml of Erthromyci*n* and 50 µg/ml . The fluorescence intensity and cell density were measured using the method explained in Section 5.4. Two samples were used for measurement and the mean was calculated at each sampling point. Figure 50 shows the fluorescence production of *C . sporogenes* harboring Pmtl_thl_evoglow plasmid (PTG)and pMTL_agr_evoglow_p3 with the native *C. sporogenes* and the *E.coli* CA434 harboring pMTL_agr_evoglow_p3(PAG3-3).

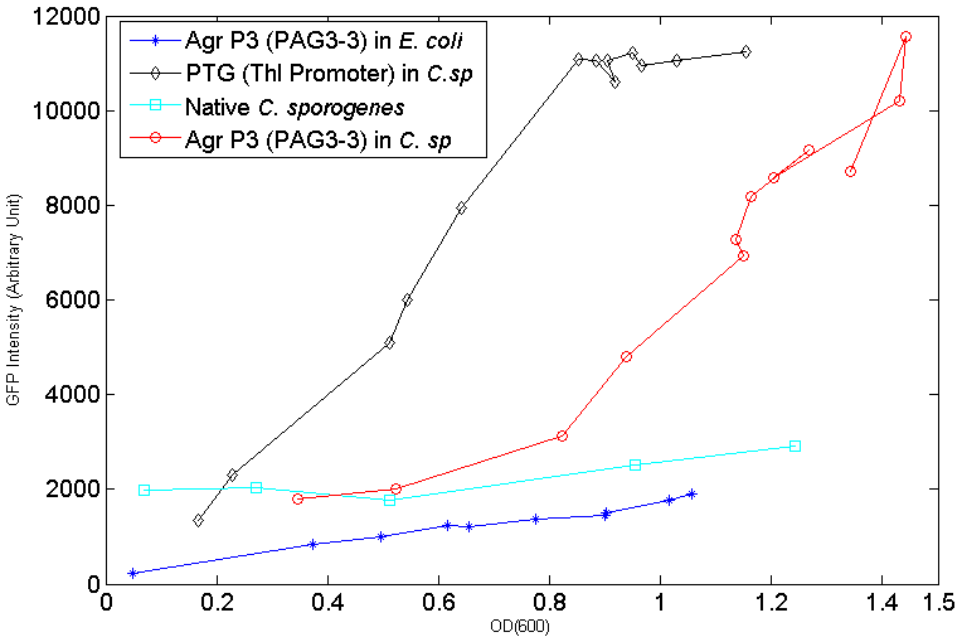

Figure 50: The behavior of the *S.aureus* quorum sensing mechanism with *P3* promoter in *C. sporogenes* and *E.coli* , fluorescence intensity versus cell density

As the figure shows, the *P3* promoter of the *agr* operon leads to a switch-like behavior in *C.sporogenes*. At low density (below OD600 of 0.8), the GFP intensity of the engineered strain is almost the same as native *Clostridium*. At higher density, the engineered strain exhibits much higher fluorescence. In contrast, the fluorescence production of the constitutive strain (positive control) is already significant at OD600 of 0.2. The figure also shows that the *P3* promoter did not express GFP in *E. coli*. As mentioned earlier, this may be caused by the lack of export of AIP to the outer membrane of the bacteria. Finally, the wild-type Clostridium strain (negative control) shows near constant fluorescence through the colony growth.

We subsequently studied the behavior of the *P3* promoter in *C. sporogenes* in three different media: TYG, TYG+0.5 Glucose and ½ TYG. Figure 51 shows the result of this study.

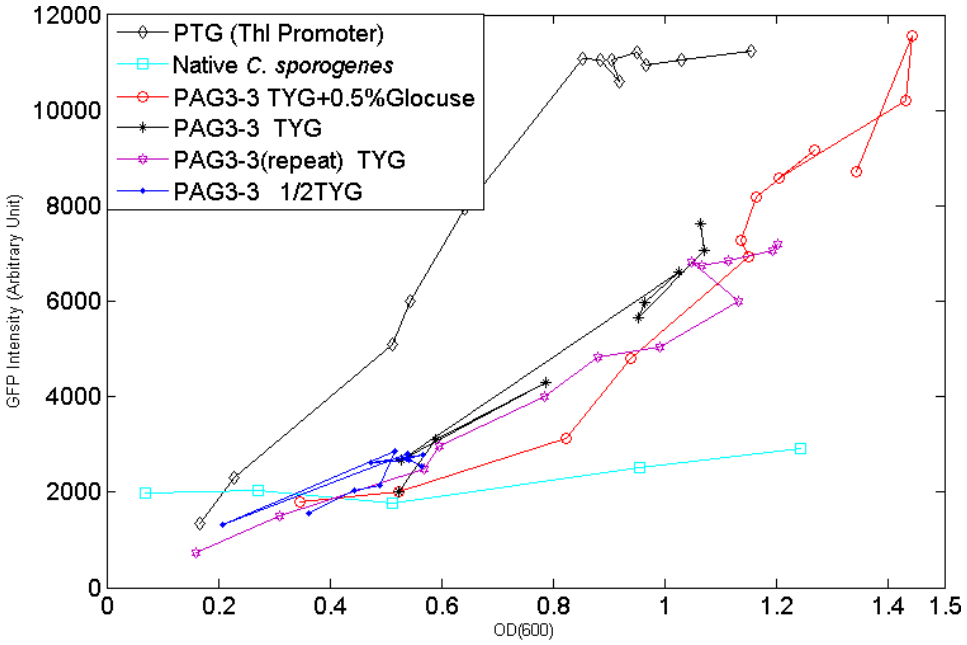

Figure 51: The behavior of *P3* promoter in *C. sporogenes* in different conditions

Engineered *C. sporogenes* could not grow beyond OD 0.6 in ½ TYG, but could grow until OD 1 in TYG. The bacteria could grow up to OD 1.5 in TYG+0.5 glucose suggesting that the bacteria stop growing in TYG because of the lack of carbon in the medium. The fluorescence intensity is fairly similar in all medium. The experiment also confirms the reproducibility of the result in Figure 50.

We conclude that the *agr* quorum sensing mechanism of S. aurous functions in *C. sporogenes* and so can be used for application in *Clostridium* mediated cancer therapy.

The *P3* promoter seems to be the best candidate for expressing density dependent aerotolerance enzyme, but we need to show that the candidate aerotolerance gene can make *C. sporogenes* aerotolerant. In the next section the behavior of engineered *C. sporogenes* harboring pMTL_thl_noxA will be compare with native strain study in the present of oxygen.

6.6.3 Behavior of the engineered *C.sporogenes* harboring aerotolerance enzyme expressed by *thl* promoter

In order to test the hypothesis that the expression of *noxA* gene in *C. sporogenes* makes the bacteria aerotolerance, the pMTL_thl_noxA plasmid was transformed into *C. sporogenes* by conjugation, as explained in Section 5.4.2. In pMTL_thl_noxA, the *noxA* gene is cloned downstream of the *thl* promoter to express aerotolerance enzyme constitutively. TY medium (30 % Tryptone, 20% Yeast

extract) was used for aerobic growth of *C. sporogenes*. Sodium thioglycollate was removed from TYG recipe because it makes the medium anaerobic. 500 µg/ml D-Cyclocerine and 30 µg/ml of Erthromycin were added to the culture of the engineered strain. Losen et al. [102] used shaking speed to control the oxygen concentration in the medium; a similar method was used here. The native and engineered strains of *C. sporogenes* were inoculated in two 13 ml tubes, each containing 7 ml of TY medium. We made the bacteria concentration in both tubes equal to OD 0.15 and kept them for 4 hours in the incubator without shaking, to revive their growth. Then we exposed the bacteria to different concentration of oxygen by changing the shaker speed. A micro plate reader was used to measure the density of the bacteria. Recordings of the time, bacterial concentration and shaker speed were taken at each sampling point. Figure 52 shows the growth of two strains at varying radial shaker speeds over time.

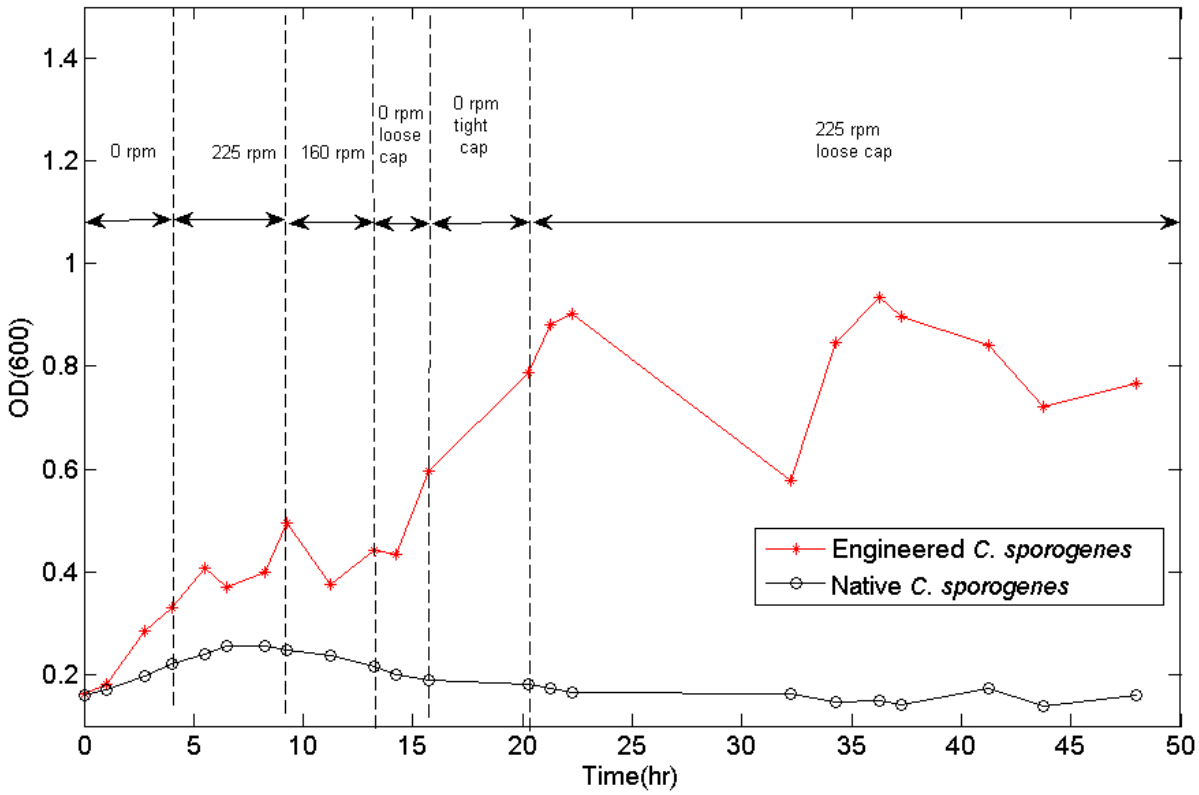

Figure 52: Comparison the behavior of native and engineered *C. sporogenes* when exposed to oxygen

The caps of both tubes were tight for the first 4 hours inside the incubator, which was set to have a temperature equal to 37 C. After four hours the shakers were turned on with radial speed of 225 rpm;

as a result both colonies started dying with about an hour delay. In order to retain their growth the radial speed was decreased to 160 rpm. The engineered strain recovered growth, while the native strain did not. Next, the shaker was turned off for two hours, to recover the growth of the native strain. The cap was held tight during the next 3 hours. The native strain could not retain its growth, while the engineered strain recovered and grew up to 0.9 OD. After 20 hrs, the cap was loosened and the shakers were turned on with radial speed of 225 rpm. The engineered colony retained its growth for two hours but started dying. Later, growth was resumed, presumably when the oxygen in the media was consumed.

To further compare the engineered *C. sporogenes* with the native strain, four cultures of the engineered bacteria were prepared, two pair at two different concentrations of 0.8 and 0.4 OD. Two liquid cultures of native were also prepared, at 0.5 and 0.2 OD. Figure 53 compares the behavior of the 6 strains in a shaker with 225 rpm and 37C temperature. The native bacteria with OD 0.2 (blue line) was sealed for the first 7 hrs to reach an OD of 0.9 and then the cap was loosened.

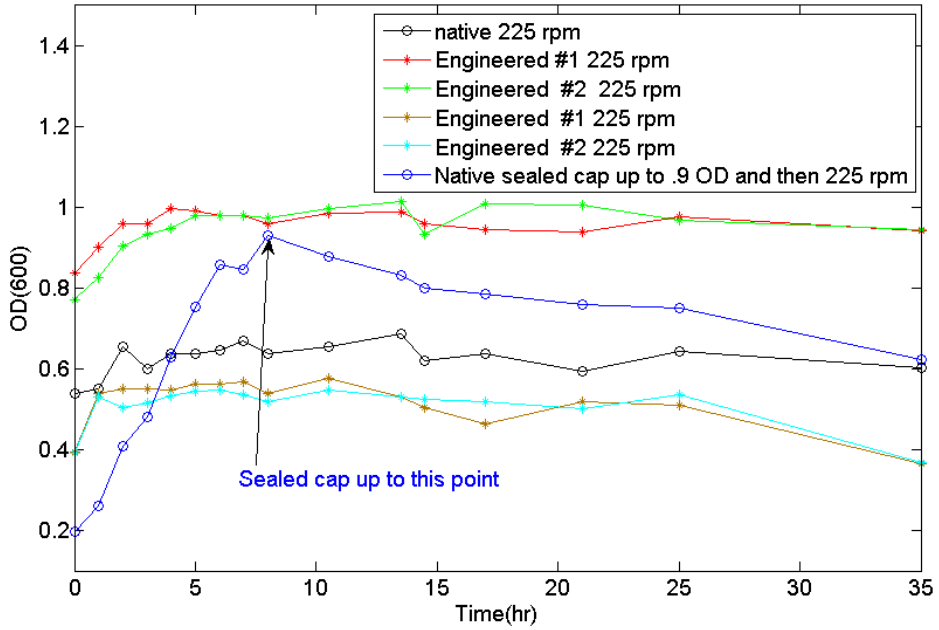

Figure 53: Comparison the behavior of native *C. sporogenes* with two different engineered strains when exposed to oxygen

As the figure shows, the native and engineered strains with OD 0.5 and 0.4 could not grow but the engineered strain with OD around 0.8 grew to 1 OD and retained its population for 35 hours. The native

strain that was grown to 0.9 OD could not retain its growth after loosening the cap and started decaying immediately after aeration. This experiments suggests that the aerotolerance strain is capable of scavenging oxygen from its environment and could grow well after aeration. These results support our hypothesis.

Chapter 7:

Conclusion and Recommendation

7.1 Conclusion

The main focus of this study was the development of a density dependent aerotolerant strain of *C. sporogenes* which would have the effective tumor colonization property of native bacteria at low density and which would be able to migrate to (and eradicate) the oxygenated part of the tumor at high density. Such a strain could not only solve the problem of tumor regrowth from outer oxygenated rim, but could also be used as a safe drug delivery system that does not affect healthy tissue. Expression of an aerotolerance enzyme under the control of a quorum sensing mechanism results in a strain with the desired properties. Key design features are the threshold population density at which bacteria becomes aerotolerant and the maximum concentration of the aerotolerance enzyme.

Two well characterized quorum sensing mechanisms were chosen as candidates for this design: from *V. fischeri* (a gram negative bacteria) and *S. aureus* (a gram positive bacteria). The lux quorum sensing mechanism of *V. fischeri* and the *agr* quorum sensing mechanism of *S. aureus* are regulated, respectively, by a small chemical called acyl homoserine lactone (AHL) and a small peptide (AIP). The dynamic behavior of these two mechanisms were studied by simulation of mathematical models in MATLAB. This analysis elucidated system dynamics, and suggested key design parameters.

The model of the lux quorum sensing mechanism (modified from [59]) confirms that the system exhibits bistability and hysteresis. The genetic circuit is 'off' at low AHL concentration (corresponding to low population density) and is 'on' at high AHL concentration. Our investigations of the effects of the *luxR* and *luxI* promoter strengths and RBS revealed that any of these features can be used tune the threshold AHL concentration, but that the final concentration of the aerotolerance enzyme can be tuned only by the expression strength of luxR. A globalized parametric sensitivity analysis showed that the maximal induced expression rate of LuxR and the degradation rate of luxR are the most significant parameters for tuning the steady-state concentration of aerotolerance enzyme, and that the threshold AHL concentration is most sensitive to the dissociation constant for LuxR and its degradation rate. The sensitivity analysis confirmed that the dissociation constant of LuxR can be used to tune the threshold activation without affecting the steady state concentration. These results suggest a design protocol: the threshold AHL concentration can be tuned by manipulation of either the *luxI* expression strength

(promoter or RBS) or by tuning the LuxR degradation rate (with, e.g. a degradation tag). Once an acceptable threshold AHL concentration has been achieved, the degree of aerotolerance (determined by the concentration of *noxA*) can be tuned independently by manipulation of the LuxR expression strength.

Our analysis of the Gustaffson et al. model [62] of the agr quorum sensing of *S. aureus* yielded similar results. Again, the system was confirmed to exhibit bistability and hysteresis: off at low AIP concentration and on when AIP concentration exceeds a threshold. We determined that the threshold AIP concentration and the final concentration of the aerotolerance enzyme both increase with the strength of expression of AgrA and AgrC. Our globalized sensitivity analysis revealed that the threshold AIP concentration is most sensitive to the Michaelis constant for activator binding, and is also highly sensitive to the degradation rates for AgrA and AgrC, and to the maximal activated expression rate of AgrC. The final value of aerotolerance enzyme is sensitive to the same parameters, except it is insensitive to the rate of degradation of AgrC. Once again, a design strategy is suggested: the degree of aerotolerance can be tuned by the degradation rate of AgrA or expression strength of AgrC, and the threshold AIP concentration can subsequently be independently adjusted by altering the the rate of degradation of AgrC.

We complemented this model-based design of the genetic circuit with a model that simulates the time-varying growth of the engineered bacteria in a tumor environment (assumed, for simplicity, to be a radially symmetric sphere). Bacterial growth was coupled to the genetic circuit by considering a simplified mechanism that represents both the gram positive and the gram negative quorum sensing systems. Production, degradation, and diffusion of the aerotolerance enzyme were modeled.

Simulation of this mathematical model predicted migration of the engineered bacteria to the oxygenated part of the tumor, while growth of the native bacteria is restricted to the hypoxic area of the tumor. We considered two key performance measures: the overall colony size in steady state, and the degree of specificity of the colony. A sensitivity analysis revealed that for both performance measures the production parameters are more significant than the degradation rates. The analysis suggests that the production rates of the aerotolerance enzyme and the autoinducer are the key design parameters that will allow tuning of the performance measures to desired values.

These modelling efforts provide guides to system design, which will be useful once the performance of the overall system has been confirmed, and is ready for tuning.

We considered three candidates for the density dependent production of aerotolerance enzyme in the engineered *Clostridium* strain: the *lux* promoter from *V. fischeri*, and the *P2* and *P3* promoters from *S. aureus*. Three genetic circuits were constructed by putting an anaerobic reporter gene under the control of these promoters. Each genetic circuit contains all elements of the associated quorum sensing mechanism. The genetic circuits were transformed into *C. sporogenes* by conjugation and the production of the reporter gene in different cell densities were assessed. The behavior of each promoter was compared with positive and negative controls (constitutive expression of reporter gene and the native bacteria, respectively). We found that the *lux* promoter was not activated in *C. sporogenes*. The *P2* promoter was found to show a behavior similar to the constitutive promoter in *C. sporogenes* (and was inactive in *E. coli*). The *P3* promoter showed the desired density-dependent expression of the reporter gene, and so appears to be a good candidate for quorum sensing therapeutic mechanism in *C. sporogenes*.

To test the hypothesis that expression of an aerotolerance enzyme can confer aerotolerance on *C. sporogenes*, the *noxA* gene of *C. aminovalericum* was cloned downstream of the *thl* promoter (a strong constitutive promoter) and the resulting plasmid was transformed into *C. sporogenes.* The behavior of the engineered *C. sporogenes* was compared with the native strain in the present of oxygen. We found that the engineered bacteria retained its growth after aeration, while the native bacteria could not grow in the presence of oxygen, as expected. Further experiments are needed to confirm this behavior, by e.g. carefully comparing growth of cultures in a range of hypoxic conditions, as measured by dissolved oxygen assays. Ideally, this would be followed by identification of the biochemical mechanism by which aerotolerance is conferred.

7.2 Recommendation and Future Directions

The preliminary work carried out in this project provides a solid foundation to explore the use of engineered *C. sporogenes* for tumor therapy. The next step will be to construct a strain containing the final product: *noxA* under the control of the *p3* quorum-sensing promoter. That system's performance can be assayed using the reporter techniques presented in Chapter 6. Once appropriate function is verified, biochemcial assays should be carried out to confirm our understanding of the response: the

AIP concentration can be measured by mass spectrometery, and the concentration of Agr mRNA and proteins can be measured by qPCR and western blot.

Once these biochemical features of the system have been confirmed, we could begin characterization of the response toward therapeutic design. This could begin with careful time-series assays of the response under various conditions (e.g. media, oxygen levels). This data could be used to refine the model (Chapter 3) of the quorum-sensing response so that it could provide predictions of the behavior of the *p3* system. At the same time, we could explore the system's design space, by altering the choice of promoters, RBS, and degradation tags, as described above. (A codon optimization exercise should also be carried out at this stage, as the agr and *noxA* genes are not native to *C. sporogenes*).

The mathematical model proposed in Chapter 4 can be expanded to include a more comprehensive mathematical model of the genetic circuit and the tumor microenvironment. The study of the bacteria migration to the tumor site and its growth in tumor before becoming aerotolerant can be included in the mathematical model.

The next step would be to investigate colony behavior in an *in vitro* tumor microenvironment [103]. Again, careful time-series measurements of colony behavior will allow refinement and specialization of the model of colony formation (Chapter 4), which will, in turn, guide an exploration of how variations in the design will affect performance in terms of colony growth and tumor regression. Once these *in vitro* characterizations are successful, the next step would be to repeat these studies in an *in vivo* environment (e.g. a mouse model), with the long term goal of entering clinical studies.

At the same time, it would be worthwhile following up with alternative designs. In particular, in our experiments, the *lux* promoter was not activate in *C. sporogenes*, but the reason remains unclear. It is possible that AHL is successfully produced in *C. sporogenes*, but cannot diffuse freely across the cell membrane. A series of experiments could be designed to elicit the reason for the lack of activation of *lux* promoter in *C. sporogenes*. The first step would be to determine whether AHL is produced in *C. sporogenes*. This can be done with an enzymatic assay or a detection technique such as HPLC. If the presence of the AHL is confirmed in the *C. sporogenes*, then the *lux* promoter can possibly be activated by expressing a receptor that facilitates export of AHL across the cell membrane.

Appendix A

Nomenclature

α	dimensionless diffusion coefficient of AHL
β	dimensionless diffusion coefficient of aerotolance enzyme
γ	dimensionless diffusion coefficient of Bacteria
$\boldsymbol{A}$	concentration of AgrA
A_e	extracellular AHL concentration
A_M	maximal concentration of autoinducer
A_p	concentration of phosphorylated AgrA
B	Concentration of AgrB
C	Concentration of AgrC
C_B	bacterial concentration
C_M	maximal concentration of bacteria
C_p	active AgrC receptor
C_x	inactive AgrC
D	concentration of AgrD
D_A	diffusion coefficient of autoinducer
D_B	diffusion coefficient of aerotolerance enzyme
D_C	diffusion coefficient of bacteria
d_A	degradation rate for AgrA
d_{Ap}	degradation of phosphorylated AgrA
d_B	degradation rate of AgrD
d_C	degradation rate of AgrC
d_{cp}	degradation rate of active AgrC receptor
d_{cx}	degradation rate of inactive AgrC receptor
d_P	degradation rate of AIP

$\boldsymbol{E}$	concentration of aerotolerance enzyme
E_M	maximal concentration of aerotolerance enzyme
G	concentration of GFP
I	concentration of LuxI
I_m	LuxI mRNA concentration
k	half-saturation constant
K	half-saturation constant
K_A	rate of production of autoinducer
K_B	rate of production of bacteria
K_E	rate of production of aerotolerance enzyme
k_1	association rate of LuxR and AHL
k_{-1}	dissociation rate of LuxR-AHL complex
K_1	ratio of the association rate k_1 to the dissociation rate k_{-1}
$k2$	association rate LuxR-AHL dimer
k_{-2}	aissociation rate LuxR-AHL dimer
K_2	ratio of association to the rate of dissociation of the dimer
K_3	maximal rates for activated transcription of R_m
K_4	dissociation constants for D-promoter binding to *luxR* promoter
$k5$	basal transcription rates for R_m
$k6$	luxR mRNA degradation rate
K_7	maximal rates for activated transcription of I_m
K_8	dissociation constants for D-promoter binding to *luxI* promoter
$k9$	basal transcription rates for I_m
$k10$	mRNA degradation rate
$k11$	per-mRNA translation rate LuxR
$k12$	degradation rate of LuxR
$k13$	per-mRNA translation rate LuxI
$k14$	degradation rate of LuxI

$k15$	per-LuxI production rate of AHL
$k16$	diffusion rate of AHL
k_A	maximal rate of activated expression of AgrA
K_A.	rate of production of autoinducer
$\boldsymbol{K_{AP}}$	Michaelis constant of activator binding of phosphorylated AgrA
k_{Aprime}	basal transcription rate of expression of AgrA
k_C	the maximal rate of activated expression of AgrC
k_{c1}	association rate of active AgrC receptor
k_{c2}	association rate of inactive AgrC receptor
k_{c3}	dissociation rate of active AgrC receptor
k_{c4}	dissociation rate of inactive AgrC receptor
k_{Cprime}	basal transcription rate of AgrC
$\boldsymbol{K_{CP}}$	Production rate of AgrC complex with native AIP
$\boldsymbol{K_{Cx}}$	Production rate of AgrC complex with inhibitor AIP
k_{dp}	dephosphorylation rate
k_D	the maximal rate of activated expression of AgrD
k_{Dp}	production rate AIP
k_{Dprime}	basal transcription rate for AgrD
$\boldsymbol{k_p}$	phosphorylation rate
$\boldsymbol{k_v}$	strength of aerotolerance enzyme
$\boldsymbol{K_v}$	dimensionless strength of aerotolerance enzyme
$\boldsymbol{M_A}$	dimensionless AHL production rate
$\boldsymbol{M_B}$	dimensionless bacterial growth rate
$\boldsymbol{M_E}$	dimensionless aerotolerance enzyme production rate
$\boldsymbol{N_A}$	dimensionless AHL degradation rate
$\boldsymbol{N_B}$	dimensionless bacterial death rate
$\boldsymbol{N_E}$	dimensionless aerotolerance enzyme degradation rate

O	Oxygen concentration
R	Concentration of LuxR
R_m	LuxR mRNA concentration
T_{AM}	maximal life time of autoinducer
T_{EM}	maximal life time of aerotolerance enzyme

Appendix B

Experimental Results

Table 15: Experimental data for comparison of GFP expression of native *E. coli* with the engineered E.coli harboring pMTL_QS_GFP plasmid with and without AHL in the media (Figure 47)

Native *E. coli*			pMTL_QS_GFP+AHL			pMTL_QS_GFP		
Time(hr)	**OD600**	**Intensity**	**Time(hr)**	**OD600**	**Intensity**	**Time(hr)**	**OD600**	**Intensity**
0	0.07	28.57	0	0.17	35.6	0	0.07	52.3
1.81	0.16	31.66	0.89	0.25	33	0.49	0.13	63.4
2.83	0.31	29.63	0	0.17	35.6	0.95	0.2	77
3.02	0.51	27.51	0.89	0.25	33	1.7	0.29	97
4.06	0.68	31.97	1.35	0.35	35.8	2.8	0.46	124
4.74	0.71	28.22	1.86	0.41	35.4	3.88	0.6	129
5.59	0.69	27.88	2.62	0.49	37.3	4.92	0.66	121
6.68	0.75	28.6	3.72	0.59	38.5	5.61	0.77	126
11.1	0.85	29.2	4.79	0.69	38.9	6.44	0.82	126
14.9	0.89	32	5.82	0.75	38.4	7.39	0.75	116
16.3	0.91	30.79	7.25	0.8	41.4	11.9	0.95	128
18.4	0.94	30.64	8.22	0.79	42.9	15.7	1.01	154
20.9	0.95	32.13	8.74	0.8	45.3	16.9	1.04	176
23.9	0.96	33.36	12.8	0.88	59.8	19.2	1.08	234
26.5	1.02	33.44	16.6	0.97	209	21.7	1.09	235
			17.8	1	237	24.8	1.11	273
			20.1	1.08	345	27.4	1.16	247
			22.6	1.11	350			

Table 16: Experimental data for comparison of florescent intensity of *C.sporogenes* and *E. coli* harboring MTL_FC_evoglow(PFCG) and pMTL_QS_GFP (PFCI) plasmids (Figure 48)

PFCG in *C. spororogenes*		PFCI in *E. coli*		PFCG in *E. coli*	
OD600	**Intensity**	**OD600**	**Intensity**	**OD600**	**Intensity**
0.07	1979.5	0.296	442.889	0.615667	2535
0.2715	2037	0.411333	889.833	0.441667	1152
0.5115	1761.5	0.5315	1245.08	0.746	3409
0.954	2510	0.598	1605.83	0.819667	4925
1.242	2901	0.646	1869.17	0.825	5465
		0.763333	3185.22	0.917333	10201
		1.039	19823.6	0.832	13132.3

Table 17: Experimental data for comparison of the behavior of the S.aureus quorum sensing mechanism with P2 promoter in *C. sporogenes* and *E.coli* (Figure 49)

PAG2 in *E. coli*		PAG2 in *C. sporogenes*		Native *C.sporogenes*		PTG in *C.sporogenes*	
OD600	**Intensity**	**OD600**	**Intensity**	**OD600**	**Intensity**	**OD600**	**Intensity**
0.0473	221	0.3045	3345	0.07	1979.5	0.167	1352.5
0.2593	779	0.572	5507	0.2715	2037	0.229	2312
0.316	908.33	0.6805	5856.5	0.5115	1761.5	0.511	5105
0.4013	1110	0.833	9280.5	0.954	2510	0.545	6000.5
0.5183	1220	0.9745	11552.5	1.242	2901	0.642	7941
0.6083	1502.7	1.028	12321			0.852	11090.5
0.6487	1460.3	1.1625	14323.5			0.885	11067
0.6767	1644	1.142	17072			0.919	10595.5
0.758	2193					0.904	11049.5
0.831	2935.7					0.95	11214.5
						0.967	10936.5
						1.029	11057
						1.155	11234

Table 18: Experimental data for comparison of the behavior of the behavior of the S.aureus quorum sensing mechanism with P3 promoter in *C. sporogenes* and *E.coli* , fluorescence intensity versus cell density (Figure 50)

PAG3 in *E. coli*		**PAG3 in *C. sporogenes***		**Native *C.sporogenes***		**PTG in *C.sporogenes***	
OD600	**Intensity**	**OD600**	**Intensity**	**OD600**	**Intensity**	**OD600**	**Intensity**
0.047667	219	0.3465	1787	0.07	1979.5	0.167	1352.5
0.372667	825	0.5235	2008	0.2715	2037	0.229	2312
0.495667	994.333	0.8225	3121.5	0.5115	1761.5	0.511	5105
0.616333	1244	0.9385	4793.5	0.954	2510	0.545	6000.5
0.655667	1200.33	1.1485	6929	1.242	2901	0.642	7941
0.775333	1374	1.1365	7282.5			0.852	11090.5
0.899	1451	1.162	8170			0.885	11067
0.901333	1501	1.2675	9169			0.919	10595.5
1.01567	1760	1.203	8575.5			0.904	11049.5
1.05567	1902	1.4315	10196.5			0.95	11214.5
		1.4425	11552.5			0.967	10936.5
		1.3415	8723.5			1.029	11057
						1.155	11234

Table 19: Experimental data for comparison of the behavior of P3 promoter in *C. sporogenes* in different conditions (Figure 51)

PAG3-3 ½ TYG		PAG3-3 *TYG*		PAG3-3 TYG(Repeat)		PAG3-3 TYG+0.5% Glocuse	
OD600	**Intensity**	**OD600**	**Intensity**	**OD600**	**Intensity**	**OD600**	**Intensity**
0.3615	1545.5	0.159	740.5	0.5235	2008	0.3465	1787
0.4435	2038	0.309	1503.5	0.588	3094	0.5235	2008
0.4885	2155	0.568	2491.5	0.786	4296	0.8225	3121.5
0.517	2866.5	0.5955	2976.5	0.527	2686	0.9385	4793.5
0.208	1319	0.784	3999.5	1.0255	6623.5	1.1485	6929
0.538	2797	0.8785	4839	0.964	5981.5	1.1365	7282.5
0.537	2702	0.991	5045.5	0.9525	5664.5	1.162	8170
0.5655	2777.5	1.1305	5987.5	1.071	7064	1.2675	9169
0.473	2618.5	1.0465	6820.5	1.064	7623	1.203	8575.5
0.541	2677	1.066	6755.5			1.4315	10196.5
0.5645	2533.5	1.1135	6861.5			1.4425	11552.5
		1.19333	7061.33			1.3415	8723.5
		1.201	7194.67				

Table 20: Comparison the behavior of native and engineered C. sporogenes when exposed to oxygen (Figure 52)

Native		Engineered	
Time(hr)	**Native**	**Time(hr)**	**Intensity**
0	0.1605	0	0.1615
1	0.1695	1	0.181
2.75	0.1965	2.75	0.2845
4	0.2205	4	0.3305
5.5	0.239	5.5	0.407
6.5	0.2545	6.5	0.369
8.25	0.255	8.25	0.399
9.25	0.247	9.25	0.4965
11.25	0.236	11.25	0.3745
13.25	0.217	13.25	0.442
14.25	0.201	14.25	0.4335
15.75	0.1895	15.75	0.5955
20.25	0.1825	20.25	0.7885
21.25	0.173	21.25	0.8825
22.25	0.166	22.25	0.9025
32.25	0.1625	32.25	0.5765
34.25	0.1475	34.25	0.846
36.25	0.1495	36.25	0.9355
37.25	0.141	37.25	0.8975
41.25	0.1725	41.25	0.841
43.75	0.1385	43.75	0.721
48	0.1605	48	0.7655

Table 21: Comparison the behavior of native C. sporogenes with two different engineered strains when exposed to oxygen (figure 53)

Time(hr)	Native sealed up to OD 0.9	Native	Engineered #2	Engineered #1	Engineered #2	Engineered #1
0	0.197	0.5385	0.39	0.395	0.772	0.8365
1	0.261	0.5505	0.53	0.539	0.8255	0.9
2	0.41	0.6565	0.503	0.5495	0.9035	0.9595
3	0.4825	0.6	0.516	0.5505	0.934	0.958
4	0.6295	0.637	0.533	0.5465	0.947	0.9985
5	0.753	0.637	0.545	0.5625	0.98	0.992
6	0.859	0.6455	0.5465	0.5635	0.9805	0.9805
7	0.845	0.6705	0.5365	0.568	0.979	0.9795
8	0.93	0.639	0.5195	0.54	0.974	0.96
10.5	0.879	0.656	0.5485	0.5765	0.9975	0.985
13.5	0.832	0.687	0.529	0.53	1.0155	0.987
14.5	0.7995	0.6205	0.525	0.505	0.9325	0.9585
17	0.7865	0.6375	0.52	0.4635	1.0075	0.9435
21	0.758	0.5935	0.5015	0.52	1.007	0.9405
25	0.7505	0.6445	0.5375	0.51	0.967	0.976
35	0.622	0.6025	0.369	0.3665	0.9455	0.943

Appendix C

Matlab Codes for Simulation and Analysis of Aerotolerant Bacteria Growth in Solid Tumors

```
function bacteria_genetic
% ---------- Anaerobic Bacteria growth in Tumour------------
% Db= diffusion coefficient,
% u= Bacteria concentration cells/um,
% x= Tumour radious um;
% The oxygen concentration is assumed as co=aa*x^2+bb*x+cc
% The bacteria growth can be modeled by the following PDE
%   In the form expected by PDEPE, the single PDE is
%
%   1/Db .*  D_ [u] = 1/x D_ [x*   Du/Dx   ] + [-
ko/Db*(DuDx*(2*aa*x+bb)+u/x*(4*aa*x+bb))+kb/Db*u*(1-u/um)]
%              Dt        Dx
%    ----         ---               ------      --------------------------
-----------------------------------
%     c            u              f(x,t,u,Du/Dx)
%
%   The equation is to hold on an interval 0 <= x <= 90 for times t >= 0.
%   The initial bacteria concentraion is zero for radious larger than Rn(
necrotic radious) and equal
%   to 8000 cells/um for the necrotic part
%   Two kinds of boundary conditions are chosen so as to show how they
%   appear in the form expected by the solver.
%
%   Bacteria concentration is zero at the outer rim of tumour x=R,
%     [u]    +     [0] .* [       Du/Dx          ] = [0]
%
%     ---          ---    ------------------------   ---
%   p(0,t,u)      q(0,t)        f(0,t,u,Du/Dx)        0
%
%    its gradient is zero at the center of the tumour.
%
%   [ 0]      +     [1] .* [   Du/Dx    ] = [0]
%
%   --------------   ---    --------------   ---
%      p(1,t,u)     q(1,t)   f(1,t,u,Du/Dx)   0


m = 2;
```

```
x = linspace(0,90,100);
x = linspace(0,200,200);
t = linspace(0,20000,100);
 %tbar=t*6.172*10^(-6);
% tbar=t;
% oxygen profile is as Co=aa*x'*x+bb*x+cc
for i=1:200
 if x(i)<=20
     Co(i)=0;
 elseif x(i)>=20 && x(i)<=90
%Co(i)=aa*x(i)^2+bb*x(i)+cc;
Co(i)=- 3.044e-005*x(i)^3 + 0.005116*x(i)^2 - 0.165*x(i) + 1.497;
 else
     Co(i)=Co(90);
end
end
xbar=x/90;
sol = pdepe(m,@pdex1pde,@pdex1ic,@pdex1bc,xbar,t);
% Extract the first solution component as u.  This is not necessary
% for a single equation, but makes a point about the form of the output.
u=sol;
u1 = sol(:,:,1);
u2 = sol(:,:,2);
u3 = sol(:,:,3);
y=trapz(xbar(20:90),u1(end,20:90))

plot(xbar(1:100),u1(end,(1:100)),'r');



% --------------------------------------------------------------------------
--

function [c,f,s] = pdex1pde(x,t,u,DuDx)
Db=.05;Da=.05;De=.05;
de=.004; da=.639;
kb=.1;ka=4.8*10^(-7);ke=0.05;kv=.15;
kb=.1;ka=4.8*10^(-7);ke=.05;
MB=100;MA=1;NA=.05;ME=1;NE=.05; NB=10^-10;kv=0;
MB=20000;MA=100;NA=.001;ME=100;NE=.001; NB=18500;kv=23;

x1 = linspace(0,90,100);
% oxygen profile
for i=1:100
 if x1(i)<=20
     Co1(i)=0;
 else
Co1(i)=- 3.044e-005*x1(i)^3 + 0.005116*x1(i)^2 - 0.165*x1(i) + 1.497;
end
end
Max_Co=max(Co1);
```

```
x2=x*90;
if x2<=20
     Co=0;
 elseif x2>=20 && x2<=90

Co=- 3.044e-005*x2^3 + 0.005116*x2^2 - 0.165*x2 + 1.497;
 else
     Co=Max_Co;
end
Co2=Co/Max_Co;

c = [1/.0001;1/1;1/0.1];
f = [1;1;1].*DuDx;

 s =[MB*u(1)*(1-u(1))-NB/(1-Co2/(kv*u(3)+1)+.00000001)*u(1);MA*u(1)-
NA*u(2);ME*u(2)*u(1)-NE*u(3)];

% ------------------------------------------------------------------------
--

function u0 = pdex1ic(xbar)
Cb0=.1;
if xbar<(20/90)
u0=[.1;0;0];
else
u0 =[0;0;0];
end

% ------------------------------------------------------------------------
--

function [pl,ql,pr,qr] = pdex1bc(xl,ul,xr,ur,t)
pl = [0;0;0];
ql = [1;1;1];
pr = [ur(1);ur(2);ur(3)];
qr = [0;0;0];
```

Bibliography

References

[1] Jain, R. K. and Forbes, N. S.(2001) Can engineered bacteria help control cancer, PNAS, 98, 14748

[2] Mengesha A., Dubois L., Chiu R.K., Paesmans K., Wouters B.G., Lambin P., Theys J. (2007) Potential and limitations of bacterial-mediated cancer therapy. Front Biosci 12: 3880–3891

[3] St. Jean, A. T., Zhang, M. M. & Forbes, N. S. Bacterial therapies: completing the cancer treatment toolbox. Curr. Opin. Biotechnol. 19, 511–517 (2008).

[4] Theys, J., Pennington, O., Dubois, L., Landuyt, W., Anné, J., Burke, P., Anlezark, G., Dûrre, P., Wouters, B.G., Minton, N.P., and Lambin, P.(2006). Repeated systemic treatment cycles of Clostridium-directed enzyme prodrug therapy results in sustained anti-tumor effects in vivo., Brit. J. Cancer, 95, 1212

[5] Ferrara, N., Smith T.N. (1997). The biology of vascular endothelial growth factor. Endocrin Rev., 18, 4

[6] Vaupel, P., Harrison, L.(2004). Tumor hypoxia: causative factors, compensatory mechanisms, and cellular response. The Oncol, 9, 4

[7] Kizaka-Kondoh, S., Inoue, M., Harada, H., and Hiraoka, M. (2003). Tumor Hypoxia: a Target for Selective Cancer Therapy. Cancer Sci., 94, 1021.

[8] Vaupel P. (2004). Tumor microenvironmental physiology and its implications for radiation oncology. Semin. Radiat. Oncol., 14, 198

[9] Brown J.M., Wilson W.R. (2004). Exploiting tumor hypoxia in cancer treatment. Nat. Rev. Cancer,4, 437

[10] Graham F.O, Coleman P.N. (1952). Infection of a secondary carcinoma by Salmonella Montevideo. BMJ. 1952, 1, 1116

[11] Bacon G.A., Burrows T.W., Yates M. (1951). The effects of biochemical mutation on the virulence of bacterium typhosum: the loss of virulence of certain mutants. Br. J. Exp. Path., 32, 85

[12] Hoiseth, S. K. J., and Stocker, B. A. D., (1981).Aromatic-dependent Salmonella tvpliimuriiim are non-virulent and effective as live vaccines. Nature (Lond.), 291,238

[13] Pawelek, J, Low, K.B., Bermudes, D. (1997). Tumor-targeted Salmonella as a novel anti-cancer vector. Cancer Res. 57, 4537

[14] Low, K.B., Ittensohn, M., Le,T. et al. (1999). Lipid A mutant Salmonella with suppressed virulence and TNF_ induction retain tumor-targeting in vivo. Nat. Biotechnol., 17, 37

[15] Zhao, M., Yang, M., Li, X. M., Jiang, P. , Baranov, E., Li, S., Xu, M., Penman, S., and Hoffman, R. M.(2005) Tumor-targeting bacterial therapy with amino acid auxotrophs of GFP expressing Salmonella typhimurium. Proc. Natl. Acad. Sci. USA, 102, 755

[16] Zhao, M., Yang, M., Ma, H., Li, X., Tan, X., Li, S., Yang, Z., and Hoffman, R.M. (2006) Targeted therapy with a Salmonella typhimurium leucine-arginine auxotroph cures orthotopic human breast tumors in nude mice. Cancer Research, 66, 7647

[17] Toso, J. F., Gill, V. J., Hwu, P., Marincola, F. M., Restifo, N. P., Schwartzentruber, D. J., Sherry, R. M., Topalian, S. L., Yang, J. C., Stock, F., Freezer, L. J., Morton, K. E., Seipp, C., Haworth, L., Mavroukakis, S., White, D., MacDonald, S., Mao, J., Sznol, M. & Rosenberg, S. A. (2002). Phase I Bacterial-mediated cancer therapy 3891 study of the intravenous administration of attenuated Salmonella typhimurium to patients with metastatic melanoma. J. Clin. Oncol., 20,142

[18] Connell, H. (1935). The study and treatment of cancer by proteolytic enzymes. A preliminary report. Can. Med. Ass. J. 33, 364

[19] Parker, R., Plummber, H., Siebenmann C., & Chapman, M. (1947) Effect of histolyticus infection and toxin on transplantable mouse tumors. Proc. Soc. Exp. Biol. Med. 66, 461

[20] Malmgren, R. A. & Flanigan, C. C. (1955). Localization of the vegetative form of Clostridium tetani in mouse tumors following intravenous spore administration. Cancer Res., 15, 473

[21] Möse, J. R. & Möse, G. (1964). Oncolysis by Clostridia. I. Activity of Clostridium Butyricum (M-55) and Other Nonpathogenic Clostridia against the Ehrlich Carcinoma. Cancer Res. 24, 212

[22] Gericke, D., Dietzel, F. and Ruster, I.(1979). Further progress with oncolysis due to local high frequency hyperthermia, local x-irradiation and apathogenic clostridia. J. Microw. Power, 14,163

[23] Thiele, E.H., Arison, R.N. and Boxer, G.E. (1964). Oncolysis by clostridia III. Effects on clostridia and chemotherapeutic agents on rodent tumors. Cancer Res., 24, 222

[24] Carey, R.W., Holland, J.F., Whang, H.Y., Neter, E. and Bryant, B. (1967). Clostridial oncolysis in man. Eur. J. Cancer 1967 3, 37

[25] Schlechte, H., Schwabe, K., Mehnert, W.H., Schulze, B. and Brauniger, H.(1982) Chemotherapy for tumors using clostridial oncolysis, antibiotics and cyclophosphamide: model trial on the UVT 15264 tumor. Arch. Geschwulstforsch.52, 41

[26] Gericke, D., Dietzel, F. and Ruster, I. (1979). Further progress with oncolysis due to local high frequency hyperthermia, local x-irradiation and apathogenic clostridia. J. Microw. Power, 14, 163

[27] Mose, J.R. (1979) Versuche zur verbesserung der onkolyse mitdem clostridienstamm. Zentralbl Bakteriol Mikrobiol Hyg. 244, 541

[28] Dang, L. H., Bettegowda, C., Huso, D. L., Kinzler, K. W. & Vogelstein, B.(2001) Combination bacteriolytic therapy for the treatment of experimental tumors. Proc. Natl. Acad. Sci. USA., 98, 15155

[29] Minton, N. P. & Oultram, J. D. (1988): Host: vector systems for gene cloning in Clostridium. Microbiol. Sci., 5, 310

[30] Lambin, P., Theys, J., Landduyt, W., Rijken, P., Van der Kogel, A., Van der Schueren, E., Hodgkiss, R., Fowler, J., Nuyts, S., De Bruijn, E., Van Mellaert, L. & Anne, J.(1998) Colonization of clostridium in the body is restricted to the hypoxic and necrotic areas of tumors. Anaerobes, 4, 183

[31] Van Mellaert, L., Barbe, S., & Anne, J.(2006). Clostridium spores as anti-tumor agents. Trends. Microbiol. 14, 190

[32]. Liu, S. C., Minton, N. P., Giaccia, A. J., & Brown, J. M., (2002). Anticancer efficacy of systemically delivered anaerobic bacteria as gene therapy vectors targeting tumor hypoxia/necrosis. Gene Therapy, 9, 291

[33] Minton N.P. (2003). Clostridium in cancer therapy. Nature review Microbiology, 1, 237

[34]. Yazawa, K., Fujimori, M., Amano, J., Kano, Y., & Taniguchi, S. (2000) . Bifidobacterium longum as a delivery system for cancer gene therapy: selective localization and growth in hypoxic tumors. Cancer Gene Therapy, 7, 269

[35] Kawasaki, S., Nakagawa, T., Nishiyama, Y., Benno, Y. , Uchimura, T., Komagata, K., Kozaki, K., and Niimura, Y. (1998). Effect of oxygen on the growth of Clostridium butyricum (type species of the genus Clostridium), and the distribution of enzymes for oxygen and for active oxygen species in clostridia. J. Ferment. Bioeng., 86, 368

[36] Holdernan, L. V., Cato, E. P., and Moor, W. E. C. (1997). Anaerobe laboratory manual, fourth edition. Anaerobe laboratory Virginia Polytechnic Institute and State University, Virginia, USA

[37] O'Brien, R. W., and Morris, J. G. (1971). Oxygen and growth and metabolism of Clostridium acetobutylicum. J. Gen. Microbial., 68, 307

[38] Niimura, Y., Koh, E., Uchimura, T., Ohara, N., and Kozaki, M. (1989). Aerobic and anaerobic metabolism in a facultative anaerobe EPOl lacking cytochrome, quinone and catalase. FEMS. Microbial. Lett., 61, 79

[39] Niimura, Y., Oh&hi, K., Yarita, Y., Hidaka, M., Masaki, H., Uchimura, T., Suzuki, H., Kozaki, M., and Uozumi, T. (1993). A flavoprotein functional as NADH oxidase from Amphibacillus xylanus EpOl: purification and characterization of the enzyme and structural analysis of its gene. J. Bacterial., 175, 7945

[40] Nllura, Y., Ohnishi, K., Nishiyama, Y., Kawasaki, S., Miyaji, T., Suzuki, H., Nishino, T., and Massey, V.(1997). Amphibacillus xylanus NADH oxidase/alkyl hydroperoxide reductase flavoprotein. Flavins and Flavoproteins. University of Calgary Press, Canada, p. 741-750.

[41] Niimura, Y., Poole, L. B., and Massey, V.(1995). Amphibacillus xylanus NADH oxidase and Salmonella typhimurium alkylhydroperoxide reductase flavoprotein components show extremely high scavenging activity for both alkyl hydroperoxide and hydrogen peroxide in the presence of S. typhimurium alkyl-hydroperoxide reductase 22-kDa protein component. J. Biol. Chem., 270, 25645

[42] Niimura, Y. and Massey, V. (1996) Reaction mechanism of Amphibacillus xylanus NADH oxidase/alkyl hydroperoxide reductase flavoprotein. J. Biol. Chem., 271, 30459

[43] Kawasaki, S., Watamura, Y., Ono, M., Watanabe, T., Takeda, K., and Niimura. Y. (2005). Adaptive responses to oxygen stress in obligatory anaerobes Clostridium acetobutylicum and Clostridium aminovalericum. Appl. Environ. Microbiol, 71, 8442

[44] Guedon, E., and Petitdemange. H. (2001). Identification of the gene encoding NADH-rubredoxin oxidoreductase in Clostridium acetobutylicum. Biochem. Biophys. Res. Commun. 285, 496

[45] Kawasaki, S., Ishikura, J., Watamura, Y., and Niimura. Y. (2004) Identification of O2-induced peptides in an obligatory anaerobe, Clostridium acetobutylicum. FEBS. Lett., 571, 21

[46] Kawasaki, S., Mimura, T., Satoh, T., Takeda, K., and Niimura, Y.(2006). Response of the microaerophilic bifidobacterium Species, B. boum and B. thermophilum, to oxygen, Applied and Environmental Microbiology. 72, 6854

[47] Kawasaki, S., Ishikura, J., Chiba, D., Nishino, T., and Niimura. Y.,(2004). Purification and characterization of an H2O-forming NADH oxidase from Clostridium aminovalericum: existence of an oxygen-detoxifying enzyme in an obligate anaerobic bacteria. Arch. Microbiol. 181, 324

[48] Zhang L.B., Tachi M, Kanno E., et al. (2009). Contribution of quorum sensing to the development of biofilm and virulence of pseudomonas aeruginosa in rat wound infection , Wound Repair and Regeneration, A3

[49] Eberl, L., Winson, M. K., Sternberg, C., Stewart, G. S. A. B., Christiansen, G., Chhabra, S. R., Bycroft, B., Williams, P., Molin, S. & Givskov, M. (1995). Involvement of N-butanoyl-L-homoserine lactone autoinducers in controlling the multicellular behavior of Serratia liquefaciens. Mol. Microbiol. 20, 127

[50] Hugouvieux-Cotte-Pattat, N., Condemine, G., Nasser, W. & Reverchon, S. (1996). Regulation of pectinolysis in Erwinia chrysanthemi. Annu. Rev. Microbiol., 50, 213

[51] Ruby, E. G. & McFall-Ngai, M. J. (1992). A squid that glows in the night: development of an animal-bacterial mutualism. J. Bacteriol. 174, 4865

[52] Nealson K.H., Hastings J.W. (1979). Bacterial bioluminescence: its control and ecological significance. Microbiol. Rev., 43, 496

[53] Waters C.M., Bassler B.L. (2005). Quorum sensing: cell-to-cell communication in bacteria. Annu. Rev. Cell Dev. Biol., 21, 319

[54] Hanzelka, B.L., and Greenberg., E.P. (1996). Generation of cell-to-cell signals in quorum sensing: Acyl homoserine lactone synthase activity of a purified Vibrio fischeri LuxI protein. Proc. Natl. Acad. Sci., 93, 9505
[55] Miyashiro, T. and Ruby, E.G. (2012). Shedding light on bioluminescence regulation in Vibrio fischeri. Mol Microbiol. 84: 795

[56] Sturme, M.H.J.; Kleerebezem, M.; Nakayama, J.; Akkermans, A.D.L.; Vaughan, E.E.; De Vos, W.M. (2002). Cell to cell communication by autoinducing peptides in gram-positive bacteria. Antonie Van Leeuwenhoek, 81, 233

[57] Yarwood J.M. and Schlievert P.M. (2003). Quorum sensing in Staphylococcus infections. J Clin. Invest., 112, 1620

[58] Leonard, P.G., Bezar, I., Sidote, D.J. and Stock, A.M. (2012) Identification of a hydrophobic cleft in the LytTR domain of AgrA as a locus for small molecule interactions that inhibit DNA binding. Biochemistry, 51:10035

[59] Goryachev A.B., Toh D.J., and Lee T. (2006). Systems analysis of a quorum sensing network: Design constraints imposed by the functional requirements, network topology and kinetic constants, Biosystems, 83, 178

[60] Williams, J. W., Cui, X., Levchenko, A., and Stevens, A. M. (2008). Robust and sensitive control of a quorum-sensing circuit by two interlocked feedback loops. Molecular systems biology 4, 234

[61] Kuttler, C., and Hense, B.A. (2008) Interplay of two quorum sensing regulation systems of Vibrio fischeri. J Theor Biol 251: 167

[62] Gustafsson E., Nilsson P., Karlsson S., Arvidson S. (2004) Characterizing the dynamics of the quorum-sensing system in Staphylococcus aureus. J Mol Microbiol Biotechnol , 8:232

[63] Karlsson, D.; Karlsson, S.; Gustafsson, E.; Normark, B. H.; Nilsson P.,(2007) Modeling the regulation of the competence-evoking quorum sensing network in Streptococcus pneumoniae. Biosystems , 90 : 211.

[64] Jabbari, S.; King, J. R.; Koerber, A. J.; Williams, P. J. (2010) Mathematical modelling of the agr operon in Staphylococcus aureus. Math. Biol. , 61: 17

[65] Benner, S.A., Sismour, A.M. (2005) Synthetic biology. Nature Reviews Genetics 6: 533

[66] Szallasi Z., Stelling, J., and Perival V. (2006). System Modeling in Cellular Biology from concept to nuts and bolts. MIT Press

[67] Ellis T, Adie T, Baldwin GS. 2011. DNA assembly for synthetic biology: from parts to pathways and beyond. Integr. Biol. 3:109

[68] Anderson, J.C., Dueber, J.E., Leguia, M., Wu, G.C., Goler, J.A., et al (2010). BglBricks: a flexible standard forbiological part assembly. J. Biol. Eng. 4:1

[69] Densmore, D., Hsiau, T.H., Kittleson, J.T., DeLoache, W., Batten, C., Anderson, J.C. (2010) Algorithms for automated DNA assembly. Nucleic Acids Res. 38:2607

[70] Bilitchenko, L., Liu, A., Cheung, S.,Weeding, E., Xia, B., et al. (2011) Eugene: a domain specific language forspecifying and constraining synthetic biological parts, devices, and systems. PLoS ONE 6:e18882

[71] Carlson, R. (2009). The changing economics of DNA synthesis. Nat. Biotechnol. 27:1091

[72] Carr, P.A., Church, G.M. (2009) Genome engineering. Nat. Biotechnol. 27:1151

[73] Weiss, R. and Knight, T. (2000) "Engineered Communications for Microbial Robotics" Proceedings of the Sixth International Meeting on DNA Based Computers (DNA6)

[74] You, L., Cox III, R.S., Weiss, R., Arnold, F. H. (2004). Programmed Population by Cell–Cell Control by Communication and Regulated Killing. Nature, 428, 868

[75] Basu, S.; Mehreja, R.; Thiberge, S.; Chen, M.-T.; Weiss, (2004) R. Spatiotemporal control of gene expression with pulse-generating networks. Proceedings of the National Academy of Sciences of the United States of America , 101, 6355

[76] Basu, S., Gerchman, Y., Collins, C.H., Arnold, F.H., and Weiss, R. (2005). A synthetic Multicellular System for Programmed Pattern Formation. Nature, 434, 1130

[77] Balagaddé, F.K., Song, H., Ozaki, J., Collins, C.H., Barnet, M., Arnold, F.H., Quake, S.R., You, L., (2008) A synthetic Escherichia coli predator-prey ecosystem. Mol Syst Biol.; 4:187

[78] Anderson, J. C., Clarke, E. J., Arkin, A. P. & Voigt, C. A. (2006) Environmentally controlled invasion of cancer cells by engineered bacteria. J. Mol. Biol. 355, 619

[79] Royo, J. L. et al. (2007) In vivo gene regulation in Salmonella spp. by a salicylate-dependent control circuit. Nature Methods 4, 937

[80] Xiang, S., Fruehauf, J. & Li, C. J. (2006) Short hairpin RNA-expressing bacteria elicit RNA interference in mammals. Nature Biotech. 24, 697

[81] Prindle, A., Selimkhanov, J., Danino, T., Samayoa, P., Goldberg, A., Bhatia, S.N., Hasty, J. (2012) Genetic Circuits in Salmonella typhimurium. ACS Synth Biol.; 1-458

[82] MATLAB and Statistics Toolbox Release 2012b, The MathWorks, Inc., Natick, Massachusetts, United States.

[83] De Mey, M., Maertens, J., Lequeux, G.J., Soetaert, W.K. and Vandamme, E.J. (2007). Construction and model-based analysis of a promoter library for E. coli: an indispensable tool for metabolic engineering. BMC Biotechnology, 7, 34.

[84] B. F. Pfleger, D. J. Pitera, C. D. Smolke, and J. D. Keasling. (2006). "Combinatorial engineering of intergenic regions in operons tunes expression of multiple genes." Nat. Biotechnol. 24:1027-1032.

[85] Haseltine E.L., Arnold F.H. (2008). Implications of rewiring bacterial quorum sensing. Appl Environ Microbio.,74:437–445

[86]B. Zargar, P. Chen, and B.P. Ingalls, "A synthetic biology approach to bacteria mediated tumor targeting," Proceedings of the Conference on Foundations of Systems Biology in Engineering (FOSBE), Denver, Colorado, August 2009.

[87] Brahimi-Horn, M. C., Pouysségur, J. (2007). Oxygen, a Source of Life and Stress. FEBS. Lett., 581, 3582

[88] Wei, M.Q., Mengesha, A., Good, D., West, C., Anné, J., (2008) Bacterial Targeted Tumour Therapy-dawn of a New Era. Cancer Lett., 259, 16.

[89] Higuchi, M., Yamamoto, Y., and Kamio, Y. (2000). Molecular Biology of Oxygen Tolerance in Lactic Acid Bacteria: Functions of NADH Oxidases and Dpr in Oxidative Stress. J. Biosci. and Bioeng., 90, 484.

[90] Sakamoto, M., Uchimura, T., and Komagata, K. (1996). Comparison of H2O-forming NADH Oxidase from Leuconostoc mesenteroides subsp. mesenteroides NRIC 1541T and H2O2-forming NADH Oxidase from Sporolactobacillus inulinus NRIC 1133T, J Ferm. and Bioeng., 82, 531.

[91], Young, D.I., Young, M. (1990) Conjugative plasmid transfer from Escherichia coli to Clostridium acetobutylicum. J Gen Microbiol, 136(5):819-26.

[92] Simon R, et al. A broad host range mobilization system for in vivo genetic engineering: transposon mutagenesis in Gram negative bacteria. Bio-Technology 1: 784-791, 1983.

[93] Canton B. (2008) Engineering the interface between cellular chassis and synthetic biological systems.PhD Thesis, MIT

[94] http://parts.igem.org/Part:BBa_C0261

[95] http://parts.igem.org/Part:BBa_I13504

[96] Heap J.T., Pennington O.J., Cartman S.T., Minton N.P. (2009). A modular system for Clostridium shuttle plasmids. J. Microbiol. Methods 78:79 –85.

[97] Lyras, D., Rood, J.I. (1998). Conjugative transfer of RP4-oriT shuttle vectors from Escherichia coli to Clostridium perfringens. Plasmid. 1998;39(2):160-4.

[98] Drepper T, Huber R, Heck A, Circolone F, Hillmer AK, et al. (2010). Flavin mononucleotide-based fluorescent reporter proteins outperform green fluorescent protein-like proteins as quantitative in vivo real-time reporters. Appl Environ Microbiol 76: 5990–5994.

[99] Dong, Y.H., L.H. Wang, J.L. Xu, H.B. Zhang, X.F. Zhang, and L.H.Zhang. (2001). Quenching quorum-sensing-dependent bacterialinfection by an N-acyl homoserine lactonase. Nature 411, 813-817.

[100] Koenig R.L., Ray J.L., Maleki S.J., Smeltzer MS, Hurlburt B.K. (2004) Staphylococcus aureus AgrA binding to the RNAIII-agrregulatory region. J Bacteriol 186(22):7549–7555.

[101] Thoendel M, Horswill AR. 2009. Identification of Staphylococcus aureus AgrD residues required for autoinducing peptide biosynthesis. J. Biol. Chem. 284(33):21828-38

[102] Losen M., Frölich B., Pohl M, Büchs J. (2004). Effect of Oxygen Limitation and Medium Composition on Escherichia coli Fermentation in Shake-Flask Cultures. Biotechnology Progress , 20:1062-1068

[103] Shin C.S., Kwak B., Han B., Park K. (2013) Development of an in vitro 3D tumor model to study therapeutic efficiency of an anticancer drug. Mol Pharm. 10(6):2167-75.